## PUBLISHER:

**Address of Publisher & Editor's Office:**

GDAŃSK UNIVERSITY
OF TECHNOLOGY
Faculty
of Ocean Engineering
& Ship Technology

ul. Narutowicza 11/12
80-233 Gdańsk, POLAND
tel.: +48 58 347 13 66
fax: +48 58 341 13 66
e-mail: office.pmr@pg.gda.pl

**Account number:**
**BANK ZACHODNI WBK S.A.**
I Oddział w Gdańsku
41 1090 1098 0000 0000 0901 5569

**Editorial Staff:**
**Tadeusz Borzęcki** Editor in Chief
e-mail: tadbor@pg.gda.pl
**Przemysław Wierzchowski** Scientific Editor
e-mail: e.wierzchowski@chello.pl
**Jan Michalski** Editor for review matters
e-mail: janmi@pg.gda.pl
**Aleksander Kniat** Editor for international relations
e-mail: olek@pg.gda.pl
**Kazimierz Kempa** Technical Editor
e-mail: kkempa@pg.gda.pl
**Piotr Bzura** Managing Editor
e-mail: pbzura@pg.gda.pl
**Cezary Spigarski** Computer Design
e-mail: biuro@oficynamorska.pl

**Domestic price:**
single issue: 25 zł

**Prices for abroad:**
single issue:
- in Europe EURO 15
- overseas USD 20

**ISSN 1233-2585**


POLISH MARITIME RESEARCH

*in internet*

***www.bg.pg.gda.pl/pmr/pmr.php***

# POLISH MARITIME RESEARCH


No 3 (79) 2013 Vol 20


## CONTENTS

# Editorial

POLISH MARITIME RESEARCH is a scientific journal of worldwide circulation. The journal appears as a quarterly four times a year. The first issue of it was published in September 1994. Its main aim is to present original, innovative scientific ideas and Research & Development achievements in the field of :

**Engineering**, **Computing & Technology**, **Mechanical Engineering**,

which could find applications in the broad domain of maritime economy. Hence there are published papers which concern methods of the designing, manufacturing and operating processes of such technical objects and devices as : ships, port equipment, ocean engineering units, underwater vehicles and equipment as well as harbour facilities, with accounting for marine environment protection.
The Editors of POLISH MARITIME RESEARCH make also efforts to present problems dealing with education of engineers and scientific and teaching personnel. As a rule, the basic papers are supplemented by information on conferences , important scientific events as well as cooperation in carrying out international scientific research projects.

# Scientific Board

**POLISH MARITIME RESEARCH** 3(79) 2013 Vol 20; pp. 3-13
10.2478/pomr-2013-0029

# Method of determining the degree of liquid aeration in a variable capacity displacement pump

**Zygmunt Paszota**, Prof.
Gdansk University of Technology, Poland

ABSTRACT

*The Author concludes, that there is a possibility of determining a concrete value of the liquid aeration coefficient ε during the pump operation by finding such value of ε with which the increase $\Delta M_{Pm|\Delta p_{Pi}=p_n,\ q_{Pgv}}$ of torque of mechanical losses is proportional to the indicated torque $M_{Pi|\Delta p_{Pi}=p_n,\ q_{Pgv}}$ determined with a fixed value $\Delta p_{Pi}$ = cte of increase of pressure in the pump working chambers. The fixed value $\Delta p_{Pi}$ assumed in searching the liquid aeration coefficient ε equals to the nominal pump operation pressure $p_n$ ($\Delta p_{Pi} = cte = p_n$). The increase $\Delta M_{Pm|\Delta p_{Pi}=p_n,\ q_{Pgv}}$ of torque of mechanical losses with a fixed value of $\Delta p_{Pi}$ ($\Delta p_{Pi} = cte$) is proportional to the pump geometrical working capacity $q_{Pgv}$, therefore: only with taking into account the aeration coefficient ε of liquid displaced by the pump the relation $\Delta M_{Pm|\Delta p_{Pi}=p_n,\ q_{Pgv}} \sim q_{Pgv}$ can be obtained from tests. The method, proposed by the Author, of determining the working liquid aeration coefficient ε, is presented in this paper and has been practically applied for the first time by Jan Koralewski in his investigations of the influence of viscosity and compressibility of aerated hydraulic oil on volumetric and mechanical losses in a pump of HYDROMATIK A7V.58.1.R.P.F.00 type [8, 9].*

**Key words**: hydrostatic drive; variable capacity displacement pump; liquid aeration; method of determining the degree of liquid aeration

## INTRODUCTION

In references [1– 4] the Author evaluated the effect of working liquid compressibility on the picture of volumetric and mechanical losses in a high-pressure variable capacity displacement pump. The considerations are based on the assumptions made in the, developed by the Author, theoretical and mathematical models of torque of mechanical losses in a pump used in a hydrostatic drive [5 –7]. It is assumed in the models, that increase $M_{Pi|\Delta p_{Pi},\ q_{Pgv}}$ of torque of mechanical losses in the pump „working chambers - shaft" assembly is proportional to torque $M_{Pi}$ indicated in the pump working chambers:

$$\Delta M_{Pm|\Delta p_{Pi}} \sim M_{Pi}$$

In references [1– 4] the Author introduced also a working liquid compressibility coefficient $k_{lc|p_n}$. Coefficient $k_{lc|p_n}$ determines the decrease, as an effect of liquid compressibility, of active volume of working liquid displaced during one pump shaft revolution with the increase $\Delta p_{Pi} = p_n$ of pressure in the working chambers equal to the pump nominal pressure $p_n$, compared with active volume equal to theoretical working capacity $q_{Pt}$ or geometrical working capacity $q_{Pgv}$ per one shaft revolution, determined with the increase $\Delta p_{Pi}$ of pressure in the working chambers equal to zero – $\Delta p_{Pi} = 0$:

$$k_{lc|p_n} = \frac{q_{Pt} - q_{Pt|\Delta p_{Pi}=p_n}}{q_{Pt}}$$

and

$$k_{lc|p_n} = \frac{q_{Pgv} - q_{Pgv|\Delta p_{Pi}=p_n}}{q_{Pgv}} = \frac{b_P\, q_{Pt} - b_P\, q_{Pt|\Delta p_{Pi}=p_n}}{b_P\, q_{Pt}}$$

The Author has also concluded that it is possible to evaluate the effect of liquid compressibility coefficient $k_{lc|p_n}$ on the value of increase $\Delta M_{Pm|\Delta p_{Pi}=p_n,\ q_{Pgv}}$ of torque of mechanical losses in the pump „working chambers - shaft" assembly and to evaluate the effect of $k_{lc|p_n}$ coefficient on the value of the coefficient of volumetric losses in the pump working chambers due to leakage.

Searching the value of liquid compressibility coefficient $k_{lc|p_n}$, which with the increase $\Delta p_{Pi}$ of pressure in working chambers, equal to the pump nominal pressure $p_n$, will cause an increase $\Delta M_{Pm|\Delta p_{Pi}=p_n,\, q_{Pgv}}$ of torque of mechanical losses proportional to $q_{Pgv}$, i.e. to the indicated torque $M_{Pi|\Delta p_{Pi}=p_n,\, q_{Pgv}}$ the Author determined, in the pump HYDROMATIK A7V.58.1.R.P.F.00 type, tested by Jan Koralewski in his doctor dissertation [8] the approximate value of the oil compressibility coefficient during the tests as equal to $k_{lc|32\ MPa} = 0.030$.

Taking into account the working liquid compressibility evaluated by the coefficient $k_{lc|32\ MPa} = 0.030$. Author determined approximate values of new coefficients of volumetric and mechanical losses in the tested pump.

The Author concludes, that there is a possibility of determining a concrete value of the liquid aeration coefficient ε during the pump operation by finding such value of ε with which the increase $\Delta M_{Pm|\Delta p_{Pi}=p_n,\, q_{Pgv}}$ of torque of mechanical losses is proportional to the indicated torque $M_{Pi|\Delta p_{Pi}=p_n,\, q_{Pgv}}$ determined with a fixed value $\Delta p_{Pi}$ = cte of increase of pressure in the pump working chambers. The fixed value $\Delta p_{Pi}$ assumed in searching the liquid aeration coefficient ε equals to the nominal pump operation pressure $p_n$ ($\Delta p_{Pi}$ = cte = $p_n$).

The increase $\Delta M_{Pm|\Delta p_{Pi}=p_n,\, q_{Pgv}}$ of torque of mechanical losses with a fixed value of $\Delta p_{Pi}$ ($\Delta p_{Pi}$ = cte) is proportional to the pump geometrical working capacity $q_{Pgv}$, therefore:

**only with taking into account the aeration coefficient ε of liquid displaced by the pump the relation $\Delta M_{Pm|\Delta p_{Pi}=p_n,\, q_{Pgv}} \sim q_{Pgv}$ can be obtained from tests.**

The method, proposed by the Author, of determining the working liquid aeration coefficient ε, is presented in this paper and has been practically applied for the first time by Jan Koralewski in his investigations of the influence of viscosity and compressibility of aerated hydraulic oil on volumetric and mechanical losses in a pump of HYDROMATIK A7V.58.1.R.P.F.00 type [8, 9].

## COMPRESSIBILITY OF WORKING LIQUID IN THE PUMP

Compressibility of liquid at a given temperature is characterized by variation of its mass density ρ as a function of pressure p. In order to facilitate the calculations, the curve of variation ρ = f(p) is represented by an approximate algebraic relation. Most often a linear approximation is used:

$$\frac{\Delta\rho}{\rho} = \frac{\Delta p}{B} \tag{1}$$

It may be said, that relation (1) defines a **modulus B of the liquid volume elasticity** valid for a certain temperature and for a certain pressure.

Numerical indications regarding the value of B of hydraulic oils are the following [10]:

– at the normal temperature (20 °C), close to B = 1500 MPa for the used hydraulic oils,
– B increases with the pressure (by about 1% every 2 MPa up to 20 MPa for the used oils ($a_p$ = 0.005/1 MPa)),
– B decreases when the temperature increases (about 1% every 2 °C up to 100 °C for the used oils ($a_\vartheta$ = - 0.005/1 °C)).

In working chambers of the tested piston pump [8, 9], during their connection with the inlet channel, was slight overpressure $p_{P1i} \approx 0.05$ MPa (i.e. absolute pressure $p_{P1ia} \approx 0.15$ MPa). Let's assume that the value of modulus B of the hydraulic oil volume elasticity, at the temperature ϑ = 20 °C, equals to:

$$B_{|p_{P1ia} \approx 0.15\ Mpa;\ \vartheta = 20\ °C} = 1500\ MPa \tag{2}$$

Therefore, the dependence of modulus B of oil on the increase $\Delta p_{Pi}$ of pressure in the working chambers and on the increase Δϑ of oil temperature may be described by the expression:

$$B = B_{|p_{P1ia} \approx 0.15\ Mpa;\ \vartheta = 20\ °C}\,(1 + a_p \Delta p_{Pi} + a_\vartheta \Delta\vartheta) \tag{3}$$

**Modulus B of hydraulic oil volume elasticity decreases very quickly when oil is aerated, i.e. when the oil aeration coefficient ε is greater than zero (ε > 0)**.

The oil aeration coefficient ε is the ratio of volume $V_a$ of air to volume $V_0 = V_o + V_a$ of mixture of oil volume $V_o$ and air volume $V_a$ ($\varepsilon = V_a/V_0 = V_a/(V_o + V_a)$). The oil aeration coefficient ε is determined at the absolute pressure $p_{P1ia}$ in the pump working chambers during their connection with the inlet channel.

Let's suppose, that volume $V_0$ of aerated oil in the pump working chambers, at initial absolute pressure $p_{P1ia}$ in the chambers (Fig. 6), contains a volume of air equal $V_a = \varepsilon V_0$ and a volume of oil equal $V_o = (1 - \varepsilon)V_0$.

An increase $\Delta p_{Pi}$ of pressure in the pump working chambers causes a decrease of the oil and air mixture volume by the value ΔV (assuming a hypothesis of compression of air $pV_a$ = cte) equal to:

$$\Delta V = \Delta V_o + \Delta V_a = \frac{V_o}{B}\Delta p_{Pi} + \frac{V_a}{p_{P1ia} + \Delta p_{Pi}}\Delta p_{Pi} \tag{4}$$

If the aeration coefficient ε is small, which is a general case, $V_o$ is close to $V_0$. Therefore it can be written:

$$\Delta V = V_0\left(\frac{1}{B} + \frac{\varepsilon}{p_{P1ia} + \Delta p_{Pi}}\right)\Delta p_{Pi} \tag{5}$$

Therefore, **with the oil aeration coefficient ε greater than zero (ε > 0), modulus B of oil volume elasticity must be replaced by modulus B' of volume elasticity** defined by the relation:

$$\frac{1}{B'} = \frac{1}{B} + \frac{\varepsilon}{p_{P1ia} + \Delta p_{Pi}} \tag{6}$$

or, in the conditions of changing pressure and temperature of the aerated oil, by the relation:

$$\frac{1}{B'} = \frac{1}{B_{|p_{P1ia} \approx 0.15\ MPa,\ \vartheta = 20°C}(1 + a_p \Delta p_{Pi} + a_\vartheta \Delta\vartheta)} + \frac{\varepsilon}{p_{P1ia} + \Delta p_{Pi}} \tag{7}$$

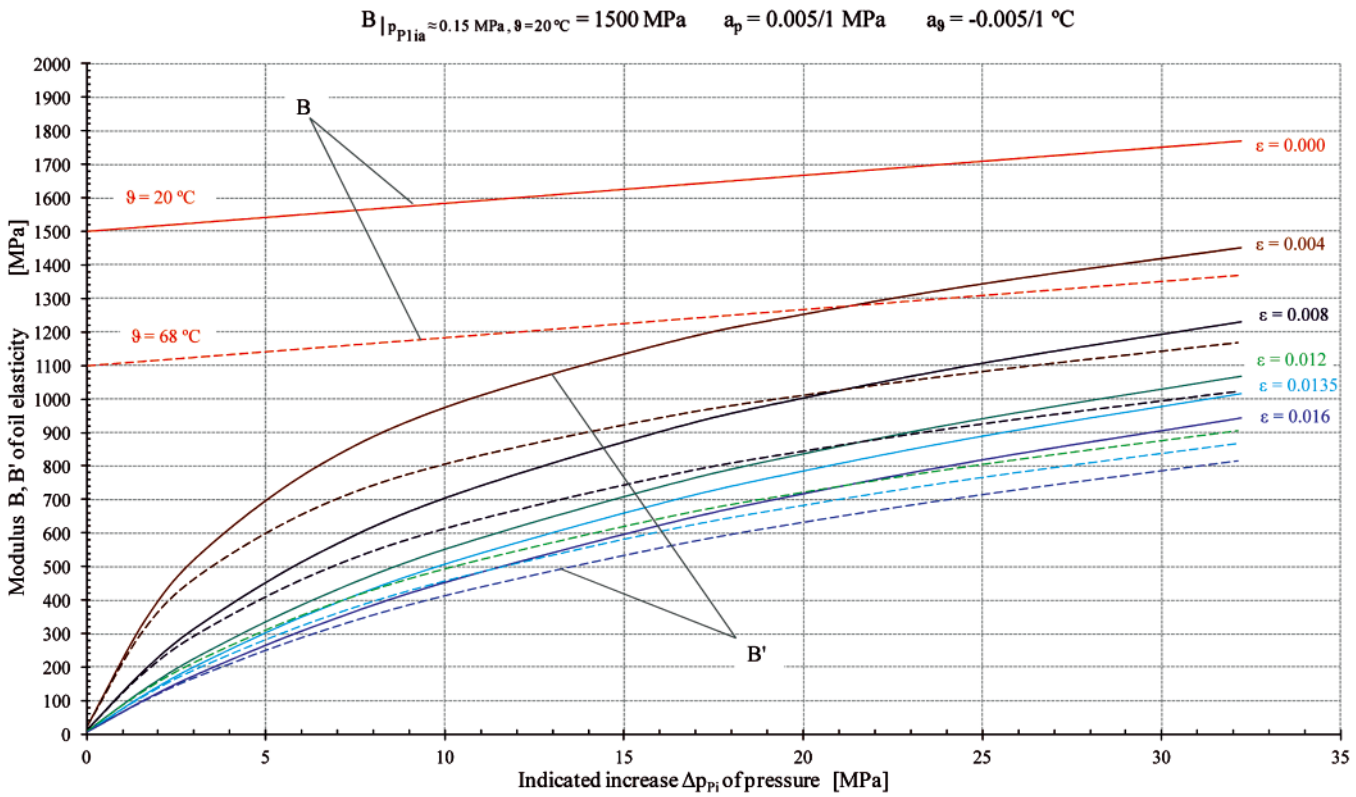


*Fig. 1. Modulus B of volume elasticity of non-aerated hydraulic oil (ε = 0) and modulus B' of aerated oil (ε > 0) as relations dependent on indicated increase $\Delta p_{Pi}$ of pressure in the pump working chambers, with limit values ϑ = 20 °C (continuous line) and ϑ = 68 °C (dashed line) of hydraulic oil temperature adopted during the investigations [8, 9]. It was assumed that modulus B of oil volume elasticity at absolute pressure $p_{PIia} \approx 0.15$ MPa in the pump working chambers during their connection with the inlet channel and at oil temperature ϑ = 20 °C is equal to B = 1500 MPa. Also assumed was the value of coefficient $a_p$ = 0.005/1 MPa of the change of modulus B of oil due to increase $\Delta p_{Pi}$ of pressure in the working channels and coefficient $a_\vartheta$ = - 0.005/1 °C of the change of modulus B due to change of oil temperature ϑ*

Fig. 1 presents the modulus B of volume elasticity of non-aerated hydraulic oil (ε = 0) and modulus B' of aerated oil (ε > 0) as relations dependent on indicated increase $\Delta p_{Pi}$ of pressure in the pump working chambers, with limit values ϑ = 20 °C and ϑ = 68 °C of oil temperature adopted during the investigations [8, 9].

**The displacement pump with variable geometric working capacity $q_{Pgv}$ per one shaft revolution is tested with different fixed values of $q_{Pgv}$ .**

Variable (set during the test) geometrical working capacity $q_{Pgv}$ of working chambers per one shaft revolution equals to the difference between maximum chambers capacity (capacity increasing to that maximum value during connection of the chamber with the pump inlet channel) and minimum chamber capacity (capacity decreasing to that value during connection of the chambers with the pump outlet (discharge) channel). The initial volume $V_0$ of oil (Fig. 6), which is compressed due to increase $\Delta p_{Pi}$ of pressure in the pump chambers, corresponding to setting $q_{Pgv}$ of the variable geometrical working capacity, is in a variable capacity pump equal to:

$$V_0 = 0.5q_{Pt} + 0.5q_{Pgv} \tag{8}$$

When the variable (set) geometrical working capacity $q_{Pgv}$ reaches the maximum value equal to the pump theoretical working capacity $q_{Pt}$ ($q_{Pgv} = q_{Pt}$), volume $V_0$ of compressed oil is equal to:

$$V_0 = 0.5q_{Pt} + 0.5q_{Pt} = q_{Pt} \tag{9}$$

The change ΔV of liquid volume (Fig. 6), due to the liquid compression under the increase $\Delta p_{Pi}$ of pressure in the pump chambers, is equal to the loss $q_{Pvc}$ of pump capacity per one shaft revolution:

$$\Delta V = q_{Pvc} \tag{10}$$

The loss $q_{Pvc}$ of pump capacity per one shaft revolution (Fig. 2), resulting from the compression of non-aerated (or aerated) oil at the setting $q_{Pgv}$ of geometrical variable working capacity, is determined (in reference to (5) and (6)) by the expression:

$$q_{Pvc} = \frac{(0.5q_{Pt} + 0.5q_{Pt})\Delta p_{Pi}}{B'} \tag{11}$$

and with $q_{Pgv} = q_{Pt}$ , by expression:

$$q_{Pvc} = \frac{q_{Pt}\,\Delta p_{Pi}}{B'} \tag{12}$$

and, after replacing 1/B' by expression (7), by the formula:

$$q_{Pvc} = (0.5q_{Pt} + 0.5q_{Pgv})\cdot \left[\frac{1}{B|_{p_{PIia}\approx 0.15\ MPa,\ \vartheta=20\,°C}(1 + a_p\Delta p_{Pi} + a_\vartheta\Delta\vartheta)} + \frac{\varepsilon}{p_{PIia} + \Delta p_{Pi}}\right]\Delta p_{Pi} \tag{13}$$

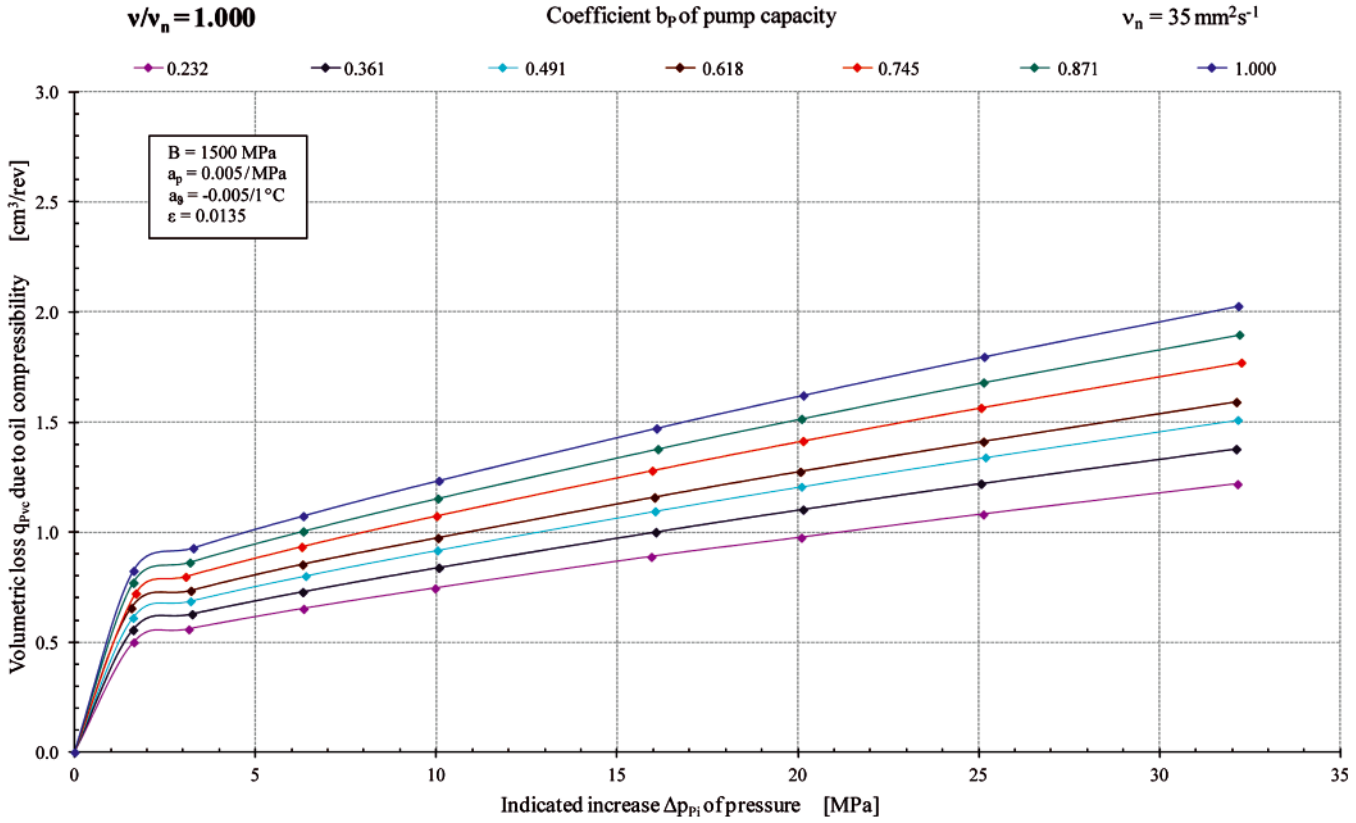


***Fig. 2.*** *Loss $q_{Pvc}$ of pump capacity during one pump shaft revolution due to compressibility of aerated (ε = 0.0135) liquid, decreasing the active volume of liquid displaced by the pump compared with the theoretical working capacity $q_{Pt}$ ($b_P$ = 1) or geometrical working capacity $q_{Pgv}$ (0 < $b_P$ < 1) (pump of HYDROMATIK A7V.DR.1.R.P.F.00 type) [8, 9]*

and also, with $q_{Pgv} = q_{Pt}$, by the formula:

$$q_{Pvc} = q_{Pt} \cdot \left[ \frac{1}{B_{|p_{Pl\,ia} \approx 0.15\ \mathrm{MPa},\, \vartheta = 20\,^{\circ}\mathrm{C}} (1 + a_p \Delta p_{Pi} + a_\vartheta \Delta\vartheta)} + \frac{\varepsilon}{p_{Pl\,ia} + \Delta p_{Pi}} \right] \Delta p_{Pi} \qquad (14)$$

Fig. 2 presents an example (with assumed oil aeration coefficient ε = 0.0135) of the results of calculations of the loss $q_{Pvc} = f(\Delta p_{Pi})$ of the tested pump capacity per one shaft revolution, taking into account formula (13) for setting $q_{Pgv}$ of the geometrical variable working capacity and formula (14) for the maximum setting $q_{Pgv} = q_{Pt}$, i.e. the case of pump theoretical working capacity.

The change of $q_{Pvc}$ as a function of indicated increase $\Delta p_{Pi}$ of pressure in the working chambers, presented in Fig. 2, takes into account the influence of changing volumes $V_0$ (Fig. 6) of compressed liquid in the working chambers, the changes being an effect of the principle of operation of a variable capacity $q_{Pgv}$ per one shaft revolution displacement pump (with variable $b_P$ coefficient).

Loss $q_{Pvc}$ of pump capacity during one shaft revolution due to the liquid compressibility decreases the active liquid volume displaced by the pump compared with the theoretical working capacity $q_{Pt}$ or geometrical variable working capacity $q_{Pgv}$ (determined at $\Delta p_{Pi} = 0$). This fact should be taken into account in the evaluation of intensity $q_{Pv} = Q_{Pv}/n_P$ of volumetric losses in the working chambers as well as in the evaluation of increase $\Delta M_{Pm|\Delta p_{Pi}}$ of the torque of mechanical losses in the „working chambers - shaft" assembly, the losses caused by the increase $\Delta p_{Pi}$ of pressure in the pump working chambers with determined values of the chamber geometrical working capacity $q_{Pgv}$.

In the considerations, notions have been introduced of **theoretical active working capacity $q_{Pt|\Delta p_{Pi} = p_n}$ and of geometrical active working capacity $q_{Pgv|\Delta p_{Pi} = p_n}$ as capacities the pump has in the working chambers at the increase $\Delta p_{Pi}$ of pressure in the chambers equal to the nominal pressure $p_n$ of system operation**. The active working capacities $q_{Pt|\Delta p_{Pi} = p_n}$ and $q_{Pgv|\Delta p_{Pi} = p_n}$ can be determined from the equations:

$$q_{Pt|\Delta p_{Pi} = p_n} = q_{Pt} - q_{Pvc|p_n} \qquad (15)$$

$$q_{Pgv|\Delta p_{Pi} = p_n} = q_{Pgv} - q_{Pvc|p_n} \qquad (16)$$

Also a notion has been introduced of **the coefficient $k_{lc|p_n}$ of working liquid compressibility in the pump**.

**Coefficient $k_{lc|p_n}$ of the working liquid compressibility in the pump determines the degree of decrease, as an effect of liquid compressibility** (without taking into account the chamber leakage)**, of the liquid active volume displaced by the pump during one shaft revolution at the increase $\Delta p_{Pi}$ of pressure in the pump working chambers equal to the nominal pressure $p_n$ of system operation, compared with the active volume displaced by the pump at $\Delta p_{Pi} = 0$**. Coefficient $k_{lc|p_n}$ is defined by the formulae:

$$k_{lc|p_n} = \frac{q_{Pt} - q_{Pt|\Delta p_{Pi}=p_n}}{q_{Pt}} = \frac{q_{Pvc|p_n}}{q_{Pt}} \quad (17)$$

or:

$$k_{lc|p_n} = \frac{q_{Pgv} - q_{Pgv|\Delta p_{Pi}=p_n}}{q_{Pgv}} = \frac{q_{Pvc|p_n}}{q_{Pvg}} \quad (18)$$

**The knowledge of coefficient $k_{lc|p_n}$ of the liquid compressibility in the pump allows to evaluate numerically the subdivision of volumetric losses in the pump into the losses due to oil leakage in the working chambers and losses due to liquid compressibility**.

In a variable capacity pump operating with setting $q_{Pgv}$ of geometrical variable working capacity (determined at $\Delta p_{Pi} = 0$), the coefficient $k_{lc|p_n}$ is described (in reference to (13) and (18)) by the formula:

$$k_{lc|p_n} = \frac{q_{Pvc|\Delta p_{Pi}=p_n}}{q_{Pgv}} = \frac{0.5q_{Pt} + 0.5q_{Pgv}}{q_{Pgv}} \cdot \left[ \frac{1}{B_{|p_{P1ia} \approx 0.15\ MPa, \vartheta = 20\ ^\circ C}\ (1 + a_p p_n + a_\vartheta \Delta\vartheta)} + \frac{\varepsilon}{p_{P1ia} + p_n} \right] p_n \quad (19)$$

and with $q_{Pgv} = q_{Pt}$ (in reference to (14) and (17)) by the formula:

$$k_{lc|p_n} = \frac{q_{Pvc|\Delta p_{Pi}=p_n}}{q_{Pt}} = \left[ \frac{1}{B_{|p_{P1ia} \approx 0.15\ MPa, \vartheta = 20\ ^\circ C}\ (1 + a_p p_n + a_\vartheta \Delta\vartheta)} + \frac{\varepsilon}{p_{P1ia} + p_n} \right] p_n \quad (20)$$

Therefore, in a displacement pump, operating at theoretical working capacity $q_{Pt}$ per one shaft revolution, the working liquid compressibility coefficient $k_{lc|p_n}$ (formula (20)) is a combined effect of modulus B of hydraulic oil volume elasticity, oil aeration coefficient $\varepsilon$ and also liquid temperature $\vartheta$ (increase $\Delta\vartheta$ to the reference temperature $\vartheta = 20$ °C) and absolute pressure $p_{P1ia}$ in the working chambers during their connection with the inlet channel, as well as the system nominal pressure $p_n$ .

In the same displacement pump operating with variable capacity $q_{Pgv}$ per one shaft revolution, the value of working liquid compressibility coefficient $k_{lc|p_n}$ (formula (19)) increases in comparison with the value $k_{lc|p_n}$ during the pump operation with the theoretical working capacity $q_{Pt}$ . This is an effect of the increased ratio of initial liquid volume ($V_0$ in Fig. 6) subjected to compression, i.e. the volume ($0.5q_{Pt} + 0.5q_{Pgv}$) (formula (8)), to the set working volume $q_{Pgv}$ . **Therefore, decreasing the $q_{Pgv}$ setting causes in a variable capacity displacement pump an increase of $k_{lc|p_n}$ coefficient** (formula (19)).

## IMPORTANCE OF THE ACCURACY OF EVALUATION OF $q_{Pt}$ AND $q_{Pgv}$ FOR THE ACCURACY OF EVALUATION OF THE INTENSITY OF VOLUMETRIC LOSSES AND TORQUE OF MECHANICAL LOSSES IN THE PUMP

It is important, particularly during investigation of a pump of variable capacity per one shaft revolution, to determine precisely the theoretical capacity $q_{Pt}$ per one pump shaft revolution and geometrical capacities $q_{Pgv}$ per one pump shaft revolution. Geometrical capacities $q_{Pgv}$ change in the $0 \le q_{Pgv} \le q_{Pt}$ range and the corresponding coefficients $b_P = q_{Pgv}/q_{Pt}$ of the pump capacity change in the $0 \le b_P \le 1$ range. Therefore, precise evaluation of the coefficient $b_P = q_{Pgv}/q_{Pt}$ depends on the precision of evaluation of $q_{Pgv}$ and $q_{Pt}$ .

The pump theoretical working capacity $q_{Pt}$ and geometrical working capacities $q_{Pgv}$ are determined at the indicated increase $\Delta p_{Pi}$ of pressure in the pump working chambers equal to zero ($\Delta p_{Pi} = 0$); the working capacities are determined by approximation at the point $\Delta p_{Pi} = 0$ of the line $q_P = Q_P/n_P = f(\Delta p_{Pi})$ describing, at a pump constant setting (but the value of $b_P$ coefficient unknown exactly), the capacity $q_P$ displaced during one pump shaft revolution as dependent on the indicated increase $\Delta p_{Pi}$ . The line $q_P = f(\Delta p_{Pi})$ runs through the measurement points obtained in the investigation.

Fig. 3 presents examples of dependence $q_P = f(\Delta p_{Pi})$ of capacity $q_P$ per one shaft revolution of an axial piston pump on the indicated increase $\Delta p_{Pi}$ of pressure in the working chambers at the coefficient $b_P = 1$ of pump capacity per one shaft revolution [8, 9]. These are examples of searching the theoretical working capacity $q_{Pt}$ per one pump shaft revolution and also the evaluation of subdivision of the intensity $q_{Pv}$ of volumetric losses per one shaft revolution into the volumetric loss $q_{Pvl}$ due to oil leakage in the working chambers and volumetric loss $q_{Pvc}$ due to compressibility of non-aerated (or aerated) oil.

Loss $q_{Pvc} = f(\Delta p_{Pi})$ per one shaft revolution, determined from formula (13), due to liquid compressibility, occurring at setting $q_{Pgv}$ of the pump variable geometrical working capacity (or from formula (14) at setting $q_{Pt}$ of the pump theoretical working capacity) is added to capacity $q_P = f(\Delta p_{Pi})$ per one shaft revolution shown by the line running through the test measurement points. The result of adding $q_{Pvc} = f(\Delta p_{Pi})$ to $q_P = f(\Delta p_{Pi})$ is pump capacity $q_{P\ without\ compressibility} = f(\Delta p_{Pi})$ as a difference between $q_{Pgv}$ (or $q_{Pt}$) and the volumetric loss $q_{Pvl}$ due to oil leakage (independent of the liquid compressibility):

$$(q_{P\ without\ compressibility} = q_{Pvc} + q_P) = f(\Delta p_{Pi}) \quad (21)$$

$$(q_{P\ without\ compressibility} = q_{Pgv}\ (\text{or } q_{Pt}) - q_{Pvl}) = f(\Delta p_{Pi}) \quad (22)$$

Approximation of the $q_{P\ without\ compressibility} = f(\Delta p_{Pi})$ line at $\Delta p_{Pi} = 0$ allows to determine the $q_{Pgv}$ (or $q_{Pt}$):

$$q_{P\ without\ compressibility\ |\Delta pPi\ =\ 0} = q_{Pgv}\ (\text{or } q_{Pt}) \quad (23)$$

As shown in Fig. 3, the pump theoretical working capacities $q_{Pt}$ , at point $\Delta p_{Pi} = 0$ of the $q_P = f(\Delta p_{Pi})$ line, obtained from tests and including also the liquid compressibility, as well as of the

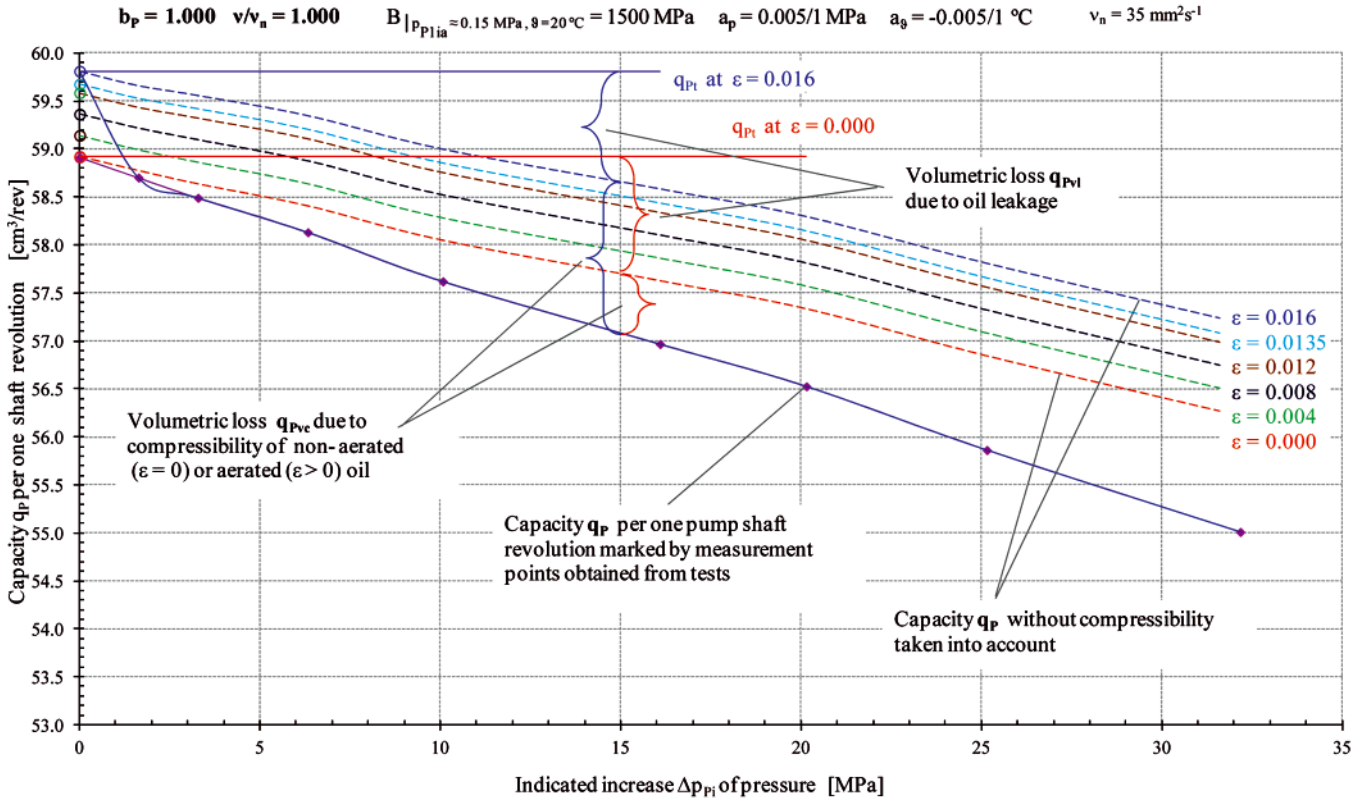


***Fig. 3.*** *Dependence of pump capacity $q_P$ per one shaft revolution on the indicated increase $\Delta p_{Pi}$ of pressure in the working chambers, at the coefficient $b_P$ = 1 of pump capacity; the val-ues $q_{Pgv}$ of geomet rical working volume and qPt of theoretical working volume per one shaft revolution (determined at $\Delta p_{Pi}$ = 0) and subdivision of the intensity $q_{Pv} = q_{Pvl} + q_{Pvc}$ of volu-metric losses per one shaft revolution into volumetric loss $q_{Pvl}$ due to oil leakage in the cham-bers and volumetric loss $q_{Pvc}$ due to compressibility of non-aerated (or aerated) oil dependent on the value of oil aeration coefficient ε (ε = 0 to 0.016); viscosity coefficient v/vn = 1, oil temperature ϑ = 43 °C (pump of the HYDROMATIK A7V.DR.1.R.P.F.00 type) [8, 9]*

($q_{P\ without\ compressibility} = q_{Pvc} + q_P$) = f($\Delta p_{Pi}$) line taking into account compressibility of non-aerated (ε = 0) oil, have practically the same value $q_{Pt}$ = 58.9 cm³/rev. Approximation of the ($q_{P\ without\ compressibility} = q_{Pvc} + q_P$) = f($\Delta p_{Pi}$) line at $\Delta p_{Pi}$ = 0 point, taking into account the aerated oil compressibility, shows an increase of $q_{Pt}$ value practically proportional to oil aeration coefficient ε. This is clearly presented in Fig. 4. For example, theoretical working capacity with ε = 0.0135, reaches the value $q_{Pt}$ = 59.57 cm³/rev.

Fig. 5 presents the subdivision of volumetric losses $q_{Pv}$ = = f($\Delta p_{Pi}$) in the tested pump into loss $q_{Pvc}$ = f($\Delta p_{Pi}$) due to liquid compressibility and loss $q_{Pvl}$ = f($\Delta p_{Pi}$) due to oil leakage at different values of liquid aeration coefficient ε, with the theoretical working capacity $q_{Pt}$ per one pump shaft revolution. The lines of $q_{Pvl}$ = f($\Delta p_{Pi}$) loss due to oil leakage do not change at different oil aeration coefficient ε value, but lines $q_{Pvc}$ = f($\Delta p_{Pi}$) due to oil compressibility differ clearly, as well as lines ($q_{Pv}$ = = $q_{Pvl} + q_{Pvc}$) = f($\Delta p_{Pi}$) of volumetric losses $q_{Pv}$ = f($\Delta p_{Pi}$) as a sum of $q_{Pvl}$ = f($\Delta p_{Pi}$) of loss due to leakage and $q_{Pvc}$ = f($\Delta p_{Pi}$) of loss due to liquid compressibility.

During a careful investigation of a displacement pump pressing non-aerated working liquid, the accuracy of determining the theoretical working volume $q_{Pt}$ and geometrical working volumes $q_{Pgv}$ is of an order of one per mille. Accuracy of estimation of the value of coefficients $b_P$ of pump capacity is then also very high.

The accuracy of evaluation of $q_{Pt}$ and $q_{Pgv}$ is significantly worse when the working liquid is aerated. This is an effect of

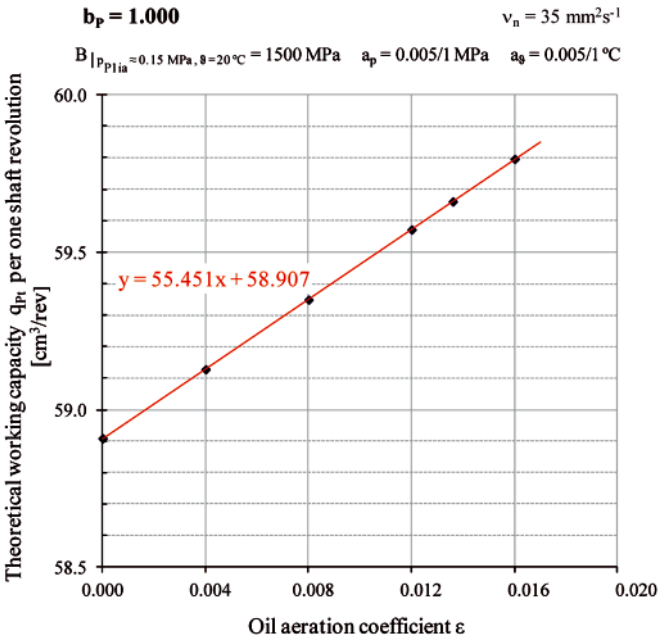


***Fig. 4.*** *Effect of evaluation of theoretical working capacity $q_{Pt}$ per one pump shaft revolution resulting from assumption of aeration coefficient ε of the pump displaced oil; evaluation $q_{Pt}$ (Fig. 3) is a result of approximation, at $\Delta p_{Pi}$ = 0. of the relation of pump capacity $q_P$ per one shaft revolution to the indicated increase $\Delta p_{Pi}$ of pressure in the working chambers taking into account the aerated oil compressibility (at a given oil aeration coefficient ε) (pump HYDROMATIK A7V.DR.1 .R.P. F.00 type) [8, 9]*

the fact, that the aerated liquid in the working chambers filled during their connection with the low-pressure inlet channel decreases its volume because of great compressibility of non-

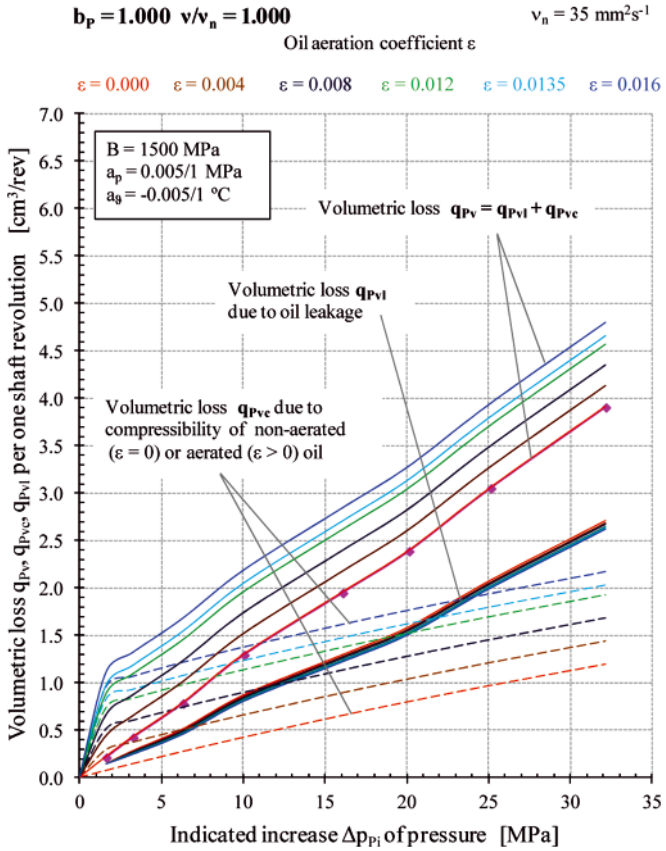


*Fig. 5. Subdivision of volumetric loss $q_{Pv} = f(\Delta p_{Pi})$ in the pump into loss $q_{Pvc} = f(\Delta p_{Pi})$ due to oil compressibility and loss $q_{Pvl} = f(\Delta p_{Pi})$ due to oil leakage at different values of oil aeration coefficient ε and value $v/v_n = 1$ of oil viscosity coefficient in the tested pump with theoretical working capacity $q_{Pt}$ ($b_P = 1$) (pump HYDROMATIK A7V.DR.1.R.P.F.00 type) [8, 9]*

dissolved air in the liquid, after connection of the working chambers with the discharge channel where pressure may be only a little higher than in the inlet channel.

**Without knowledge of the coefficient ε of aeration of the liquid flowing into the pump working chambers, it is impossible to determine the quantities $q_{Pt}$ and $q_{Pgv}$ precisely**.

**At the same time, precise knowledge of $q_{Pt}$ and $q_{Pgv}$ is important in evaluation of the volumetric and mechanical losses in the pump**.

The intensity $q_{Pv} = Q_{Pv}/n_P$ of volumetric losses $Q_{Pv}$ in the pump working chambers per one pump shaft revolution is evaluated as a difference between $q_{Pt}$ (or $q_{Pgv}$) and $q_P$ determined during the investigation at changing values of the indicated increase $\Delta p_{Pi}$ of pressure in the chambers.

**Increase $\Delta M_{Pm|\Delta p_{Pi}}$ of the torque of mechanical losses in the pump „working chambers - shaft" assembly**, compared with torque $M_{Pm|\Delta p_{Pi}=0}$ of mechanical losses in the no-load pump, is an effect of increased friction forces in the assembly resulting from the influence of the torque $M_{Pi}$ indicated in the working chambers upon the assembly and **is proportional to $M_{Pi}$** .

Increase $\Delta M_{Pm|\Delta p_{Pi}}$ of the torque of mechanical losses in the pump „working chambers - shaft" assembly is determined during the investigations as a difference $\Delta M_{Pm|\Delta p_{Pi}} = M_{Pm} + - M_{Pm|\Delta p_{Pi}=0}$ between torque $M_{Pm}$ of losses in the assembly and torque $M_{Pm|\Delta p_{Pi}=0}$ of losses in the assembly of a no-load pump.

Torque $M_{Pm}$ of losses is determined as a difference $M_{Pm} = M_P - M_{Pi}$ between torque $M_P$ measured directly on the shaft and torque $M_{Pi}$ indicated in the working chambers. Therefore, **extremely important, for determination of torque $M_{Pm}$ of mechanical losses and of increase $\Delta M_{Pm|\Delta p_{Pi}}$ of torque of mechanical losses, is precision of determination of torque $M_{Pi}$ indicated in the working chambers** (defined by formulae (35) and (36)).

## WORK OF THE DELIVERY OF COMPRESSED WORKING LIQUID DURING ONE PUMP SHAFT REVOLUTION AND TORQUE INDICATED IN THE PUMP WORKING CHAMBERS

In order to deliver compressed working liquid during one pump shaft revolution, **a certain work E is required, which is a sum of**:

- **the work of compression itself − $E_1$,**
- **the work of displacement at constant pressure − $E_2$** .

Let's calculate the theoretical values (efficiencies equal to 1) of the two works. For that purpose, the pump delivering the compressed liquid is presented in a simplified way by a piston of cross-section S moving in a cylinder, which, by two valves $R_1$ and $R_2$ (acting as a distributer), can communicate with, respectively:

- space filled with liquid at constant absolute pressure $p_{P1ia}$ ,
- volume $C_2$ filled with liquid at constant absolute pressure $p_{P2ia}$ (Fig. 6).

Piston in Fig. 6 performs stroke from position $x_o$ to the bottom of cylinder i.e. to position 0

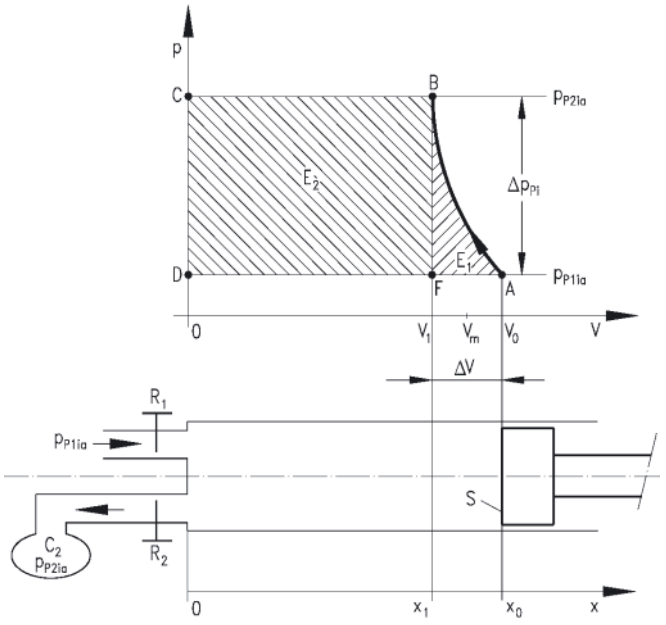


*Fig. 6. Work of the delivery of compressed working liquid during one displacement pump shaft revolution (simplified diagram)*

**Initial position**: piston at $x_0$ . Volume open to liquid at pressure $p_{P1ia}$ : $V_0$ . $R_1$ opened, $R_2$ closed.

**1st phase**: $R_1$ is closed, piston pushed from $x_0$ to $x_1$ (volume $V_1$). This is the point where liquid, closed in the cylinder, achieves the pressure $p_{P2ia}$ . The work delivered by the piston is **the work of compression**:

$$E_1 = -\int_{x_0}^{x_1} (p - p_{P1ia})\, S dx = -\int_{V_0}^{V_1} (p - p_{P1ia})\, dV \tag{24}$$

Work $E_1$ is represented by area ABFA.

**2nd phase**: $R_2$ is opened and the piston is pushed (in the case of $b_P = q_{Pgv}/q_{Pt} = 1$) from $x_1$ to 0. i.e., to the bottom of cylinder. The liquid is discharged into $C_2$ . The work delivered by the piston is **the work of displacement**:

$$E_2 = -\int_{x_1}^{0} (p_{P2ia} - p_{P1ia})\, S dx = -\int_{V_1}^{0} (p_{P2ia} - p_{P1ia})\, dV = (p_{P2ia} - p_{P1ia}) V_1 \tag{25}$$

Work $E_2$ is represented by area BCDFB.

**3rd phase**: $R_2$ is closed, $R_1$ opened and we return to the initial position. This operation is carried out without work performed by the pump.

The total work $E = E_1 + E_2$ is represented by the dashed areas in Fig. 6.

One of the definitions of the modulus B of liquid volume elasticity is the following:

$$\frac{\Delta V}{V} = -\frac{\Delta p}{B} \text{ where } V = -\frac{V}{B}\, dp \tag{26}$$

Therefore, the compression work is:

$$E_2 = -\int_{V_0}^{V_1} (p - p_1)\, dV = \int_{p_1}^{p_2} (p - p_1) \frac{V}{B} dp = \frac{V}{B} \frac{(p - p_1)^2}{2} \Bigg|_{p_1}^{p_2} \tag{27}$$

During operation of pump with theoretical capacity $q_{Pt}$ per one shaft revolution ($b_P = 1$), the change of V (Fig. 6) during compression work in relation to $V_0$ is small. The compression curve may be replaced by linear approximation and the V quantity in equation (27) by mean value $V_m = (V_0 + V_1)/2$:

$$E_1 = \frac{V_m}{B} \frac{(p_2 - p_1)^2}{2} \tag{28}$$

Therefore:

$$E_2 = V_1 (p_{P2ia} - p_{P1ia}) \text{ (acc. to (25))}$$

and:

$$E = E_1 + E_2 = (p_2 - p_1)\left[V_1 + \frac{V_m (p_2 - p_1)}{2B}\right] = (p_2 - p_1)\left[V_1 + \frac{\Delta V}{2}\right]$$

$$E = (p_2 - p_1) V_m$$

$$E = V_m (p_{P2ia} - p_{P1ia}) \tag{29}$$

Formula (29) describing the work E may be replaced by the expression:

$$E = \left[V_0 - \frac{\Delta V}{2}\right](p_{P2ia} - p_{P1ia}) = \left[V_0 - \frac{\Delta V}{2}\right] \Delta p_{Pi} \tag{30}$$

In a real displacement pump with variable capacity per one shaft revolution, with the geometrical working capacity setting $q_{Pgv}$ , work E performed by the pump in the working chambers during one shaft revolution (after replacing in formula (30) the original volume $V_0$ by volume $q_{Pgv}$ , the change $\Delta V$ of liquid volume due to liquid compressibility by loss $q_{Pvc}$ of pump capacity during one shaft revolution (formula (8) and the loss $q_{Pvc}$ by formula (11)), is described by the expressions:

$$E = \left(q_{Pgv} - \frac{q_{Pvc}}{2}\right) \Delta p_{Pi} \tag{31}$$

and:

$$E = \left\{1 - \frac{1}{2}\left[\frac{1}{B_{|p_{P1ia} \approx 0.15\ \text{MPa}, \vartheta = 20\,^{\circ}\text{C}} (1 + a_p \Delta p_{Pi} + a_\vartheta \Delta\vartheta)} + \frac{\varepsilon}{p_{P1ia} + \Delta p_{Pi}}\right] \Delta p_{Pi}\right\} q_{Pgv} \Delta p_{Pi} \tag{32}$$

and with $q_{Pgv} = q_{Pt}$ (in reference to (12)) by the expressions:

$$E = \left(q_{P_{Pt}} - \frac{q_{Pvc}}{2}\right)\Delta p_{Pi} \tag{33}$$

and:

$$E = \left\{1 - \frac{1}{2}\left[\frac{1}{B_{\left|p_{P1ia} \approx 0.15\ MPa,\, \vartheta = 20\,^{o}C\right.}(1 + a_p \Delta p_{Pi} + a_\vartheta\, \Delta\vartheta)} + \frac{\varepsilon}{p_{P1ia} + \Delta p_{Pi}}\right]\Delta p_{Pi}\right\}\, q_{Pt}\, \Delta p_{Pi} \tag{34}$$

It has to be mentioned, that in formula (32), describing the work E performed by the pump with setting $q_{Pgv}$ per one shaft revolution, the $q_{Pgv}$ value is determined by approximation of the $(q_P + q_{Pvc}) = f(\Delta p_{Pi})$ line at point $\Delta p_{Pi} = 0$. At the same time, the formula (32) contains the value $q_{Pvc} = f(\Delta p_{Pi})$ describing a loss of capacity per one shaft revolution due to the liquid compressibility taking into account the change $\Delta V$ (Fig. 6) of liquid volume resulting from the variable capacity pump operation mode, i.e. the compressed volume $V_0$ (Fig. 6) equal to $V_0 = 0.5q_{Pt} + 0.5q_{Pgv}$ .

Torque $M_{Pi}$ indicated in the pump working chambers, corresponding to work E in the chambers during one shaft revolution, is then, with $q_{Pgv}$ setting, described by the formula:

$$M_{Pi} = \frac{E}{2\Pi} = \left\{1 - \frac{1}{2}\left[\frac{1}{B_{\left|p_{P1ia} \approx 0.15\ MPa,\, \vartheta = 20\,^{o}C\right.}(1 + a_p \Delta p_{Pi} + a_\vartheta\, \Delta\vartheta)} + \frac{\varepsilon}{p_{P1ia} + \Delta p_{Pi}}\right]\Delta p_{Pi}\right\}\frac{q_{Pgv}\, \Delta p_{Pi}}{2\Pi} \tag{35}$$

and with $q_{Pgv} = q_{Pt}$ by the formula:

$$M_{Pi} = \frac{E}{2\Pi} = \left\{1 - \frac{1}{2}\left[\frac{1}{B_{\left|p_{P1ia} \approx 0.15\ MPa,\, \vartheta = 20\,^{o}C\right.}(1 + a_p \Delta p_{Pi} + a_\vartheta\, \Delta\vartheta)} + \frac{\varepsilon}{p_{P1ia} + \Delta p_{Pi}}\right]\Delta p_{Pi}\right\}\frac{q_{Pt}\, \Delta p_{Pi}}{2\Pi} \tag{36}$$

## METHOD OF DETERMINING THE WORKING LIQUID AERATION COEFFICIENT ε

**As it so far has not been possible to determine the coefficient ε of aeration of the working liquid flowing into the pump**, and therefore not possible to take the liquid compressibility into account, both at the small increase $\Delta p_{Pi}$ of pressure in the pump working chambers and in the full range of increase $\Delta p_{Pi}$ of pressure − up to the hydrostatic drive system nominal pressure $p_n$ , **the pictures of volumetric losses and mechanical losses in the pump, determined by the applied methods, are deformed**. For instance, if the compressibility of working liquid, the liquid in fact aerated, is not taken into account, a picture of negative increase $\Delta M_{Pm|\Delta p_{Pi}}$ of torque of mechanical losses in the pump „working chambers - shaft" assembly is obtained as an effect of increased torque $M_{Pi}$ indicated in the working chambers due to the increase of geometrical working volume $q_{Pgv}$ (of $b_p$ coefficient), which is an illogical result (Fig. 7).

**A method of determining the coefficient ε of working liquid aeration may be searching for value of ε which was used for determining the values $q_{Pgv}$ of geometrical working capacities causing an increase $M_{Pm|\Delta p_{Pi}}$ of torque of mechanical losses in the pump „working chambers - shaft" assembly proportional to torque $M_{Pi}$ indicated in the working chambers** (formula (35)), **a torque $M_{Pi}$ resulting from $q_{Pgv}$ and from ε at the constant value $\Delta p_{Pi}$ of indicated increase of pressure in the chambers.** It is assumed, that during searching for $q_{Pgv}$ and ε, the increase $M_{Pm|\Delta p_{Pi}}$ of the torque of mechanical losses is determined at a constant value of indicated increase $\Delta p_{Pi}$ of pressure in the pump working chambers equal to the system nominal pressure $p_n$ ($\Delta p_{Pi} = p_n$).

**Therefore, it is assumed, that with a fixed value $\Delta p_{Pi} = p_n$ of the indicated increase of pressure in the pump working chambers, the increasing torque $M_{Pi}$ in the chambers** (formula (35))**, described by the expression**:

$$\mathbf{M_{Pi}} = \left\{\mathbf{1 - \frac{1}{2}\left[\frac{1}{B_{\left|p_{P1ia} \approx 0.15\ MPa,\, \vartheta = 20\,^{o}C\right.}(1 + a_p p_n + a_\vartheta\, \Delta\vartheta)} + \frac{\varepsilon}{p_{P1ia} + p_n}\right]p_n}\right\}\frac{q_{Pgv}\, p_n}{2\Pi} \tag{37}$$

**must be accompanied by proportional increase $\Delta M_{Pm|\Delta p_{Pi} = p_n}$ of torque of mechanical losses in the pump „working chambers - shaft" assembly**:

$$\Delta M_{Pm|\Delta p_{Pi} = p_n;\, q_{Pgv}} \sim M_{Pi|\Delta p_{Pi} = p_n;\, q_{Pgv}} \tag{38}$$

**or**

$$\Delta M_{Pm|\Delta p_{Pi} = p_n;\, q_{Pgv}} \sim q_{Pgv}\,(b_P) \tag{39}$$

With fixed values of B, $a_p$ , $a_\vartheta$ , $\vartheta$, $p_{P1ia}$ and $p_n$ , **expressions (38) and (39) can be obtained only with one value ε of the aeration coefficient**, which was assumed for determining of $q_{Pgv}$ values and of the pump capacity $b_P$ coefficient values.

Fig. 7 presents results of searching for the oil aeration coefficient ε during pump tests [8, 9].

With the assumption of non-compressible (B = ∞) and non-aerated (ε = 0) liquid, i.e. with the assumption of the liquid compressibility coefficient $k_{lc|p_n} = 0$ the picture of $\Delta M_{Pm|\Delta p_{Pi}=p_n} = f(M_{Pi|\Delta p_{Pi}=p_n})$ relation has the form of a descending straight line:

from value $\Delta M_{Pm} = 1.87$ Nm at $q_{Pgv} = 0$
to value $\Delta M_{Pm} = 0.53$ Nm at $q_{Pgv} = q_{Pt}$ .

With the assumption of compressible and non-aerated (ε = 0) liquid, the picture of $\Delta M_{Pm|\Delta p_{Pi}=p_n} = f(M_{Pi|\Delta p_{Pi}=p_n})$ relation has the form of an ascending straight line:

from value $\Delta M_{Pm} = 1.86$ Nm at $q_{Pgv} = 0$
to value $\Delta M_{Pm} = 2.79$ Nm at $q_{Pgv} = q_{Pt}$ .

With the assumption of compressible and aerated (ε = 0.008) liquid, the picture of $\Delta M_{Pm|\Delta p_{Pi}=p_n} = f(M_{Pi|\Delta p_{Pi}=p_n})$ relation has the form of an ascending straight line:

from value $\Delta M_{Pm} = 0.76$ Nm at $q_{Pgv} = 0$
to value $\Delta M_{Pm} = 1.77$ Nm at $q_{Pgv} = q_{Pt}$ .

With the assumption of compressible and aerated (ε = 0.016) liquid, the picture of $\Delta M_{Pm|\Delta p_{Pi}=p_n} = f(M_{Pi|\Delta p_{Pi}=p_n})$ relation has the form of an ascending straight line:

from value $\Delta M_{Pm} = -0.35$ Nm at $q_{Pgv} = 0$
to value $\Delta M_{Pm} = 0.74$ Nm at $q_{Pgv} = q_{Pt}$ .

With the oil aeration coefficient ε = 0.0135, the picture $\Delta M_{Pm|\Delta p_{Pi}=p_n;\, q_{Pgv}} = f(M_{Pi|\Delta p_{Pi}=p_n;\, q_{Pgv}})$ has the form of an ascending straight line:

from value $\Delta M_{Pm} = 0$ at $q_{Pgv} = 0$
to value $\Delta M_{Pm} = 1.03$ Nm at $q_{Pgv} = q_{Pt}$ .

Figure 8 presents, in reference to results presented in figure 7, a linear relation of the increase $\Delta M_{Pm|\Delta p_{Pi}=p_n;\, q_{Pgv}=0}$ of torque of mechanical losses to the assumed value of the oil aeration coefficient ε. **The relation shown in figure 8 allows to find with high accuracy the value of oil aeration coefficient ε, with which the increase $\Delta M_{Pm|\Delta p_{Pi}=p_n;\, q_{Pgv}=0}$ of the torque of mechanical losses at $q_{Pgv} = 0$ ($b_P = 0$) equals zero**:

$$\Delta M_{Pm|\Delta p_{Pi}=p_n;\, q_{Pgv}=0;\, \varepsilon} = 0 \qquad (40)$$

**The oil aeration coefficient ε during the pump testing (pump HYDROMATIK A7V.DR.1.R.P.F.00 type) corresponding to the situation described by formula (40), had the value ε = 0.0135** [8, 9].

## CONCLUSIONS

1. The Author concludes, that there is a possibility of determining a concrete value of the liquid aeration coefficient ε during the pump operation by finding such value of ε with which the increase $\Delta M_{Pm|\Delta p_{Pi}=p_n;\, q_{Pgv}}$ of torque of mechanical losses is proportional to the indicated torque $\Delta M_{Pm|\Delta p_{Pi}=p_n;\, q_{Pgv}}$ determined with a fixed value $\Delta p_{Pi}$ = cte of increase of pressure in the pump working chambers.

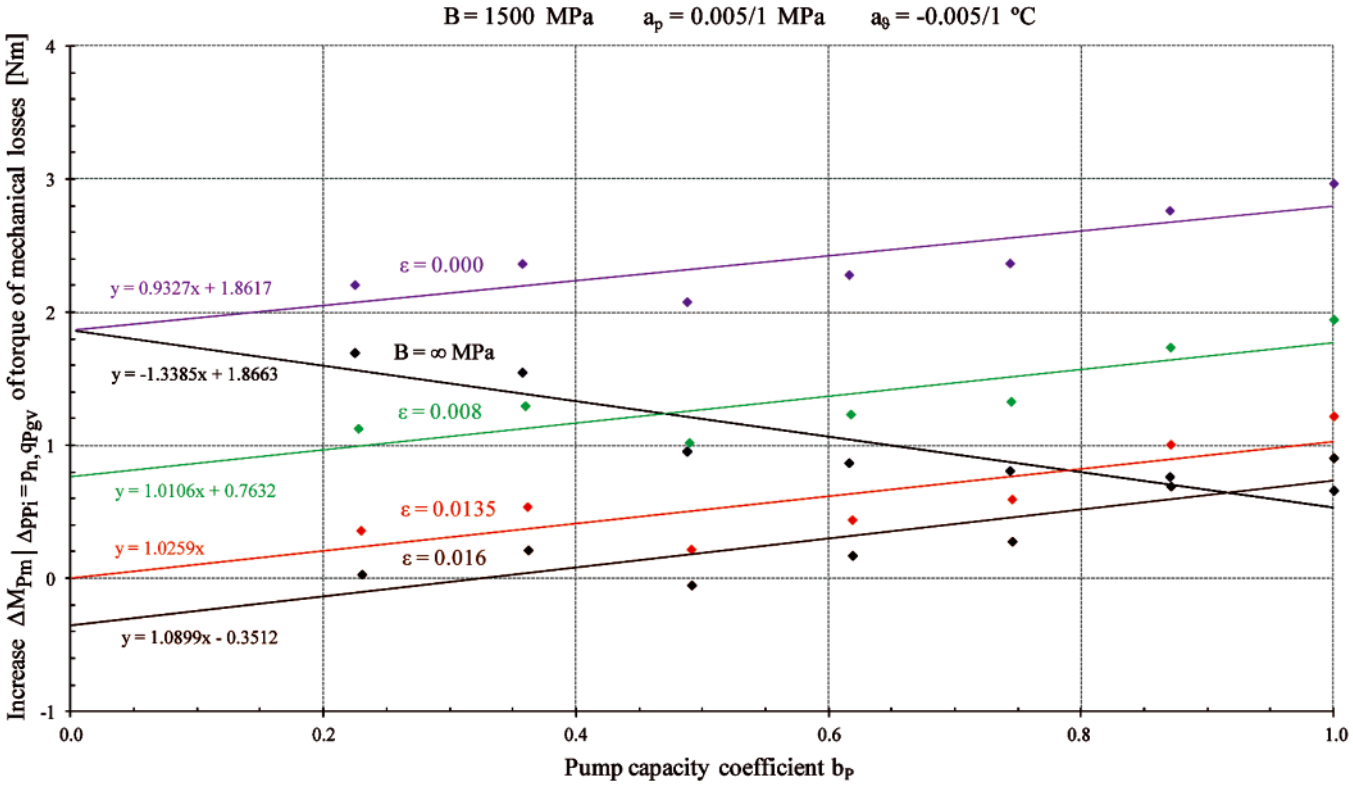


*Fig. 7. Picture of the relations of increase $\Delta M_{Pm|\Delta p_{Pi}=32\ MPa;\, q_{Pgv}}$ of torque of mechanical losses in the pump „working chambers - shaft" assembly (pump HYDROMATIK A7V.DR.1.R.P.F.00 type) to the geometrical working capacity $q_{Pgv}$ ($b_P$ coefficient) with assumed values of modulus B of hydraulic oil elasticity and oil aeration coefficient ε; the line $\Delta M_{Pm|\Delta p_{Pi}=32\ MPa;\, q_{Pgv}}$ corresponding to ε = 0.0135 is an effect of the straight line picture presented in Fig. 8 [8, 9]*

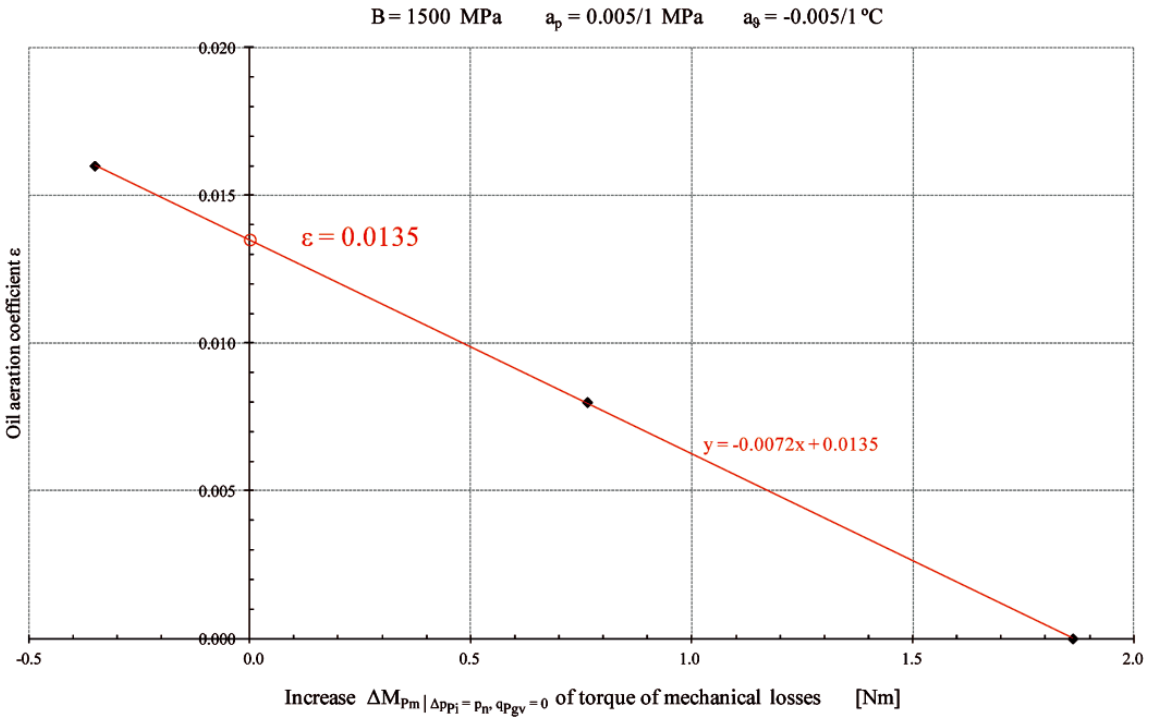


***Fig. 8.*** *Straight line relation of the oil aeration coefficient ε to the assumed increase $\Delta M_{Pm|\Delta p_{Pi} = 32\ MPa;\ q_{Pgv} = 0}$ of torque of mechanical losses (pump HYDROMATIK A7V.DR.1.R.P.F.00 type) [8, 9]*

2. The fixed value $\Delta p_{Pi}$ assumed in searching the liquid aeration coefficient ε equals to the nominal pump operation pressure $p_n$ ($\Delta p_{Pi}$ = cte = $p_n$).
3. The increase $\Delta M_{Pm|\Delta p_{Pi} = p_n;\ q_{Pgv}}$ of torque of mechanical losses with a fixed value of $\Delta p_{Pi}$ ($\Delta p_{Pi}$ = cte) is proportional to the pump geometrical working capacity $q_{Pgv}$ , therefore: only with taking into account the aeration coefficient ε of liquid displaced by the pump the relation $\Delta M_{Pm|\Delta p_{Pi} = p_n;\ q_{Pgv}} \sim q_{Pgv}$ can be obtained from tests.
4. The method, proposed by the Author, of determining the working liquid aeration coefficient ε, is presented in this paper and has been practically applied for the first time by Jan Koralewski in his investigations of the influence of viscosity and compressibility of aerated hydraulic oil on volumetric and mechanical losses in a pump of HYDROMATIK A7V.58.1.R.P.F.00 type [8, 9].

## BIBLIOGRAPHY


1. Paszota Z.: *Effect of the working liquid compressibility on the picture of volumetric and mechanical losses in a high pressure displacement pump used in a hydrostatic drive. Part I Energy losses in a drive system, volumetric losses in a pump* //International Scientific-Technical Conference Hydraulics and Pneumatics, Wrocław, 16 – 18 maja 2012 / Ośrodek Doskonalenia Kadr SIMP - Wrocław : ODK SIMP we Wrocławiu, 2012,
2. Paszota Z.: *Effect of the working liquid compressibility on the picture of volumetric and mechanical losses in a high pressure displacement pump used in a hydrostatic drive. Part II Mechanical losses in a pump* //International Scientific-Technical Conference Hydraulics and Pneumatics, Wrocław, 16 – 18 maja 2012 / Ośrodek Doskonalenia Kadr SIMP - Wrocław : ODK SIMP we Wrocławiu, 2012,
3. Paszota Z.: *Effect of the working liquid compressibility on the picture of volumetric and mechanical losses in a high pressure displacement pump used in a hydrostatic drive. Part I Energy losses in a drive system, volumetric losses in a pump* // Polish Maritime Research, Vol. 19, 2/2012
4. Paszota Z.: *Effect of the working liquid compressibility on the picture of volumetric and mechanical losses in a high pressure displacement pump used in a hydrostatic drive. Part II Mechanical losses in a pump* // Polish Maritime Research, Vol.19 3/2012
5. Paszota Z.: *Theoretical and mathematical models of the torque of mechanical losses in the pump used in a hydrostatic drive*. (in Polish). Chapter in the monograph: „Research, design, production and operation of hydraulic systems" (in Polish) Adam Klich, Antoni Kozieł and Edward Palczak editors. „Cylinder" Library. „Komag" Mining Mechanisation Centre, Gliwice 2011
6. Paszota Z.: *Theoretical and mathematical models of the torque of mechanical losses in the pump used in a hydrostatic drive*. (in Polish). „Napędy i sterowanie", scientific monthly 10/2011
7. Paszota Z.: *Theoretical and mathematical models of the torque of mechanical losses in the pump used in a hydrostatic drive*. Polish Maritime Research, Vol. 18, 4/2011
8. *Koralewski J.: Effect of the liquid viscosity on the energy characteristics of variable capacity piston pump* (in Polish). Doctor dissertation (continued). Gdańsk University of Technology, Faculty of Ocean Engineering and Ship Technology
9. Koralewski J.: *Effect of oil viscosity and compressibility on determination of volumetric losses in a variable capacity piston pump* (In Polish). Paper submitted to the „Cylinder" 2013 Conference. Centrum Mechanizacji Górnictwa „Komag", Gliwice 2013
10. Guillon M.: *Theory and calculation of hydraulic systems* (in Polish). Wydawnictwa Naukowo-Techniczne Warszawa 1967


## CONTACT WITH THE AUTHOR


Prof. Zygmunt Paszota
Faculty of Ocean Engineering
and Ship Technology
Gdansk University of Technology
Narutowicza 11/12
80-233 Gdansk, POLAND
e-mail: zpaszota@pg.gda.pl

**POLISH MARITIME RESEARCH** 3(79) 2013 Vol 20; pp. 14-19
10.2478/pomr-2013-0030

# Energy efficiency of a hydrostatic drive with proportional control compared with volumetric control

**Grzegorz Skorek**, Ph.D.
Gdynia Maritime University, Poland

ABSTRACT

*There are uninvestigated areas connected with behaviour of elements in hydraulic systems with different structures. Unawareness of proportions of the energy, volumetric, pressure and mechanical losses in elements is often the case. Problems connected with energy efficiency are essential for improvement of functionality and quality of hydrostatic drive systems, characterised by unquestioned advantages but also by relatively low efficiency in comparison with other types of drive. Energy efficiency of hydrostatic transmissions, particularly those with throttling control of the motor speed, and also efficiency of the hydraulic servo-mechanism systems may be in fact higher than the values most often quoted in publications on the subject. Possibility of calculating the real value of the hydraulic system overall efficiency as a function of many parameters influencing it, becomes a tool of complete evaluation of the designed system quality. The paper compares efficiencies of systems with cylinder proportional control and efficiency of the system volumetric control by a variable capacity pump. Presented are also two schematic diagrams of the investigated hydrostatic systems, their principle of operation and problems of studying losses in elements and energy efficiency of systems consisting of a feed assembly, control set and cylinder.*

**Key words**: hydrostatic system; control structures; proportional directional valve; cylinder; energy losses; energy efficiency

## INTRODUCTION

In searching for the energy saving solutions, computer-aided methods of calculating the energy efficiency of systems have been developed and improved.

The hydrostatic systems play a very important role in modern machines. Great number of the nowaday constructed machines have more or less developed hydrostatic or electric-hydrostatic drive systems and in many cases those systems are the most important parts of the machines. Component elements – hydraulic linear motors (cylinders) – are widely applied in machines used on land and aboard ships. Unquestioned advantages of cylinders are: capability of performing the translational motion, reliability, simple construction, the effective force to weight ratio.

The required speed $v_M$ and load $F_M$ of the driven machine are a result of its operation cycle and tasks to be performed. The driven machine current speed and load values are independent of the type and structure of the machine driving system.

The current speed and load of the hydrostatic system driven machine have a direct or indirect impact on the mechanical, volumetric and pressure losses in the hydraulic motor, pump and other elements of the system with a given motor speed control structure, the losses resulting also from the hydraulic oil viscosity.

If, as an effect of the increasing, required by the driven machine, hydraulic motor operating speed $v_M$ or increasing, required by the machine, motor load $F_M$ , and also as an effect of the mechanical, volumetric and pressure losses in the hydrostatic driving system elements, the maximum driving system capability, determined by the maximum pump capacity $Q_{Pmax}$ or maximum pressure $p_{P2max}$ in the pump discharge conduit limited to the system nominal pressure $p_n$ , is used up, then further increase of $v_M$ or $F_M$ will not be possible [4÷9].

The maximum pump capacity $Q_{Pmax}$ is less than its theoretical capacity $Q_{Pt}$. The pump theoretical capacity $Q_{Pt}$ is a product of the theoretical capacity $q_{Pt}$ per one pump shaft revolution and the no-load pump shaft speed $n_{P0}$. The pump $Q_{Pmax}$ capacity results from the loaded pump speed $n_P$, lower than the $n_{P0}$ speed. At the same time, volumetric losses occur in the pump [4÷9].

The system nominal pressure $p_n$ is a maximum permissible pressure $p_{P2max}$ for its continuous operation, determined in the pump discharge conduit.

Maximum values of the hydrostatic drive system hydraulic motor speed $v_{Mmax}$ and load $F_{Mmax}$ are limited by the maximum pump capacity $Q_{Pmax}$ and the system (pump) nominal pressure $p_n$ , and also by the mechanical, volumetric and pressure losses in other system elements, which are also an effect of the working liquid viscosity [4÷9].

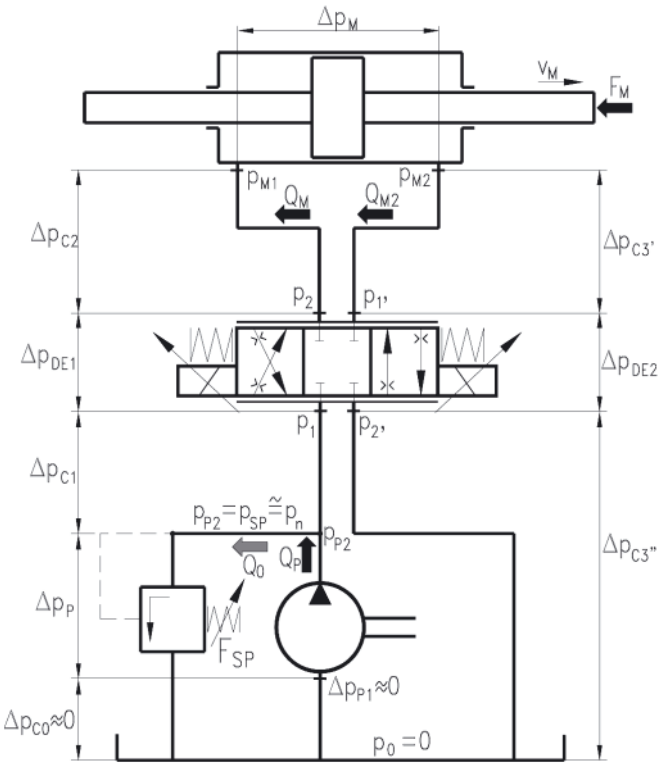


***Fig. 1.*** *Diagram of the investigated system fed at constant pressure – a p = cte structure [1÷3]*

The most often used proportional control system of a linear hydraulic motor is a system (Fig. 1), where the proportional directional valve is fed by a constant capacity pump cooperating with an overflow valve stabilizing a constant feed pressure level (p = cte). Such system achieves high energy efficiency, close to the efficiency of a system without throttling control, only at a point of maximum values of the motor load coefficient $\overline{M}_M$ and speed coefficient $\overline{\omega}_M$. With decreasing motor load, and particularly with simultaneous decreasing motor speed, the system efficiency $\eta$ decreases rapidly [1÷3].

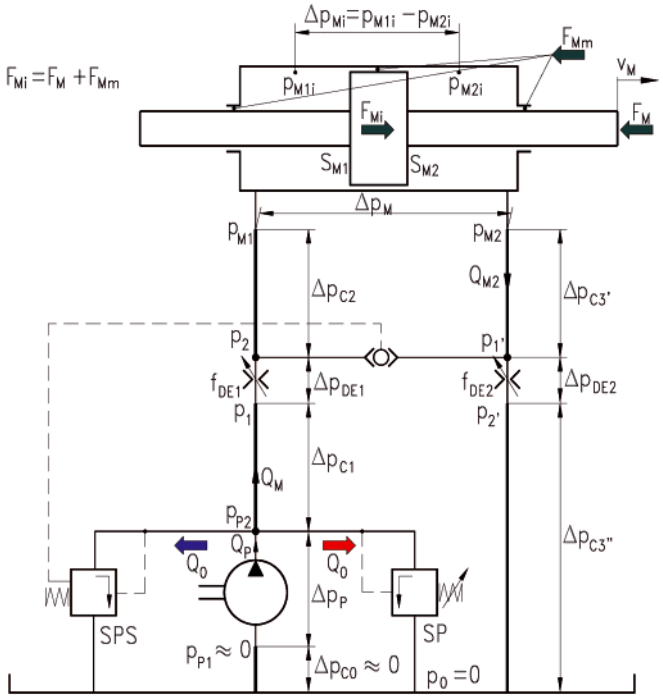


***Fig. 2.*** *Diagram of the investigated system with proportional directional valve fed by a constant capacity pump cooperating with an overflow valve controlled in a variable pressure system – p = var [1÷3]*

There are possibilities of reducing the energy losses in elements (pump, throttling control assembly and hydraulic motor, particularly the linear motor) of a system with proportional control, i.e. possibilities of increasing the energy efficiency of a system with throttling valve.

The hydrostatic system of drive and linear hydraulic motor proportional control may be fed by a constant capacity pump cooperating with an overflow valve stabilizing the proportional directional valve feed pressure at the nominal pressure level (Fig. 1), or by a pump cooperating with an overflow valve controlled by the receiver inlet pressure. The variable pressure (p = var) (Fig. 2) system makes it possible to reduce losses in the pump, in the control assembly and in the linear hydraulic motor [1÷3].

In a variable pressure (p = var) system, the structural pressure and volumetric losses in the throttling control assembly, mechanical losses in the cylinder and pump as well as volumetric losses in the pump can be significantly reduced. The mathematical description of losses and efficiency is presented in reference [1].

The hydrostatic system structure has an essential influence on the system efficiency. Its impact is most often considered with the assumption of an ideal pump and motor and also with supposition that energy losses in the real pump and motor will cause further proportional decrease of the system overall efficiency. However, the picture of mutual impact of losses in all the hydrostatic system elements appears much more complex [8].

## IMPORTANCE OF THE INVESTIGATIONS

Problems connected with energy efficiency are of basic importance for improvement of functionality and quality of the hydrostatic drive systems, characterised by unquestioned advantages but also by relatively low efficiency in comparison with other types of drive. Publications describing the influence of particular design and operating parameters on the hydrostatic system efficiency are valuable. They make it possible to work out system configurations with losses reduced to a minimum.

Energy efficiency of hydrostatic transmissions, particularly those with throttling control of the motor speed, and also efficiency of the hydraulic servo-mechanism systems may be in fact higher than the values most often quoted in publications on the subject. Possibility of calculating the real value of the hydraulic system overall efficiency as a function of many parameters influencing it, becomes a tool of complete evaluation of the designed system quality. The capability of making such evaluation is important because the hydrostatic control systems are used in various machines and equipment, and also due to increasing power of the hydrostatic drive at the time of constantly increasing costs of energy generation [8].

In a system with too low efficiency, the load, first of all of the pump, increases, which leads to increased risk of failure and the necessary repair or replacement, as well as to a shorter service life. The too low system efficiency, most often resulting from intensive throttling of the stream of liquid, is also a source of rapid deterioration of operational characteristics, particularly the hydraulic oil lubricating properties, which is an effect, among other reasons, of too high temperature of the working liquid – the hydrostatic transmission power medium.

Comparison of power losses in the elements provides information facilitating design of a new system.

Comparison of energy balances from the point of view of the power of losses in different systems gives a broader view for choosing an optimum solution.

## COMPARISON OF THE ENERGY EFFICIENCY OF VARIOUS SYSTEM VERSIONS

Investigations of the efficiency of elements and systems, taking into account detail analysis of the sources of particular energy losses, may be included in the basic scope of research into the hydrostatic drive and control systems.

The energy efficiency, one of the most important system characteristics, is defined as the ratio of, by the driven device currently demanded, useful power $P_{Mu}$ of the hydraulic motor to the power $P_{Pc}$, corresponding to $P_{Mu}$, obtained by the pump on its shaft from the (electric or combustion) motor driving the pump. In case of improper choice of the system type, the consequence may be increased hydraulic oil temperature, i.e. decreased oil viscosity and, in turn, lower efficiency of the system elements, and also an impact on the system run characteristics. Therefore, the energy efficiency may be a decisive factor for usability of a system in a specific case. But its detailed analysis quite often leads to design improvements of the system elements. However, improving the quality of hydrostatic systems does not consist exclusively in the improvements of their elements [1].

Figures 3 and 4 present the overall efficiency η of a constant pressure (p = cte) and a variable pressure (p = var) system with proportional control and a system with volumetric control by a variable capacity pump ($Q_P$ = var) as a function of the load coefficient $\overline{M}_M$ at different values of the cylinder speed coefficient $\overline{\omega}_M$.

In the case of a system with volumetric control by a variable capacity pump ($Q_P$ = var), increasing the cylinder load coefficient $\overline{M}_M$ causes rapid increase of the system overall efficiency η (Fig. 3). However, efficiency of structures with the series throttling control fed by a constant capacity pump is, with small value of the $\overline{\omega}_M$ coefficient, distinctly lower than the volumetric control efficiency with the same value of $\overline{\omega}_M$, because the structural losses are high.

Increase of the cylinder speed causes a proportional increase of efficiency of the p = cte and p = var systems, but with an increase of the cylinder speed $v_M$ the relative increase of efficiency of the system fed by a variable capacity pump is smaller (Fig. 3).

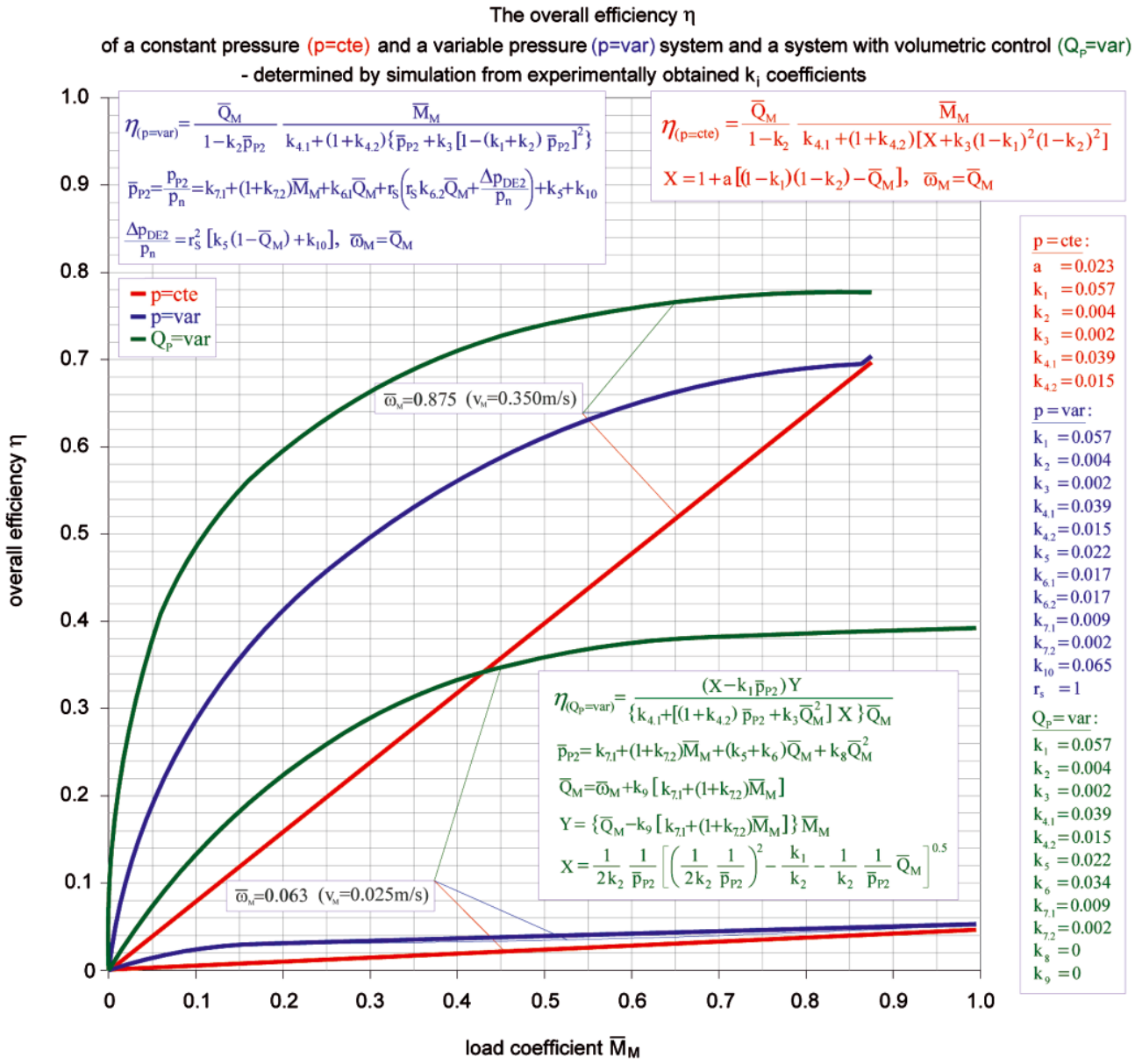


*Fig. 3. Relation of the overall efficiency η of a constant pressure (p = cte) and a variable pressure (p = var) system with proportional control and a system with volumetric control by a variable capacity pump ($Q_P$ = var) to the load coefficient $\overline{M}_M$ at different values of the cylinder speed coefficient $\overline{\omega}_M$ (efficiency determined by simulation from experimentally obtained $k_i$ coefficients ; the $v_M$ = 0.350m/s ($\overline{\omega}_M$ = 0.875) speed was the highest cylinder speed used during the tests) [1]*

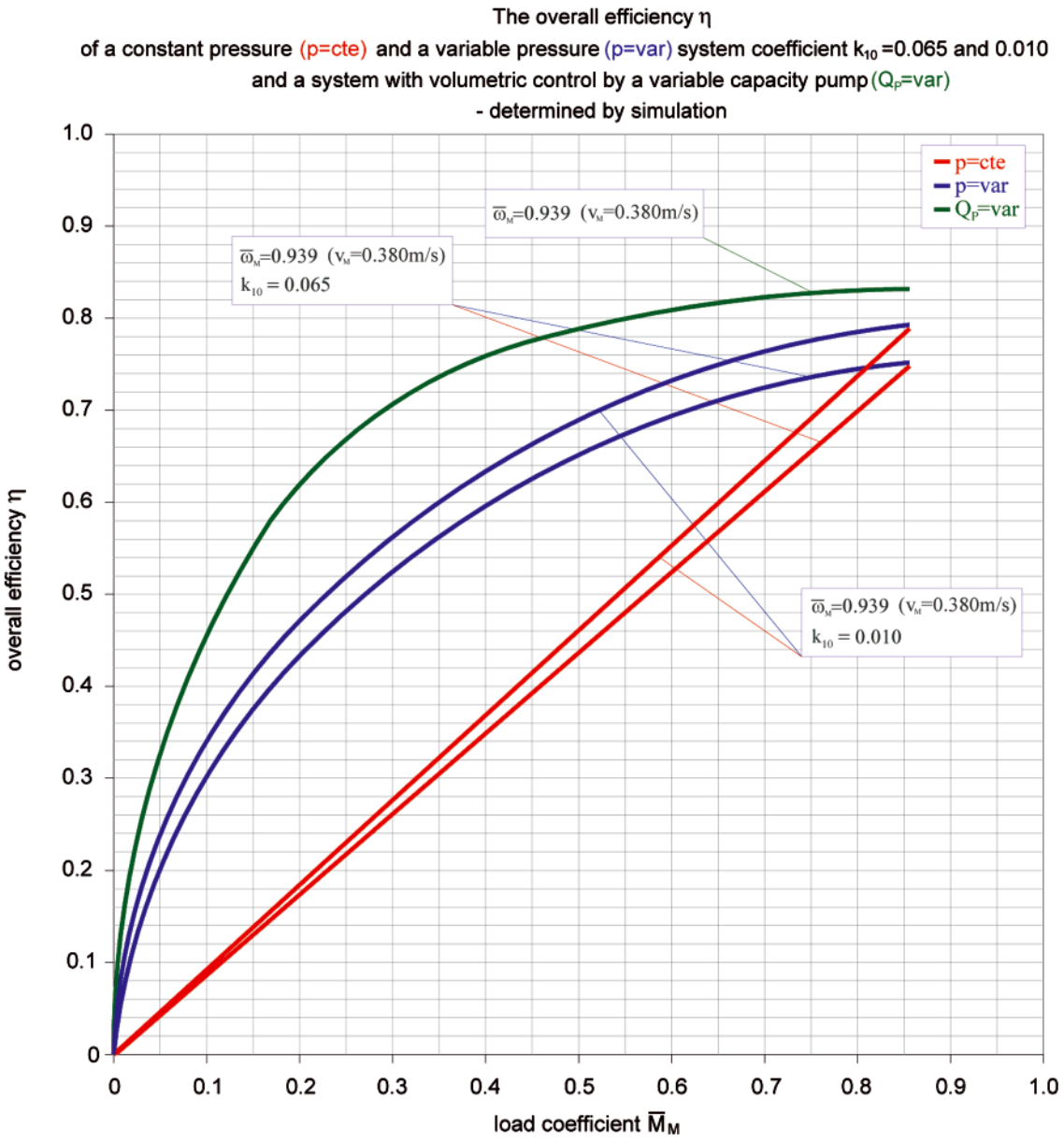


***Fig. 4.*** *Relation of the overall efficiency η of a constant pressure (p = cte) and a variable pressure (p = var) system with proportional control, with the used proportional directional valve coefficient $k_{10}$ = 0.065 and with possible use of a bigger proportional directional valve with $k_{10}$ = 0.010, as well as a system with volumetric control by a variable capacity pump ($Q_P$ = var), to the load coefficient $\overline{M}_M$ at the value of the cylinder speed coefficient $\overline{\omega}_M$ = 0.939 ($v_M$ = 0.380m/s) resulting from the maximum pump capacity $Q_{Pmax}$. Maximum $\eta_{max}$ values of the three considered systems are closer to one another [1].*

It can be seen in Fig.3 that a 14-fold increase of the cylinder speed in the investigated structures causes about 14-fold increase of their efficiency. As a comparison, a 14-fold increase of the cylinder speed in a $Q_P$ = var structure causes about 2-fold increase of its efficiency (from η = 0.39 at $\overline{\omega}_M$ = 0.063 and $\overline{M}_M$ = 0.875 to η = 0.78 at $\overline{\omega}_M$ = 0.875 and $\overline{M}_M$ = 0.875).

Fig. 4 presents efficiency η of a constant pressure (p = cte) and a variable pressure (p = var) system with proportional control, with the used proportional directional valve coefficient $k_{10}$ = 0.065 and with possible use of a bigger proportional directional valve with $k_{10}$ = 0.010, as well as a system with volumetric control by a variable capacity pump ($Q_P$ = var), as a function of the load coefficient $\overline{M}_M$ at the value of the cylinder speed coefficient $\overline{\omega}_M$ = 0.939 ($v_M$ = 0.380m/s) resulting from the maximum pump capacity $Q_{Pmax}$ .

In the maximum cylinder speed range, i.e. with the full use of the pump capacity, efficiency values of the p = cte and p = var systems with throttling control become close to the efficiency of the $Q_P$ = var system with volumetric control.

## CONCLUSIONS

1. The maximum achievable values of efficiency of systems with proportional (i.e. series throttling) control and of a system with volumetric control by a variable capacity pump are approximately similar. The compared systems were assembled of elements with the same $k_i$ coefficients of energy losses.
2. By applying a variable pressure (p = var) system, a significant increase of the energy efficiency η can be achieved with smaller cylinder loads.
3. With small cylinder speed values, the effect of using a p = var system is little, mainly due to volumetric losses connected with draining the excess liquid to the tank.
4. Optimization of hydrostatic systems means, among other aspects, a possibility of foreseeing the behaviour of an energy system in various conditions of its operation, as a function of speed and load of the hydraulic motor, working liquid viscosity, losses in the elements and particularly as

an effect of the system structure. The common acceptance and use of the objective, experimentally verified methods of determining the system energy efficiency, looking at the efficiency of entire combined system, can clarify many misunderstandings, e.g. those pertaining to the problem of maximum efficiency of specific structures. Such as an answer to the question: has a system with flow regulator different efficiency than a system with common throttling valve?

5. The Author intends to carry out further investigations of systems with proportional control, aimed at determining the influence of the working liquid (oil) viscosity on the energy efficiency.

## NOMENCLATURE

cte – constant
$f_{DE1}$ – throttling slot at the cylinder inlet
$f_{DE2}$ – throttling slot at the cylinder outlet
$F_M$ – hydraulic linear motor (cylinder) load, current force required of a linear motor
$F_{Mi}$ – force indicated on the piston of the hydraulic linear motor (cylinder)
$F_{Mm}$ – hydraulic linear motor mechanical losses
$F_{SP}$ – force of spring in the overflow valve
$k_1$ – coefficient of relative volumetric losses per one shaft revolution of fixed capacity pump
$k_2$ – coefficient of relative decrease in pump rotational speed
$k_3$ – coefficient of relative pressure losses (flow resistance) in internal pump ducts, at theoretical pump delivery $Q_{Pt}$
$k_{4.1}$ – coefficient of relative mechanical losses in pump, at $\Delta p_{Pi} = 0$
$k_{4.2}$ – coefficient of relative increase of mechanical pump losses, at increase in pressure in pump working chambers
$k_5$ – coefficient of relative pressure losses (flow resistances) in the line joining the pump with throttle control unit, at theoretical pump delivery $Q_{Pt}$
$k_{6.1}$ – coefficient of relative pressure losses (flow resistances) in the line joining the throttle control unit with hydraulic motor, at theoretical pump delivery $Q_{Pt}$
$k_{6.2}$ – coefficient of relative pressure losses (flow resistances) in hydraulic motor outlet line, at theoretical pump delivery $Q_{Pt}$
$k_{7.1}$ – coefficient of relative mechanical losses in hydraulic motor – cylinder, at a force $F_M = 0$
$k_{7.2}$ – coefficient of relative increase of mechanical losses in motor – cylinder, at increase of force $F_M$
$k_8$ – coefficient of relative pressure losses (flow resistances) in internal ducts of hydraulic motor, at theoretical pump delivery $Q_{Pt}$
$k_9$ – coefficient of relative volumetric losses in hydraulic motor
$k_{10}$ – coefficient of relative minimum pressure decrease in 2-way flow control valve, which still ensures the flow regulation, or coefficient of relative pressure decrease in 3-way flow control valve
$k_{11}$ – coefficient of relative pressure decrease $\Delta p_{DE}$ in directional control valve (servovalve, proportional valve) demanded by a maximum throttling section $f_{DEmax}$ for receiving flow intensity equal theoretical pump delivery $Q_{Pt}$
$\overline{M}_M$ – hydraulic motor relative load coefficient $\overline{M}_M = F_M / F_{Mn}$
$p_0$ – the reference pressure in the oil reservoir
$p_1$ – pressure at the cylinder feed proportional valve inlet
$p_2$ – pressure in the outlet conduit from proportional valve to the cylinder
$p_{1'}$ – pressure in the inlet conduit to the proportional valve from the cylinder
$p_{2'}$ – pressure in the outlet conduit from proportional valve to the oil reservoir
$p_n$ – nominal (rated) working pressure of hydrostatic transmission (hydraulic system)
$p_{M1}$ – pressure in the inlet conduit to the cylinder
$p_{M2}$ – pressure in the outlet conduit from the cylinder
$p_{M1i}$ – pressure in the inlet chamber of the cylinder
$p_{M2i}$ – pressure in the cylinder discharge chamber
$p_{P1}$ – pressure in the pump inlet
$p_{P2}$ – pump supplying pressure
$p_{SP}$ – operating pressure overflow valve
$p_{SP0}$ – opening pressure overflow valve for ($Q_0 = 0$)
$p_{SPS}$ – operating pressure overflow valve controlled by the receiver inlet pressure
$\Delta p_{C0}$ – pressure drop in the inlet conduit to the pump
$\Delta p_{C1}$ – pressure drop in the inlet conduit to the control unit
$\Delta p_{C2}$ – pressure drop in the line between the control unit and cylinder
$\Delta p_{C3'}$ – pressure drop in the outlet conduit from cylinder to the proportional valve
$\Delta p_{C3''}$ – pressure drop in the outlet conduit of the cylinder from the proportional valve
$\Delta p_{DE1}$ – pressure drop in the proportional directional valve throttling slot $f_{DE1}$ (at the cylinder inlet)
$\Delta p_{DE2}$ – pressure drop in the $f_{DE2}$ proportional valve throttling slot (at the cylinder outlet)
$\Delta p_M$ – decrease of pressure (pressure drop) in hydraulic linear motor (cylinder)
$\Delta p_{Mi}$ – pressure drop indicated between inlet and outlet chamber of the cylinder
$\Delta p_P$ – increase of pressure in the pump
$\Delta p_{Pp1}$ – pressure drop in the inlet channel pump (and the distributor, if any)
$\Delta p_{Pp2}$ – pressure drop in the pump outlet duct (and the distributor, if there is one)
$Q_0$ – intensity of flow directed through the overflow valve to the oil reservoir
$Q_M$ – hydraulic linear motor absorbing capacity, intensity of flow to hydraulic linear motor
$Q_{M2}$ – intensity of flow from the hydraulic linear motor (cylinder)
$Q_P$ – pump delivery
$\eta$ – energy efficiency
$S_{M1}$ – effective area of the hydraulic linear motor piston in its inlet chamber
$S_{M2}$ – effective area of the hydraulic linear motor piston in its outlet chamber
SP – overflow valve
SPS – overflow valve controlled by the receiver inlet pressure
var – variable
$v_M$ – hydraulic linear motor speed
$\overline{\omega}_M$ – hydraulic linear motor speed coefficient – ratio of instantaneous speed to the nominal one of a hydraulic linear motor – $\overline{\omega}_M = v_M / v_{Mn}$

## BIBLIOGRAPHY


1. Skorek G.: *Charakterystyki energetyczne układu hydraulicznego o sterowaniu proporcjonalnym siłownika zasilanego pompą o stałej wydajności w systemie stałego i zmiennego ciśnienia*. Doctor dissertation, 2008
2. Skorek G.: *Badania laboratoryjne zachowania energetycznego wybranych elementów układu hydraulicznego o sterowaniu proporcjonalnym siłownika zasilanego pompą o stałej wydajności*. XV Ogólnopolska Konferencja Naukowo-Techniczna – Cylinder 2005, „Badanie, Konstrukcja i Eksploatacja Układów Hydraulicznych", 19-21 September 2005
3. Skorek G.: *Zachowanie energetyczne układów hydraulicznych o sterowaniu proporcjonalnym liniowego silnika hydraulicznego*. X Jubileuszowe Seminarium „Napędy i Sterowanie 2004", Gdańsk, 18 February 2004
4. Paszota Z.: *Metoda oceny sprawności energetycznej układów z silnikiem hydraulicznym liniowym – siłownikiem*. Politechnika

Gdańska, Wydział Oceanotechniki i Okrętownictwa, Research report No. 611/95, Gdańsk, 1995
5. Paszota Z.: *Model strat i sprawności energetycznej układu hydraulicznego o sterowaniu proporcjonalnym siłownika zasilanego pompą o stałej wydajności w systemie zmiennego ciśnienia*. Rozdział w monografii p.t.: "Badanie, konstrukcja, wytwarzanie i eksploatacja układów hydraulicznych" - Biblioteka „Cylinder" pod redakcją Edwarda Palczaka, Centrum Mechanizacji Górnictwa Komag, 2005
6. Paszota Z.: *Energy Saving in a Hydraulic Servomechanism System – Theory and Examples of Laboratory Verification*. Brodogradnja, Journal of Naval Architecture and Shipbuilding Industry, Zagreb, June 2007, Volume 58, Number 2
7. Paszota Z.: *Hydrauliczny układ indywidualny z pompą o stałej wydajności i ze sterowaniem proporcjonalnym siłownika – model strat i sprawności energetycznej*. Materiały VI Seminarium „Napędy i Sterowanie'2000", Gdańsk 23 – 25.02.2000, Gdańsk: Politechnika Gdańska, 2000
8. Paszota Z.: *Podwyższanie sprawności energetycznej kierunkiem rozwoju napędu hydrostatycznego*. Hydraulika i Pneumatyka, Zeszyt 5/98, 1998
9. Paszota Z.: *Losses and energy efficiency of drive motors and systems. Replacement of the Sankey diagram of power decrease in the direction of power flow by a diagram of power increase opposite to the direction of power flow opens a new perspective of research of drive motors and systems*. Polish Maritime Research 1 (77) Vol. 20, 2013

---

**CONTACT WITH THE AUTHOR**

Grzegorz Skorek, Ph.D.
Department of Engineering Sciences
Faculty of Marine Engineering,
Gdynia Maritime University
Morska 81/87
81-225 Gdynia, POLAND
e-mail: grzesko@am.gdynia.pl

**POLISH MARITIME RESEARCH** 3(79) 2013 Vol 20; pp. 20-27
10.2478/pomr-2013-0031

# Multi-source-supplied parallel hybrid propulsion of the inland passenger ship STA.H. Research work on energy efficiency of a hybrid propulsion system operating in the electric motor drive mode

**Jakub Kowalski**, M. Sc.
**Wojciech Leśniewski**, Ph. D.
**Wojciech Litwin**, Ph. D.
Gdansk University of Technology, Poland

ABSTRACT

*In the Faculty of Ocean Engineering and Ship Technology, Gdansk University of Technology, design has recently been developed of a small inland ship with hybrid propulsion and supply system. The ship will be propelled by a specially designed so called parallel hybrid propulsion system.*
*The work was aimed at carrying out the energy efficiency analysis of a hybrid propulsion system operating in the electric motor drive mode and at performing the noise pollution measurements.*
*The performed investigations have shown that a significant impact on the efficiency and on the acoustic emission has the type of belt transmission applied.*

**Key words**: hybrid ship propulsion; ship propulsion

## INTRODUCTION

In recent years an unusual development in practically all fields of science has been witnessed. In effect, new machines and equipment with increasing capabilities are being designed and produced and the progress has not left shibuilding out.

In most of the now constructed ships the conventional propulsion with an internal combustion engine is used. Modern propulsion units of the type are equipped with complex fittings limiting emissions of noxious compounds to the atmosphere. Attempts to limit emissions are being made even at the cost of increased fuel consumption. Modern internal combustion engines are more and more often adapted to use such non-typical fuels as vegetable oils or compressed natural gas.

Specific requirements are imposed on the inland navigation ships. Some inland waterways are under particular protection as popular recreation regions or due to their exceptional landscape values.

Looking through the shipbuilding technical literature, one can often come across the terms like ”no emission”, ”zero emission” or ”greenship” in titles of the papers. This testifies that the ”clean technologies” are now a much more meaningful issue than they used to be.

In the case of a conventional propulsion system, the ”noise pollution” is also a significant problem. Unfortunately, even a perfectly designed engine exhaust system cannot fully eliminate noise. Combustion engine is also a source of vibration, which may have a negative impact on the condition of crew and passengers, particularly during a longer voyage. Another problem are the exhaust gases, which with an adverse wind can significantly worsen the sailing comfort.

The electric propulsion has none of the above described flaws. It operates silently and generally is not a source of vibration. In addition, the most up-to-date solutions have a high, 90% exceeding efficiency. However, a problem is the motor supply source. The use of a combustion engine-driven generating set does not solve the problem, as all the above described limitations will then occur. The fuel cell appears an advisable solution in the case. Such solution was used on a ship already in 1964 [1, 2, 3, 4]. A very interesting ship is Alsterwasser launched in 2008. She is equipped with hydrogen-supplied fuel cells.

The same technology has been used also in the 212A class submarines built in 1996 by the Thyssen-Krupp Marine Systems/HDW corporation to the order of the German Navy. They are equipped with the Siemens company hydrogen-supplied fuel cells.

Therefore, the information (given at the beginning of 2013) that the Siemens company withdraws from the development work on fuel cells was a big surprise.


***Fig. 1.*** *The Alsterwasser ship launched in 2008 in Hamburg, driven with a 100 kW electric motor supplied by two 48 kW fuel cells, may take a hundred passengers on deck (http://www.zemships.eu)*

Batteries are a commonly used supply source for electric motors driving small and medium size inland vessels. Unfortunately, the cheapest classical solutions are heavy and the modern light batteries (Fig. 2) are very expensive. The price of an 1 kWh module may exceed a thousand Euro and it depends on the battery generation, manufacturer, and size of the order.

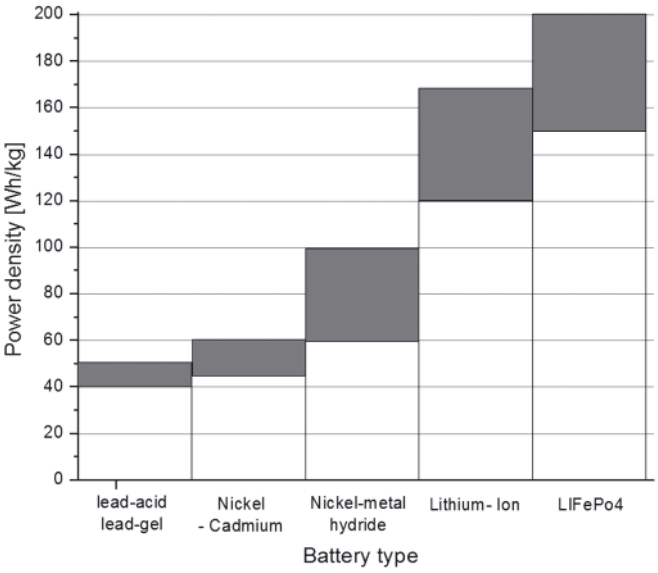


***Fig. 2.*** *Energy density of the most popular now available battery types (based on the Authors' investigation - data of 2013)*

Therefore, in most of the so far implemented solutions the lead batteries have been applied. But this creates serious problems. A service ship, e.g. a passenger vessel, is usually designed for as intensive operation as possible. It must be a source of income to repay, within a shortest possible time, the expensive investment of its designing and construction. It is also recommended to be relatively fast. Greater speed means greater number of trips, besides, the owners' experience shows that passengers get nervous when, even in touristically attractive surroundings, the trip takes too long. Greater speed means also increased demand for accumulated energy, which translates into large volume and great weight of the batteries. Great weight of batteries means in turn increased ship draught and increased hydrodynamic resistance, i.e. even greater demand for energy. Therefore, proper design of the ship hull, with as little weight as possible and low hydrodynamic resistance, are the basic questions. Very important is also a high-efficiency propulsion system.

As the Authors' experience indicates, in many cases the use of a propulsion system based exclusively on an electric motor is not justified. In preparing the "*Design of an ecological watercraft for inland waters in Poland"* project for realization, analysis was carried out of several popular sailing routes, with fragments included in the "Nature 2000" programme protection system or protected as parts of a national park. It appeared that quite long sections of waterways are touristically not particularly attractive and there are no navigating speed limits on them. Therefore, the project authors came to the conclusion that an ideal solution would be a hybrid propulsion system, being a combination of a compression ignition engine and an electric motor. Such solution allowed considerable reduction of the ship weight and the propulsion system flexibility.

## DESIGN OF THE STA.H SHIP

The designed ship has 19 m length, 5 m width and about 0.5 m draught and can take on deck from 50 to 70 passengers, depending on version. The main dimensions allow it to navigate on smaller, shallow Polish rivers, as well as on the route from Gdansk to Augustow, where the prototype unit is supposed to operate.

The design of ship is an effect of cooperation between engineers from the Faculty of Ocean Engineering and Ship Technology, Gdansk University of Technology and artists from the Academy of Fine Arts in Gdansk.

Particular effort was made to reduce the hydrodynamic resistance of the ship hull and to minimize draught. Low weight was achieved by designing the hull from aluminium. The tests of hydrodynamic resistance were performed in parallel for two versions – a single hull and a double hull (catamaran) structure. Numerical analysis by CFD method and model tests in the Faculty of Ocean Engineering and Ship Technology towing tank were carried out (Fig. 3).

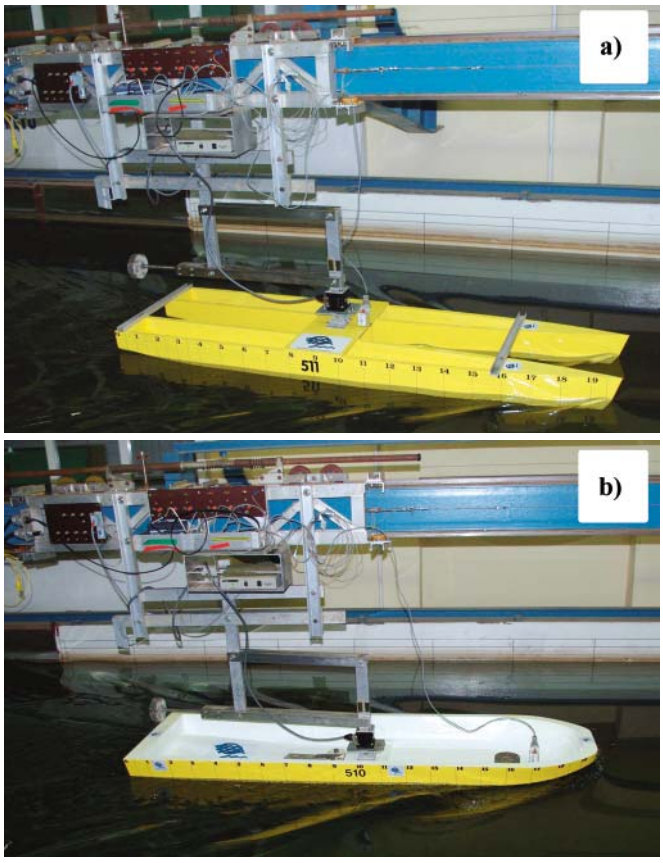


***Fig. 3.*** *Model of STA.H ship during the towing tank tests;* ***a)*** *catamaran* ***b)*** *single-hull version; photo: Mirosław Grygorowicz*

The tests showed that the catamaran had slightly lower hydrodynamic resistance than the single-hull unit. Nevertheless, the single-hull version was considered a more promising solution due to its smaller draught and smaller overall height of the vessel.

The ship propulsion system has been designed in two versions. For fast navigation in the regions with protected sections the parallel hybrid diesel-electric solution is proposed. In the other version, of a ship designed for navigation in fully protected regions, the all-electric propulsion system has been chosen. In both solutions the electric propulsion system is equipped with a hybrid multi-source supply system consisting of a battery, high power charger, photovoltaic panel module on the ship deck and the auxiliary emergency generating set. Both solutions have been accepted by the classification society.

## PROPULSION SYSTEM DESIGN

In the preliminary design stage, the propulsion power and the necessary battery weights were assumed from experience, as the results of hull hydrodynamic resistance tests were not known yet and precise estimation of power demand was impossible (Table 1). It has to be remembered, that because of the classification society requirements regarding high level of safety, two autonomous propulsion systems must be provided. In effect, a twin-screw propulsion system must be applied, which is otherwise advantageous. The most important advantage is smaller diameter of the propulsion screws, important for a small-draught inland vessel. Additionally, a twin-screw ship has better manoeuvrability.

***Tab. 1.*** *Data assumed in the preliminary design included the weights of electric system, propulsion system and supply system*

| No. | Description | Brief foredesign |
|---|---|---|
| **1** | Cruising speed with the electric motor drive [km/h] | 8 |
| **2** | Power of the electric drive [kW] | 2 x 12 |
| **3** | Time of navigating with the electric drive [h] | 3 |
| **4** | Battery capacity (with the allowance taking into account the loss of capacity) [kWh] | 2 x 40 |
| **5** | Number of batteries (75kg, 12V, 230Ah) [pcs.] | 2 x 16 |
| **7** | Battery weight [kg] | 2 x 1200 |
| **8** | Approximate weight of motors with fittings [kg] | 2 x 80 |

After the towing tank tests it appeared that the power needed to achieve the required speed is less than the value assumed in the preliminary design. However, it has to be remembered that in real conditions the impact of wind and of the hull overgrowing with water organisms may increase the power demand. Also a certain power reserve in the propulsion system is needed for manoeuvrability purposes. Finally, a three-phase alternating-current electric motor with permanent lantanide series magnets was chosen, which, supplied with 48 V voltage by means of a dedicated frequency converter, achieves the power of 10 kW. It is also important that, if needed, the motor can operate as generator driven by the main engine and batteries may be charged in this way.

The propulsion system designed by the Authors (Fig. 4) has some important advantages. It can cooperate with typical combustion engines of various power. The designed system may be installed aboard a newbuilt ship or an existing solution may be modernized. The proposed system may also be used as an electric propulsion system without the combustion engine. Another advantage is easy assembly and free access to the electric motor. In practice, the solution allows easy replacement of the drive unit in accordance with customer's demand and does not require significant structural changes.

A complete propulsion system is shown in Fig. 4 below. For the system to operate properly, the combustion engine must be equipped with a typical reduction gear, with coupling allowing to disconnect the engine from the shaft line. Then the electromagnetic clutch (4) may be remotely switched on and the electric drive activated. It is also worth noting that the solution with belt transmission makes it easy to adjust individually the transmission ratio depending on the engine type used, by exchanging the belt pulleys and belt.

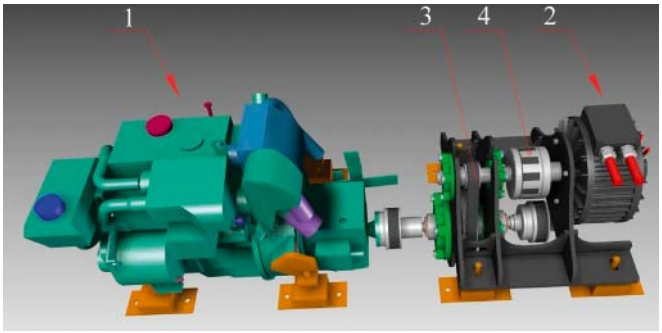


***Fig. 4.*** *Visualization of the STA.H ship hybrid propulsion system:* ***1*** *– combustion engine with reduction gear,* ***2*** *– electric motor,* ***3*** *– belt transmission,* ***4*** *– controlled clutch*

Similar solutions are now used by established manufacturers. Looking through the catalogues, participating in fairs and exhibitions, one can hear a lot about advantages of this type of drive, particularly about its noiseless operation and high energy efficiency.

## INVESTIGATIONS OF A HYBRID SYSTEM OPERATING IN THE ELECTRIC MOTOR DRIVE MODE

The propulsion system was assembled in the Faculty of Ocean Engineering and Ship Technology laboratory (Fig. 5). Combustion engine was not connected to the hybrid propulsion system test stand, as the test was aimed at evaluation of the propulsion system energy efficiency during the electric motor operation. Therefore, concentration was on the electric drive together with the belt transmission. The propulsion system was loaded with a direct-current generator (pos. 5).

In order to measure the belt transmission and the electric motor efficiency, the controlled clutch (Fig. 4 pos. 4) was replaced by a torque meter (Fig. 5 pos. 2).

The following parameters were recorded during the tests:
- rotational speed and torque on the motor shaft,
- torque on the driven shaft,
- voltage and intensity of the motor input current,
- noise during the system operation,
- temperature distribution on the surface of transmission subassemblies.

After completion of the measurements, it was possible to calculate the power of losses in the transmission gear and

*Tab. 2. Data of the two investigated drive versions*

| Drive type | First version (I) | Second version (II) |
|---|---|---|
| | Synchronic straight gear belt transmission, belt width 30 mm, pitch 8 mm | Synchronic bevel gear belt transmission, belt width 32 mm, pitch 8 mm |
| Transmission ratio / number of wheel teeth | 1:3.07 / 80 and 26 | |
| Motor power / motor rotational speed | 10 kW / 3000 rev/min | |
| Safety coefficient assumed for the drive – service factor | 1.5 | |

motor, the propulsion system (motor and frequency converter) energy efficiency, the transmission gear efficiency and the overall efficiency of the propulsion system. The results are presented in chapter 5.

Details of the two investigated drive versions are given in Table 2.

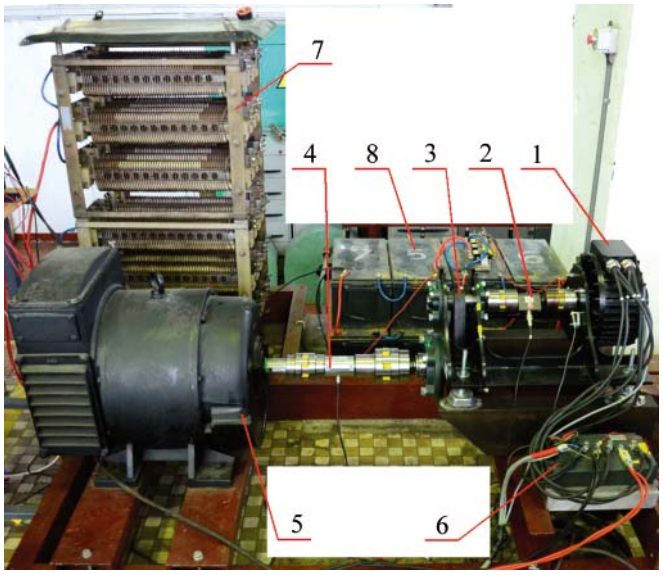


***Fig. 5.*** *Test stand for investigations of the hybrid propulsion system operating in the electric drive mode: **1** – electric motor, **2** – torque meter installed instead of controlled clutch, **3** – belt transmission, **4** – torque meter, **5** – generator, **6** – frequency converter, **7** – resistor*

## INVESTIGATION RESULTS

In designing the drive transmission system, no particular difficulties were anticipated and the solution seemed not complicated. In the drive first version (I), a high class synchronic straight gear belt transmission was used consisting of two toothed wheels and one tension roll. In order to be sure that the system will operate properly, recommended by the manufacturer prefabricated belt pulleys were acquired. The small driving wheel had flanged rims protecting against the belt slip-off.

From the beginning of measurements it appeared that the drive transmission system operated with excessive noise (Fig. 6), the noise intensity reached 87 dB.

Temperature of the transmission subassemblies was measured by means of a thermovision camera (Fig. 7 and 8). The measurements were verified by thermocouples (Sp1 and Sp2) installed on the transmission gear. Their position was changed in the consecutive measurement series, which can be seen in the illustrations. The measurements showed that temperature of the full power transmitting drive system stabilized after about forty minutes of operation.

During the investigations a new very modern type of synchronic bevel gear belt was acquired. Price of such solution was almost four times higher than that of the above described classic solution. Both solutions were compared. The second (II) version had the wheels without protective rims because of the specific gear geometry. A comparable efficiency but certainly a lower noise level was expected. Results of the measurements of temperature distributions (Fig. 8) and efficiency (Fig. 9 to 11) are presented below.

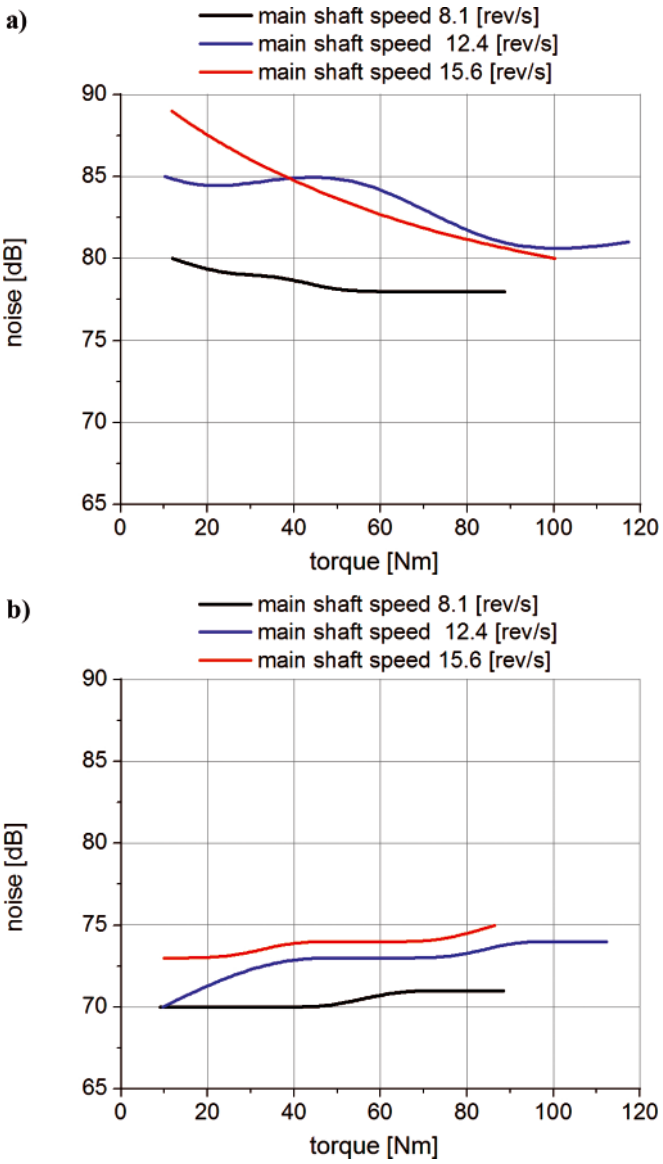


***Fig. 6.*** *Diagrams of the measured noise as a function of drive shaft torque and rotational speed: **a)** version I – straight gear belt, **b)** version II – bevel gear belt*

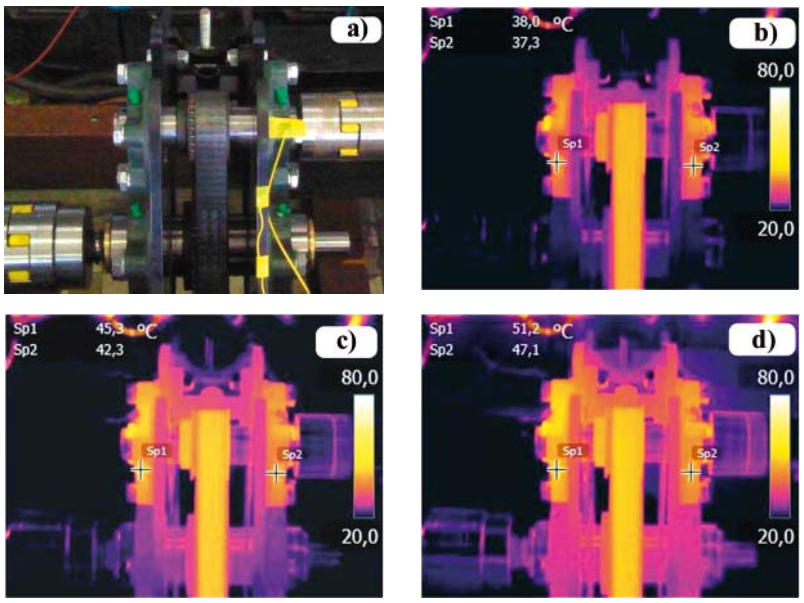


*Fig. 7. Results of temperature field measurements carried out with thermovision camera in the transmission version I;* ***a)*** *photograph of the investigated system,* ***b)*** *the system immediately after start-up,* ***c)*** *measurement after 20 minutes,* ***d)*** *measurement in stabilized state after 40 minutes of operation*

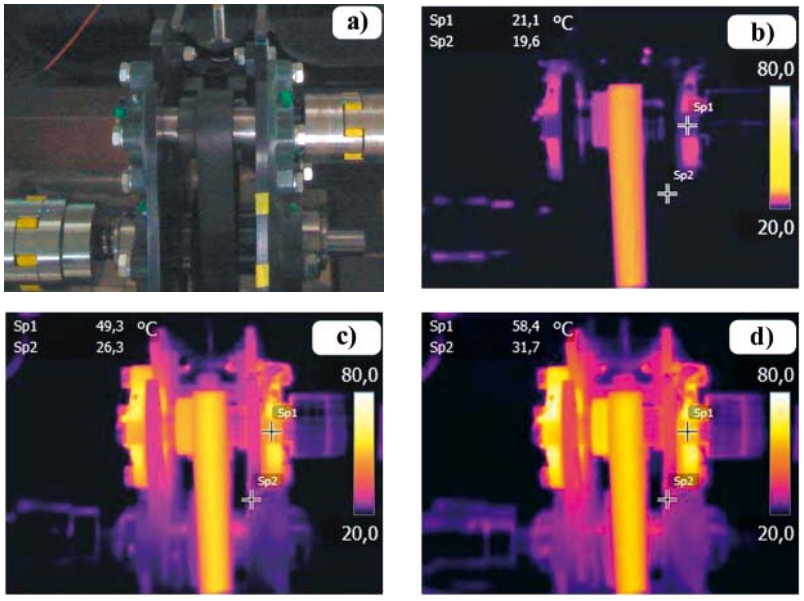


*Fig. 8. Results of temperature field measurements carried out with thermovision camera in the transmission version II;* ***a)*** *photograph of the investigated system,* ***b)*** *the system immediately after start-up,* ***c)*** *measurement after 20 minutes,* ***d)*** *measurement in stabilized state after 40 minutes of operation*

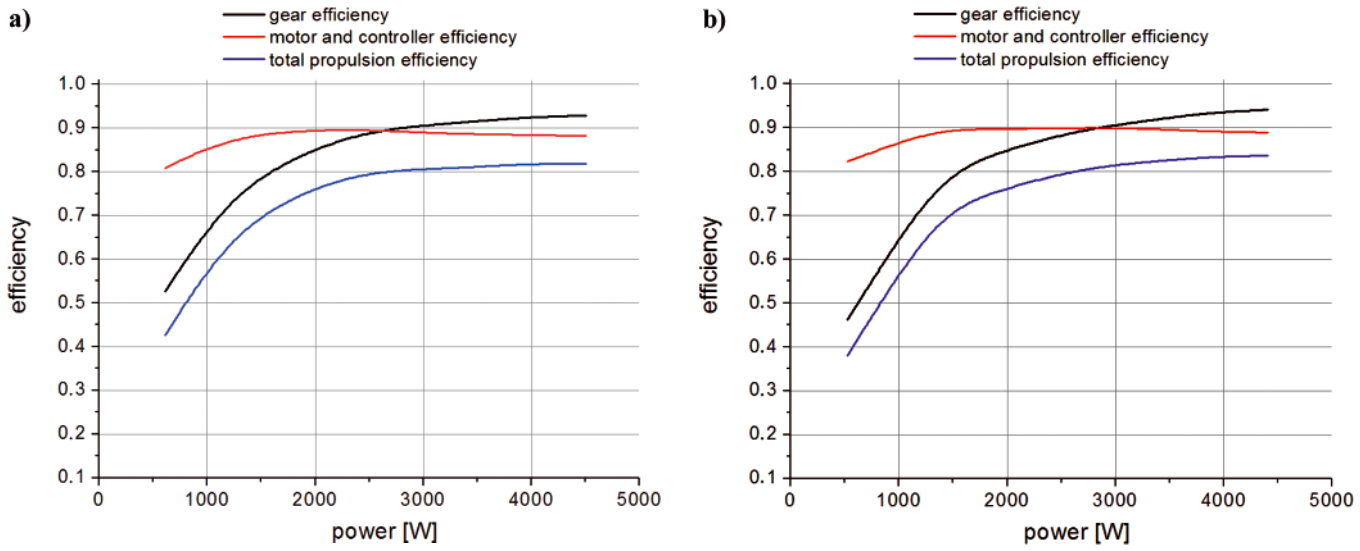


*Fig. 9. Diagrams of efficiency as a function of output power for the main shaft speed n = 8.1 rev/s;* ***a)*** *transmission with straight gear belt (version I),* ***b)*** *transmission with bevel gear belt (version II)*

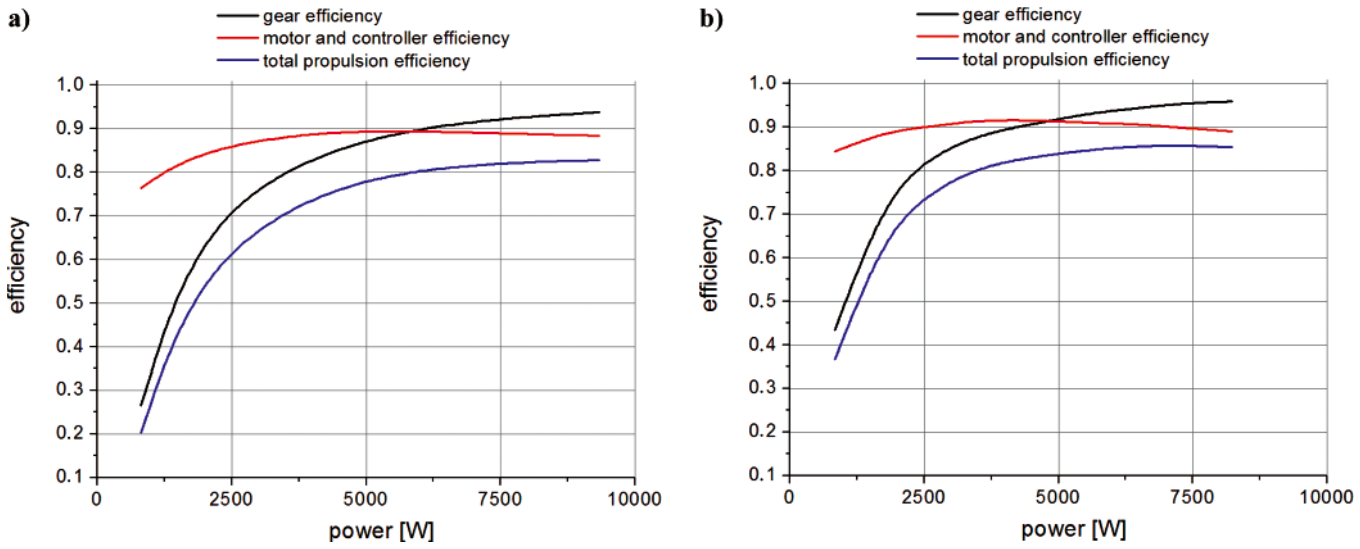


***Fig. 10.*** *Diagrams of efficiency as a function of output power for the main shaft speed n = 12.4 rev/s;* ***a)*** *transmission with straight gear belt (version I),* ***b)*** *transmission with bevel gear belt (version II)*

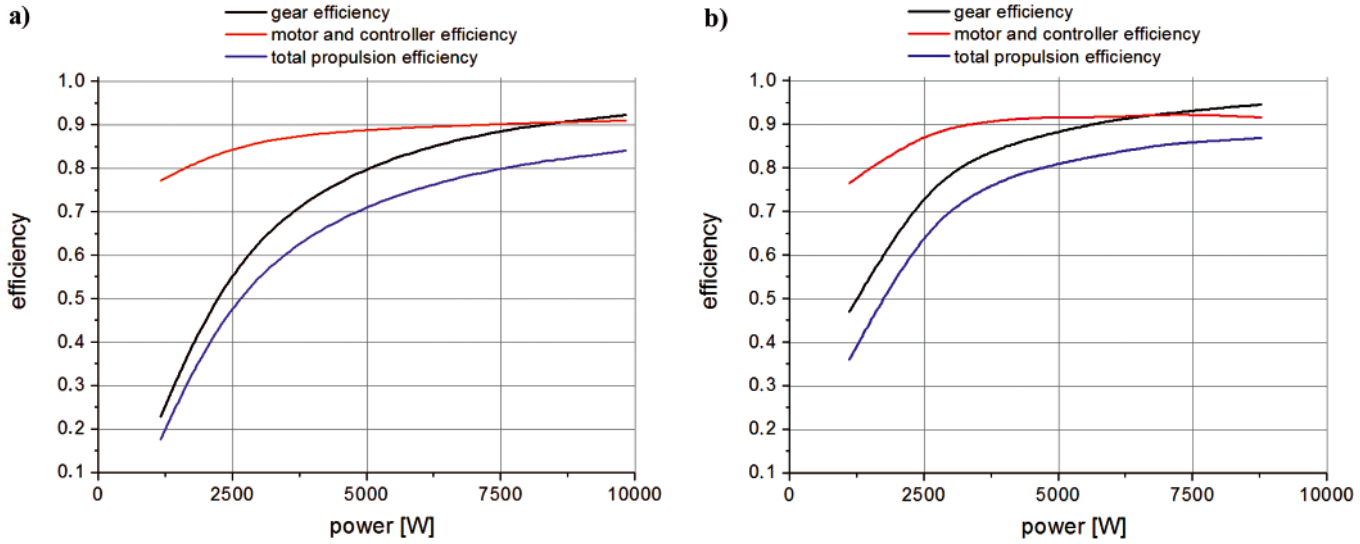


***Fig. 11.*** *Diagrams of efficiency as a function of output power for the main shaft speed n = 15.6 rev/s;* ***a)*** *transmission with straight gear belt (version I),* ***b)*** *transmission with bevel gear belt (version II)*

## DISCUSSION

The investigation results have shown that the efficiency of such belt transmissions increases with the increasing output power (Fig. 9 to 11). This is relation typical of that type of solutions. The analysis of lost power (Fig. 12 and 13) gives a picture of an interesting phenomenon. It appears that the power of energy losses does not increase with increasing output torque, but slightly decreases. In the Authors' opinion, this may be an effect of stretching the active part of the belt and slight slackening of the passive part where the tension roll is mounted. In effect, resistance on the tension roll is slightly lower. In the case of straight gear belt, the power of losses is proportional to the emitted noise (Fig. 12). Such effect cannot be seen in the transmission system with bevel gear belt, which indicates a different character of the movement resistance. In the Authors' opinion, the main source of losses and of the acoustic emissions in the case of straight gear belt is throttling the tooth space by consecutive belt teeth and making the compressed air come out sidewise. This effect can be limited by removing one flanged rim of the belt pulley or making holes in the rims to let the compressed air out. In the investigated case, removing one rim was not a promising method as the belt was several millimetres narrower than the pulley.

Worth considering is also a conception of not overdimensioning the drive system by assuming a high service factor. In designing the analysed system (after consultation with the manufacturer), the value 1.5 of service factor was assumed. In this way it will be possible to extend the transmission gear operating field in the range where the efficiency exceeds 90% (Fig. 14). However, this can be achieved at the expense of the drive durability. In the case of a typical inland vessel, which usually has a long winter break in navigation, it does not seem to be a problem as the belt can then be renewed.

In the analysed case (Fig. 14), decreasing the assumed service factor from 1.5 to 1 would cause extending the operating field where efficiency exceeds 90%.

The investigations have shown that the bevel gear belt has higher efficiency than the straight gear belt by about 5% in the whole range of rotational speed and torque where the tests were carried out. A considerable surprise was noisy operation of the straight gear belt drive system (Fig. 6 and 12), which is surely an effect of the high rotational speed of small wheel reaching 3000 rev/min.

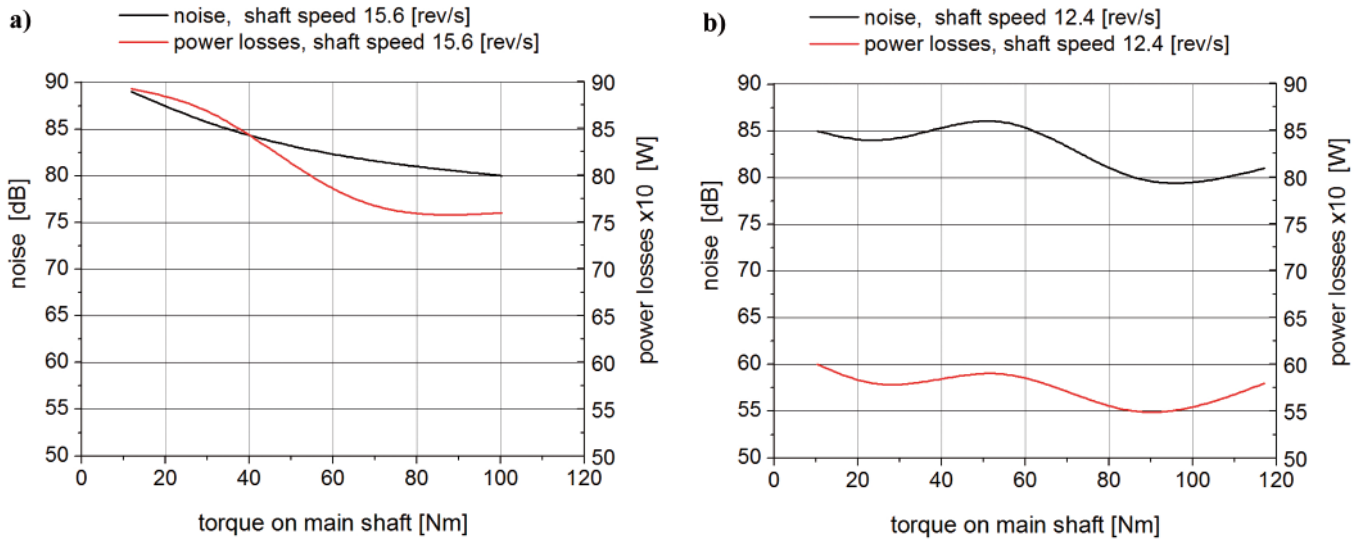


***Fig. 12.*** *Diagrams of lost power and measured noise of the drive system with straight gear belt (version I) as a function of the drive shaft torque and rotational speed:* ***a)*** *main shaft rotational speed 15.6 rev/s,* ***b)*** *main shaft rotational speed 12.4 rev/s*

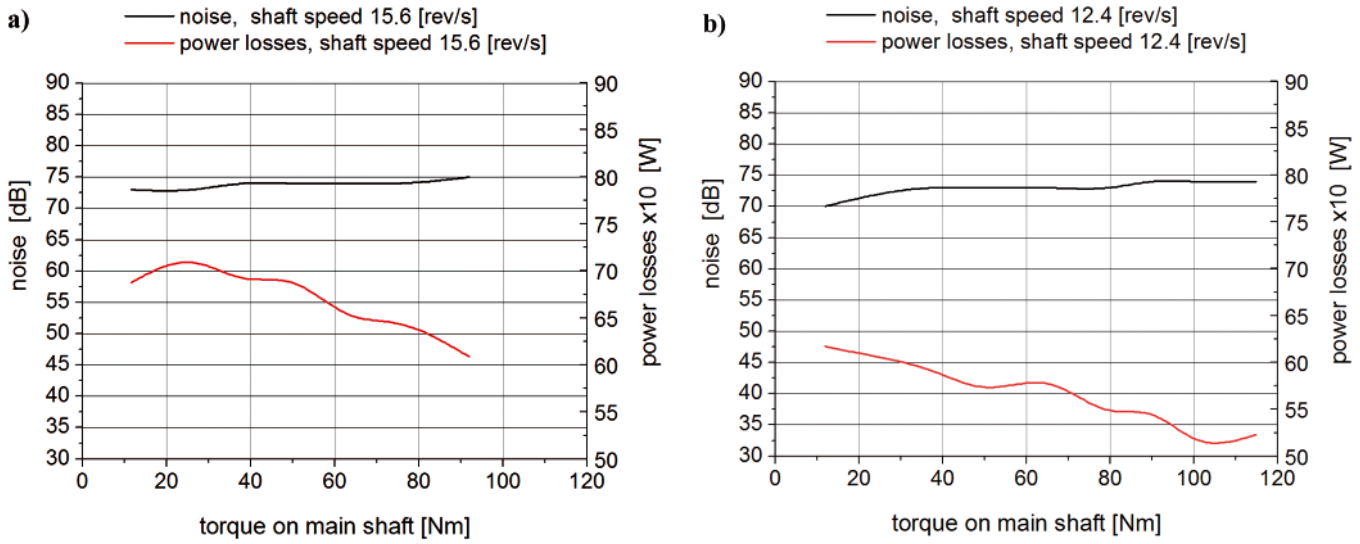


***Fig. 13.*** *Diagrams of lost power and measured noise of the drive system with bevel gear belt (version II) as a function of the drive shaft torque and rotational speed:* ***a)*** *main shaft rotational speed 15.6 rev/s,* ***b)*** *main shaft rotational speed 12.4 rev/s*

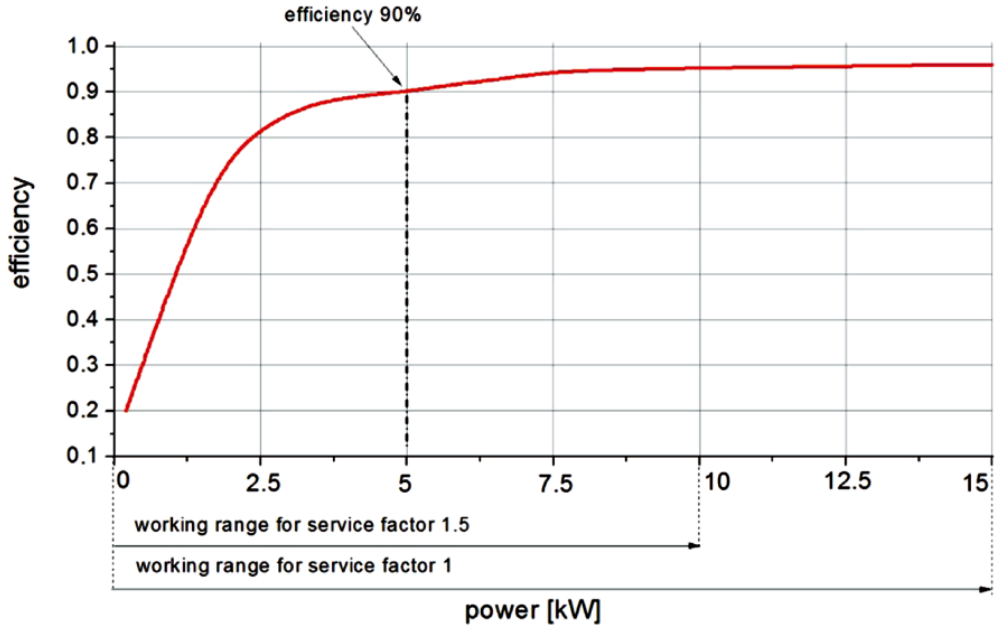


***Fig. 14.*** *Diagram of efficiency as a function of output power*

## SUMMARY AND CONCLUSIONS

The energy efficiency of a battery-supplied ship propulsion system is of primary importance. Batteries have limited capacity and the accumulated energy must be utilized economically. Cases have been known where crews accustomed for years to operate ships with conventional propulsion could not cope with a battery or photovoltaic cell-supplied electric drive of ships.

In analysing the propulsion system overall efficiency it has to be remembered, that it is a product of the efficiencies of motor, transmission gear, bearings and screw propeller. If in a ship a high efficiency screw propeller with maximum efficiency of 65% were used, then in optimum conditions the overall propulsion system efficiency would not exceed 55 %.

The tested 11 kW electric motor reached efficiency exceeding 90% in the output power range above 5.5 kW. Power of only about 10 kW was obtained during the tests. The motor did not achieve the catalogue rotational speed and torque. The Authors had experienced similar situations in the past, when the drive unit parameters differed from the catalogue values by more than 10 %. In some cases the operating parameters could be improved by reprogramming the frequency converter.

The investigations will be continued in order to compare properties of other two types of belt transmissions. Transmission with five wedge belts and transmission with a multi-wedge belt have already been designed.

**BIBLIOGRAPHY**


1. Psoma A., Sattler G.: *Fuel cell systems for submarines: from the first idea to serial production*; Journal of Power Sources 106, 2002
2. Kickulies M.: *Fuel cell power for maritime applications*; Fuel Cells Bulletin, September 2005
3. Weaver G.: *Marine applications of fuel cell technology*; Fuel Cells Bulletin, January 2003
4. McConnell Vicki P.: *Now, voyager? The increasing marine use of fuel cells*; Fuel Cells Bulletin, May 2010


**CONTACT WITH THE AUTHOR**


Jakub Kowalski, M. Sc.
Wojciech Leśniewski, Ph. D.
Wojciech Litwin, Ph. D.
Faculty of Ocean Engineering
and Ship Technology
Gdansk University of Technology
Narutowicza 11/12
80-233 Gdansk, POLAND
e-mail: wlitwin@pg.gda.pl

**POLISH MARITIME RESEARCH** 3(79) 2013 Vol 20; pp. 28-38
10.2478/pomr-2013-0032

# An Ant Colony Algorithm for efficient ship routing

**Ming-Cheng Tsou**, Associate Prof.
**Hung-Chih Cheng**, Prof.
National Kaohsiung Marine University, Kaohsiung, Taiwan, R.O.C.

ABSTRACT

*With the substantial rising of international oil price and global warming on the rise, how to reduce operational fuel consumption and decrease air pollution has become one of the pursued goals of green ship. Ship route planning is an indispensible part of the ship navigation process, especially in transoceanic crossing ship routing. The soundness of ship routing not only affects the safety of ship navigation but also the operation economy and environmental protection. This research is based on the platform of Electronic Chart Display and Information System (ECDIS), and founded on Ant Colony Algorithm (ACA) combined with the concept of Genetic Algorithm (GA), to model living organisms optimization behaviour to perform efficient ship route planning in transoceanic crossing. Besides the realization of route planning automation, ship routing will achieve the goal of optimum carbon dioxide reduction and energy conservation, and provide reference for route planning decision.*

**Key words**: ship routing; Ant Colony Algorithm; GIS; weather routing

## 1. INTRODUCTION

Almost 90% of the world's trade is carried by ship and, for the vast majority of this trade there is little or no alternative to transport by ship. Statistical data indicate that the freight carried by global commercial shipping has reached 8.919 million tons, and that this large volume has caused substantial negative environmental impacts, even though ships are the most environmentally friendly form of transportation. Still, it is estimated that 4-5 per cent of global $CO_2$ emissions come from international shipping [6]. According to statistics, there are about 52,000 registered civil ships of more than 100t capacity, annually consuming 500 million tons of fuel, producing 1.6 billion tons of carbon dioxide and 30 million tons of sulfur dioxide, causing greater global warming and air pollution. Therefore, an additional option for reducing air pollution is to decrease fuel consumption during transit [3]. From a climatic and environmental perspective sustainability has become an issue of the highest priority, and this is an imperative that cannot and should not be ignored. Within the foreseeable future shipping will still be dependent on fossil fuels. We must develop energy efficient and environmentally friendly technologies encompassing shipboard energy production, ship propulsion and ship operation. In recent years the concepts of the "green ship" and "green shipping" have been raised in the international shipping industry. The green ship concept covers the full ship life cycle, and provides total solution to pollution prevention, noxious gas emission, and energy conservation problems associated with the ship's design, production, operation, and scrapping. Therefore, shipping management should take care not only of economic efficiency, but also environment protection to prevent pollution. The coordination of efficiency and environment allows for environmentally sustainable development. In order to achieve this goal, ships already in operation can be retrofitted with energy-conserving equipment but the most direct and economical method is to plan an optimum route. Choosing the optimum route, adjusting the speed and avoiding adverse weather can not only reduce fuel consumption significantly but also improve navigational safety.

The efficiency of transoceanic ship route planning is generally determined by the following three aspects [26]:

- the accuracy of the prediction of the ship's hydrodynamic behaviour under different weather conditions;
- the accuracy of the weather forecast;
- the capability and practicability of the optimization algorithm.

This paper deals with navigation technology and focuses on the third above mentioned aspect, i.e. ship route optimization. Because optimum route determination is a multi-criterion non-linear planning issue and encompasses many constraints, a balance between navigational safety and economic efficiency should be found [18]. In other words, the applied planning framework not only has to take care of navigational safety-related risk evaluation and deviation but also avoid total cost increase due to deviation measures. In order to achieve this optimization mission we made use of the new Ant Colony Algorithm (ACA) developed in the evolutionary computation field to model and simulate how ants choose foraging paths.

We modified the ACA for marine navigation application, and integrated the Genetic Algorithm (GA) concept to improve its practical effectiveness. The geometric computation and information search function is provided by the Geographic Information System (GIS) - based platform ECDIS along with weather information for the background data required for ACA calculation. Through this research design we hoped to achieve optimum ship routing and use a more objective, quicker and more accurate model in order to:

- automatically generate a more rational recommendation route that gives consideration to both safety and economy,
- lighten the navigator's workload,
- provide a reference for route planning decision making,
- collaborate in the green shipping and environment sustainability effort.

## 2. PREVIOUS WORK

Since research in transoceanic crossing weather routing typically studies broader geographic domains, usually across the Atlantic or Pacific, it mainly considers mid- and short-term weather effects, especially the effects of wave direction and height on a ship's cross-ocean navigation speed, to achieve the goals of minimum sailing time and fuel consumption. After the appearance of an innovative paper by Hanssen and James [8], several methods have been proposed to solve the problem of minimizing sailing time. The major methods include:

1. **Isochrone method**. An Isochrone Line (Time-Front) is defined as the outer boundary of the attainable region from the departure point that is reached after a certain time. The isochrone method proposed by Hanssen and James [8] was used for a long time because it offered an easy manual calculation method. Hagiwara [7] devised a modified isochrone method suitable for computer programming. However this method can generate so-called "isochrones loops", and cannot ensure that the route will not cross land. Hence to counter these problems, Szlapczynska and Smierzchalski [19] made improvements to the isochrone method, consisting in generating the initial set of candidate routes necessary for evolutionary computation to enhance the effectiveness of initial random population generation in evolutionary computation. However this method utilizes bitmap-based algorithms and is not applicable to vector-based ECDIS.
2. **Calculus of variation**. In Bijlsma publications [1, 2, 3] application of the calculus of variation was extended to the minimization of fuel consumption. Kosmas *et al.* [11] used calculus of variation and a wave model to compute the optimum route and applied simulated annealing techniques, a type of optimization method, to accelerate algorithm convergence. This approach is limited to theoretical analysis, time-consuming in terms of calculation, and less applicable in practice [24]. Khalilov [10] states that the variation calculus method has no optimality proof.
3. **Dynamic programming**. Dynamic programming uses a grid system which divides a possible sailing region into several cells. Each crossing point of a cell boundary is a waypoint candidate. The dynamic programming solution algorithm seeks a ship's trajectory that is composed of the positions $(X, Y, T)_k$, $k = 1, 2,...,N$, and the Control $C_k$ with the initial time $T_0$ and the initial ship position X [12]. Motte *et al.* [14, 15, 16, 17] conducted a series of detailed investigations on this issue, including grid mesh size setting, system development and design. In recent years, Wei *et al*. [25], Zhou and Chen [27] and Tang *et al.* [20] have also used dynamic programming to conduct automatic ship routing to reduce the workload of navigators. In Bijlsma paper [2] the relation between optimum control theory and dynamic programming was elucidated for the case of minimal fuel routing. The development of this method has become more mature but its weaknesses include the large quantity of nodes, large amount of space required for storage, inflexibility, and slow computational speed.
4. **Network Model**. A network is a special form of graph that consists of nodes and arcs. The network has numerical parameters such as length, cost and transit time. Lee *et al.* [12], through network modelling, used a depth-first search algorithm to combine weather modelling to establish a web-based optimum ship routing system. Montes [13] modelled the Optimum Track Ship Routing (OTSR) for U.S. Navy warships using a network graph of the Western Pacific Ocean. A binary heap version of Dijkstra's algorithm determines the optimum route for given model-generated wind and sea inputs. This method is similar to the dynamic programming method, but computation is inefficient because of a large quantity of nodes.

Problems such as difficult computerization, complicated and inefficient calculations, and easily getting trapped into local optima, are found in the above-mentioned traditional solution methods. With the development of artificial intelligence and the maturing of evolutionary computation technology, more and more researchers investigate model organism optimization by using evolutionary computation technology (for example: genetic algorithms (GA), ant colony algorithms (ACA) and particle swarm optimization) and apply it to route planning solutions. Tsou [22, 23], Smierzchalski and Michalewicz, [18] and Ito *et al.* [9] used the GA in the planning of collision avoidance and coastal navigation paths and gained very good results. The present research used the ACA as the research method, emulating ants' forage path finding behaviour, and applied it to search an optimum route. The two problems are similar with regard to their nature; ships are considered as ants, optimum navigation routes as forage paths, and weather conditions as obstacles. We hope that through this conversion approach the ACA calculation efficiency and global optimum search capability can be enhanced in achieving optimum ship routing.

## 3. OPTIMUM SHIP ROUTING AND WEATHER ROUTING

The ship weather routing develops an optimum track for ocean voyages based on ship's individual characteristics for a particular transit, and forecasts of weather and sea conditions. The advent of extended range forecasting and the development of selective climatology, along with powerful computer modelling techniques, have made ship routing systems possible [4].

### *3.1. The principle of optimum ship routing*

Today, in the evaluation of optimum transoceanic routes, the primary concern, besides safety, is usually given to navigation time (or navigation speed) rather than to distance. In synthesized considerations of safety and energy conservation the shortest distance between two ports is not necessarily an optimum route. If there are many routes to choose from, under the condition that the main engine power outputs are equal, the route that takes the least amount of time is the optimum route. Shorter navigation time in itself implies less fuel consumption.

Therefore, the optimum route must consider at least the following conditions:
- safety;
- avoiding severe weather and sea conditions as much as possible;
- natural factors such as weather, sea conditions and ocean currents, to increase navigational speed as much as possible.

In order to find the optimum route, when choosing and planning the navigation route and making corrections, the following principles must always be met:
- firstly, to ensure safety, avoid severe weather and sea conditions as much as possible;
- secondly, if, under the circumstances, there is no other option but to pass through a severe sea environment, pass in the least time possible;
- thirdly, the design of navigation routes always aims to shorten navigation time and arrive ahead of the ETA (Estimated Time of Arrival);
- fourthly, as much as possible make use of natural conditions which help to increase navigation speed, such as down winds and down currents, and as much as possible avoid natural factors which work against speed of navigation, such as head seas.

The impact of wind and waves on ship speed is non-linear. In circumstances where other conditions are unchanged, their effect on ship's speed, main engine power outputs, and fuel consumption cannot be represented by a simple algebraic expression. Therefore, in terms of ship's energy conservation, if, upon planned corrections, navigation overall makes use of natural conditions that work to its advantage, and avoids natural conditions that work against it, total navigation time usually can be decreased, although the total navigation distance may be lengthened, because increased navigation speed can usually compensate for an increase in navigation distance.

### *3.2. Computation of optimum route*

Based on the above-mentioned principles of optimum route planning, the cost of the optimum route is a function of the extent of obstruction and the distance between start and end points. Therefore, solving an optimum ship route problem may be seen as finding the route with the least cost among the set of candidate routes, while taking weather conditions into consideration. The mentioned cost is not limited to distance only but may include navigation time, fuel consumption or a combination of factors. The decision variables that should be controlled are the manoeuvring of course and speed. The total computational cost (I) is calculated as the sum of the costs over each route leg (S). It is based on the ship's position (P), changes in the manoeuvring control (C) (i.e., speed and course) and the time duration (t). With these cost components, the ship routing problem can be described by the following formula:
to minimize:

$$I = \int_S f(P(s), C(s), t(s))\,ds \tag{1}$$

where:
f(P, C, t) – function of voyage cost for position, manoeuvring control and time; and $P \in R$, $C \in C_A$

Let R be a possible sailing region. The manoeuvring control variable $C_A$ is the limit of the ship's output speed and the limit of course changing range. The cost per unit distance ds is measured by fuel consumption and degree of ship safety under sailing.

## 4. ANT COLONY ALGORITHMS AND SHIP ROUTE COMPUTATION

### *4.1. The Ant Colony Algorithm principle*

The ant colony algorithm is a form of evolutionary computation that models the behaviour of real ants in search of food. The algorithm was proposed by Dorigo [5] and has been successfully used to solve many real-life problems, such as the travelling salesman problem (TSP). In the natural world, in ants' search of food, among many different possible routes from the nest to the food source, different ants will at first choose different paths but in the end nearly all ants will discover the same shortest path. This is because ants' search for the shortest path is an interactive process. They leave a certain amount of secretion (pheromones) on the path they pass, can sense the presence and intensity of the secretions and move toward the direction where the substance has a higher concentration. The amount of secretion increases with the increase in number of ants that pass by, and decreases in a certain function of time that passes by. The reason is that more ants pass by the shortest path and the speed of pheromone accumulation is higher than that of other paths. Through the continuous exchange of pheromones the optimum route between the nest and the food source is found in the end. The ACA is an optimization decision method designed according to this ability of ants in the natural world. One sets a certain number of artificial ants (ships) and follows a set of search rules to find the optimum route comprehensively. The objective of weather routing is to find the safest and most economical navigation route based on the weather and manoeuvring control conditions between the departure and destination points. The conditions and objectives are basically the same as those of the ACA.

### *4.2. Division of the marine grid system*

In order to plan the necessary deviational and directional change in the navigation route, maritime space must first be divided into grids. The grids form the basis for waypoint candidates, and the navigation route structure consists of the waypoints (Fig. 1). Motte [16] has conducted detailed comparison and analysis regarding grid mesh size setting, and suggested that the grid mesh size should be four degrees longitude by a half degree latitude.

However the experimental measures are based on the North Atlantic Ocean from Western Europe to North America and may not be applicable to other marine areas. Additionally, given the case of a near north-south travel direction, the great circle route, using four degrees longitude as the grid's horizontal width, is not always appropriate. Therefore, in this study distance is used as the basis for the setting of grid size, hence flexibility for users themselves to change settings is saved. Essentially, navigation speed should be referred to, so that grid size corresponding to about the distance of one day's navigation, can be kept. The procedure to make a grid is as follows:
- first establish a great circle route between the starting point ($L_1$, $\lambda_1$) and end point ($L_2$, $\lambda_2$), to be the basis for route planning. The Great Circle route distance (D) and the initial course (C) can be obtained from the following formula:

$$\mathrm{CosD} = \pm \mathrm{SinL}_1 \cdot \mathrm{SinL}_2 + \mathrm{CosL}_1 \cdot \mathrm{CosL}_2 \cdot \mathrm{CosDLo} \tag{2}$$

$$\mathrm{CotC} = \frac{\pm \mathrm{CosL}_1 \cdot \mathrm{TanL}_2 - \mathrm{SinL}_1 \cdot \mathrm{CosDLo}}{\mathrm{SinDLo}} \tag{3}$$

where:
DLo – the difference of longitude.

When latitude $L_1$, $L_2$ have same sign, then the signs of $SinL_1$ $SinL_2$ and $CosL_1$ $TanL_2$ are (+); otherwise they are (-).

- then set a distance X, and along the great circle route set segmentation points (Lx, λx) at intervals of X. The location (Lx, λx) of a segmentation point from a departure point with a certain distance $D_x$ and initial course C is calculated by the formula:

$$L_X = Sin^{-1}(SinL_1 \cdot CosD_x + CosL_1 \cdot SinD_x \cdot CosC) \quad (4)$$

$$\lambda_X = \lambda_1 + Cos^{-1}\left(\frac{CosD_x - SinL_1 \cdot SinL_x}{CosL_1 \cdot CosL_x}\right) \quad (5)$$

- then, using each segmentation point as a basis, extend the longitude line to the north and south and pick a set distance *Y* to establish each segmentation point, so that the coordinates have the same longitude and different latitude;
- then connect these segmentation points in the north-south, east-west direction to form a grid system.

Finally set up the coordinate and node matrix, and the route planning will be established on this grid system. With advancements in communication and positioning technology the grid system and navigational route can be dynamically adjusted continuously, according to the latest weather conditions and the latest positioning point and end point on the great circle route.

### *4.3. Implementation of Ant Colony Algorithm*

First, establish a grid system and its node matrix in the navigation area, and provide each node with the appropriate initial value in the matrix to form the initial node information concentration value matrix. Then, put all the ants on the starting point to allow them to move simultaneously toward direction of the aim, and to reach the destination point in the end (Fig. 1). In the process every ant uses the state transition rule and undergoes a selection process when gathering at the next node. Assuming that the time it takes for an ant to travel from node *a* in the node set *i* to any node *b* in the next node set i+1, is the same, and distance is not a factor here, all the ants will reach the destination simultaneously and complete a circle. After all the ants have reached the destination, calculate the objective function value (Eq. 1) based on the routes discovered by each ant. Each node is also updated with overall information quantity, and nodes that are not passed by are treated as information quantity evaporation. Repeat this process until the optimum route is discovered. The detailed explanation of the process is as follows:

#### 4.3.1. Adjustment of information quantity

The number of ants is assumed m. And, every ant chooses the next route according to the corresponding probability based on the information quantity on the route, instead of choosing the route it has previously completed. Upon completing a route circle, it produces a corresponding quantity of information concentration, based on the total distance of the route, and updates the information concentration on the route just passed.

With $\tau_{ab}$ (t) representing the information concentration on route (a, b) at t-moment, the information concentration on this route at t+1 moment is:

$$\tau_{ab}(t+1) = \rho \cdot \tau_{ab}(t) + \sum_{k=1}^{m} \Delta\tau_{ab}^{k} \quad (6)$$

where:

ρ – a constant which indicates that the residual factor of information quantity is between 0 and 1, and (1 – ρ) represents the information evaporation coefficient

$\Delta\tau_{ab}^{k}$ – the increased information quantity of ant k on route (a, b) between t and t+1 moment

$$\Delta\tau_{ab}^{k} = \begin{cases} \dfrac{Q}{d_{ab}} & \text{If the k-th ant passes through a, b in this cycle} \\ 0 & \text{else} \end{cases} \quad (7)$$

Eq. (7) indicates that the increased information concentration is related to the cost of the passed route, and:

Q is a constant which is the total information amount produced by each ant; $d_{ab}$ is the distance between node a and b, which can be calculated through Mercator Sailing, and then expressed in terms of other costs, such as time, fuel consumption etc.

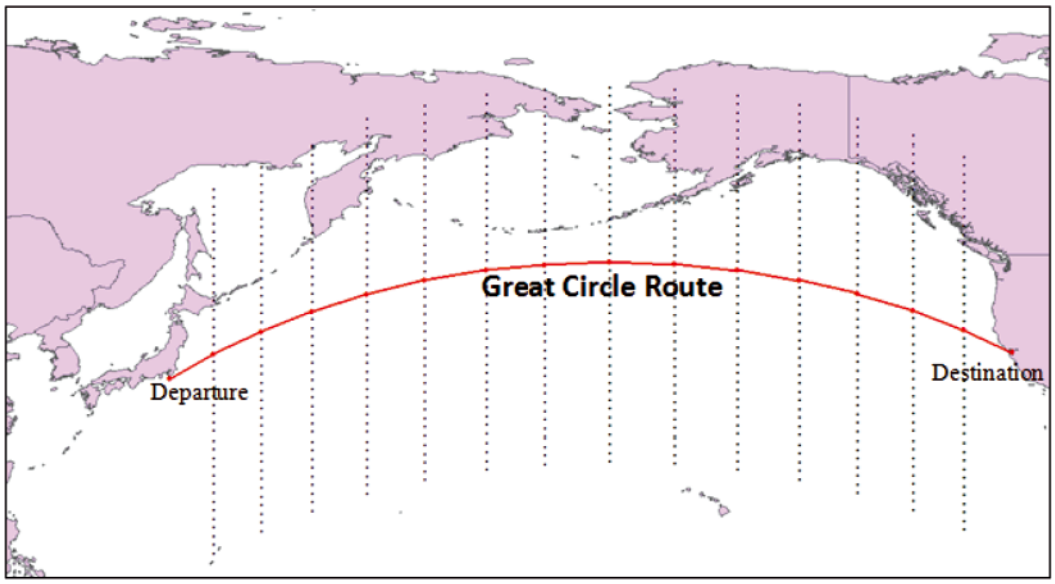


***Fig. 1.*** *Grid system and Great Circle Route*

#### 4.3.2. Waypoint selection principle

The probability of the event that the ant k which is at node a will select node b as its next destination at t moment, is:

$$P_{ab}^{k}(t)=\begin{cases}\dfrac{\tau_{ab}^{\alpha}(t)\cdot\eta_{ab}^{\beta}}{\sum\limits_{b\in N_{k(a)}}\tau_{ab}^{\alpha}(t)\cdot\eta_{ab}^{\beta}}, & \text{if } b\in N_{k(a)}\\ 0 & \text{else}\end{cases} \tag{8}$$

where:

$N_{k(a)}$ – the set of nodes that are yet to be visited by the $k^{th}$ ant at node a

$\eta_{ab}$ – heuristic information transferred from node a to node b. The information is obtained through the problem which has to be solved. In the problem the reciprocal of the cost of the points a and b, is $\eta_{ab} = 1/d_{ab}$

$\alpha$ – the relevant importance degree of residual information element concentration

$\beta$ – the relevant importance degree of the expected value

#### 4.3.3. Calculation procedure

The steps for using the ACA to determine the optimum route are listed below:

1. Initialize the information quantity on all the nodes on the navigation area, to form the initial information quantity matrix.
2. m ants in number are ready to start at the starting point A.
3. Every ant selects the next node on the matrix based on the state transition rule of Eq. 8, and reaches the destination in the end, forming a feasible route.
4. Calculate the objective function of every ant's feasible route based on Eq. 1, and keep the optimum route.
5. According to the objective function and the information quantity adjustment principle of Eq. 6, adjust the information quantity of every point.
6. Check if iteration conditions are met (if the established iteration number or minimum objective function value is reached). If the conditions are met then the search is complete. If not, repeat the procedure starting from the step (2) until the iteration conditions are met.

### *4.4. Calculation of navigation cost*

The calculation of navigation cost must take environmental conditions and ship performance conditions into account. To simplify the numerical experiment the amount of speed loss is calculated only by using the effect of waves.

#### 4.4.1. Ship response and performance

Ships travelling in the ocean are affected by wind and waves. As a result the actual speed of the ship in waves will certainly be lower than that in calm water. The degree of speed loss will affect the calculation of the speed-weather conditions as well as computed navigation time or fuel consumption costs for the ship route [14]. Speed loss is the most important among the various factors involved in ship route calculations. It is present in many route calculation formulae and has significant influence on the precision of vessel positioning and the feasibility of route optimization by weather routing. In general, there are two approaches to studying ship speed loss. The first approach is to conduct seakeeping tank and wind tunnel model tests to simulate air and water resistance on the ship body and to derive theoretical expressions to quantify the effect of wave resistance on the ship. The second approach involves the use of mathematical statistics or neural network regression to obtain empirical formula for calculating ship speed loss due to waves, by means of a large database of weather observation information (e.g. weather records or logbook) and information regarding ship conditions at the time. The formulae for speed loss obtained from the two methods can be used to produce ship performance curves or speed loss curves, as shown in Fig. 2. The effect of wave direction on speed loss is different for head seas, following seas, and beam seas. The relationship between ship orientation and wave directions is demonstrated in Fig. 3. Based on ship performance curves in combination with sea condition forecast data such as wave height, wave direction, or wind speed, the impact of ship speed loss on the total navigational costs can be calculated. Empirical formulae for ship performance curves have been the subject of a number of studies in the past, where different factors were considered. The main factors affecting ship speed loss are wind and waves, and wave size is closely related to wind speed. For simplicity of formulation and because the present study is focused on route optimization algorithms, the empirical formula recommended by Soviet Central Maritime Research Institute to calculate ship speed loss has been selected as the basis for comparison. The included main factors are wave height, wave

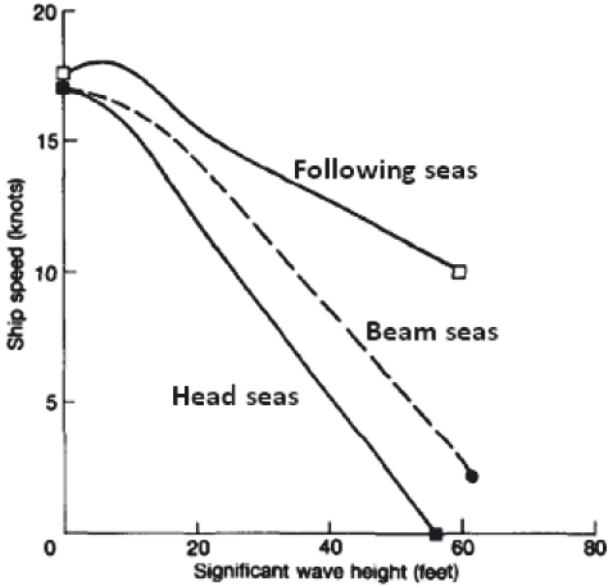


***Fig. 2.*** *James ship performance curves (Motte et al., 1988)*

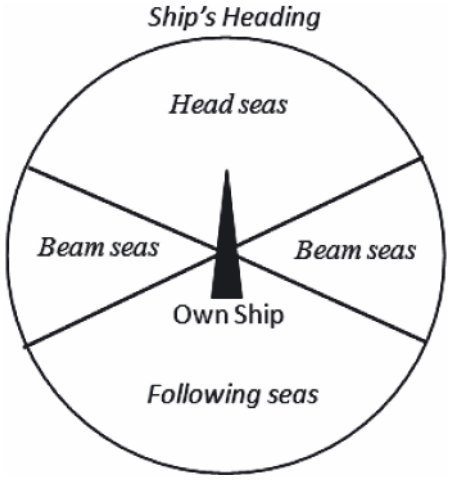


***Fig. 3.*** *Ship orientation and wave direction*

direction, and ship performance coefficient. If necessary, this can be substituted in the future by more sophisticated and accurate formulae. However, the assumed formula is sufficient for the purpose of validation of this research results. The formula is expressed as follows:

$$V = V_0 - (0.745h - 0.257qh)(1.0 - 1.35\times10^{-6} DV_0) \quad (9)$$

where:
V – the actual speed in the sea
$V_0$ – the speed in calm water
h – the wave height
q – the angle between ship heading and wave direction
D – the actual displacement of the ship (tons)

This formula is applicable to ships with displacement ranging from 5000 to 25000 tons, and speeds between 9 and 20 knots. Research has shown that when the wave height is between 0 and 5 meters, the difference between speed calculated by using this formula and the actual speed is less than 1 nautical mile. However, the calculated speed becomes slightly higher than the actual speed when the wave height is between 5 and 8 meters.

#### 4.4.2. Environmental data processing

Environmental data include geographic, navigational, and weather data, i.e. the basic background information on navigation areas, and the primary basis for cost calculation. By means of intersection calculation and measurement of navigation distance and environmental information, different cost data can be obtained. The processing and calculation method is as follows: **Geographic data**. Land and ocean distribution and danger zone (e.g. shallow waters) distributions are stored as GIS's polygon vector data. With regard to land area, overlap analysis is conducted on the marine grid system's node and land distribution. Nodes in land areas are initialized with the value of 0, while other nodes are set at a constant value. Thus, ants will not enter the nodes in the land area and will only search in the marine area.

- **Weather data**. With advances in information and communication technology in recent years, onboard internet connection by the INMARSAT ship station is often available and ample weather information is then easily accessible. Because ocean-going vessels can be only connected to the internet by satellites, which is relatively costly, only few ships use this method to gather weather information. However for the optimum route planning function in the Electronic Chart Display and Information System (ECDIS) the application of this method is an inevitable trend. In this study, the GRIB data downloaded from the internet is converted to a GIS format in the system and used for the route optimization.

The GRIB hydro-meteorological data is the standard defined by the World Meteorological Organization, and many service stations in the United States and Europe publish meteorological data in this format. In general, forecasts for the next 5 days are available, and they are updated every 6, 12 or 24 hours. The spatial resolution can reach 0.5° × 0.5°. This format offers great flexibility in that wind speed, wind direction, air pressure, seawater temperature, wave height, wave direction, and some other meteorological information can be selectively included. Such information adequately meets the requirements of weather routing. The information can be downloaded directly from the internet to the computer onboard for further processing, saving time and improving accuracy. Because the loss of ship speed is mainly caused by waves and Eq. (9) is taken into consideration, in this study wave direction and wave height are extracted from the GRIB data for subsequent calculations. The wind effect was ignored because its relationship with waves is linear.

#### 4.4.3. Calculation method

Wave direction and wave height grid data extracted from the GRIB are subsequently converted to cell layer data in the GIS to facilitate the integration with GIS computation. The weather cells are different from the nodes which constitute navigational waypoints in the navigation grid system. Next, the use of GIS's spatial analysis function is made to calculate the distance across all the cells that every candidate route passes, and find the wave height and wave direction data of the passed cells. By using ship speed loss formula the speed loss quantity can be computed. Finally, based on the distance across the cells, time/fuel consumption cost can be calculated. If navigation time is considered the primary cost, the computation formula is as follows:

$$t_j = \frac{d_j}{v - w_j} \quad (10)$$

$$T_c = \sum_{j\in J} (t_j + d_j \times F_j) \quad (11)$$

where:
$t_j$ – the required time for candidate route to pass the $j^{th}$ cell
$d_j$ – the distance for candidate route to pass the $j^{th}$ cell
v – normal speed without weather disturbance
$w_j$ – the quantity of speed loss due to waves in the $j^{th}$ cell
$T_c$ – total sailing cost
$F_j$ – additional unit distance cost factor in the $j^{th}$ cell

### *4.5. Improvements in computational performance*

#### 4.5.1. Limitations of maximum course deviation and maximum route segment length

Because a great number of nodes in the vast ocean grid system is not feasible in relation to navigation planning without proper heuristic calculation, the process is very time-consuming and much calculation capacity will be wasted. Because of limitations of maximum course deviation and maximum route segment length much unnecessary route calculation results may be spared. The course deviation angle is limited to ± 60° from the original course and the maximum route segment length cannot exceed that which can be covered in two days with the current speed. The selecting of appropriate values is a topic of further discussion.

#### 4.5.2. Determination of critical speed

While performing ship routing calculations we cannot seek only the shortest navigation time and must also consider a ship's critical speed (allowed maximum speed) while navigating in storm conditions. Thus the calculation result can produce the optimum route on the premise of safety. The calculation of critical speed is mainly related to wave height and wave direction. In this study the following formula [24] is used to impose maximum speed limits on a ship's critical speed in waves.

$$V_{Limit} = e^{0.13[\mu(q)-h]^{1.6}} + r(q) \quad (12)$$

where:
$\mu(q) = 12.0 + 1.4\times10^{-4}q^{2.3}$
$r(q) = 7.0 + 4.0\times10^{-4}q^{2.3}$

q – stands for the relative wave direction
h – stands for wave height

The formula reflects ship's critical speed under different wave conditions to ensure navigational safety.

#### 4.5.3. Limit on information quantity

When the scale of the problem increases, the information quantity of the grid point which has never been searched, will decrease near to 0, because of the information quantity evaporation coefficient (1-ρ), decreasing the algorithm's global search capability. If (1-ρ) becomes too small then the probability of a solution which has been searched, being selected, may become too large and will also affect the algorithm's global search capability [21]. Although increasing (1-ρ) may enhance an algorithm's global search capability but also decrease the algorithm's rate of convergence. Thus, a range of information quantity ($\tau_{min}$, $\tau_{max}$), is established, and if the information quantity exceeds this range the following corresponding limits are imposed:

$$\tau_{ab}(t+1) = \begin{cases} \tau_{min} & \tau_{ab}(t+1) < \tau_{min} \\ \tau_{max} & \tau_{ab}(t+1) > \tau_{max} \\ \tau_{ab}(t+1) & \text{other} \end{cases} \quad (13)$$

#### 4.5.4. The addition of crossover operations to the genetic algorithm

The crossover operation concept is added to the GA in this study. The crossover operation is processed through the searched optimum route and another ant's random route every time. If the two ants pass by the same grid point (waypoint), then a crossover operation is conducted between the two routes (excluding the starting and end points) based on the same grid point, namely, by combining the first half of route A with the second half of route B to form a new route, and also the second half of route A and the first half of route B to form another new route. If the two ants do not pass the same grid point then crossover operations are not conducted. If, after the crossover operation, a route better than the current optimum route is obtained then the optimum route information is updated, otherwise, another crossover operation is performed. The adding of crossover operations increases the ant's ability to find a better route in a search, as well as variety of solutions.

#### 4.5.5. The addition of mutation operators to genetic algorithms

In order to avoid local optima, in this study the concept of mutation operation was added to the GA through setting a certain probability value randomly selecting a grid point from the current optimum route and exchanging it with a not-yet-passed random grid point from the optimum route, to form a new route. If the new route has a lower cost than that of the original optimum route then the original optimum route is replaced with this route.

## 5. EXPERIMENT RESEARCH RESULTS

### *5.1. Condition settings of the experiment*

This experiment research simulated the navigation route from Yokohama to San Francisco, with (34°40′ N, 140°E) as the starting point coordinates, and (37°45′ N, 122°W) as the end point coordinates. The following conditions were applied to the simulation. The time spent in the algorithm is verified in the results.

- Weather conditions: the presumed weather conditions in the research had been previously ascertained. The weather cell size of wave height - wave direction weather data was set at latitude 0.5°Í longitude 0.5°. The GRIB data used was for the northern Pacific Ocean on 2011/11/25.
- Conditions of course deviation and route segment length restriction: it was assumed that the ship was located at the $X^{th}$ node (waypoint) in the node set I, and the ship's next feasible node (waypoint) was confined within the range of X ± 3 node (waypoint) in the node set I + 1. This approach was used to provide the conditions of course deviation and route segment length restriction.
- Ship performance was simulated under the output power required to maintain the navigation speed of 18 knots in calm water. The speed loss curves, as in Eq. 9, were matched with wave height and wave direction data to simulate ship speed. In the simulation the ship displacement of 18000 tons was assumed.
- Grid system size: as shown in Fig. 1, the east-west direction interval distance along the great circle route was set at 300 nautical miles, with a total of 14 points. The distance along the longitude north-south direction line was set at 60 nautical miles (1°), with a total of 44 points. Thus, a grid system consisted of 616 waypoints was established. The route was generated through the ACA search; it was generated by testing and combining the waypoints.
- ACA parameter setting: α = 3, β = 2, ρ = 0.5, Q = 1000, m (number of ants) = 100, N (number of cycles) = 100.
- Experiment environment: to perform the simulations PC of 4 GB memory and an Intel Core 2 Duo CPU 2.2 GHz processor, was used. Visual Basic 2010 was used as the programming language and the geographic information feature provided by ArcGIS Engine's COM object was used to perform spatial analysis and geometry computation.

### *5.2. Discussion of results*

The shipping routes were assessed on the basis of the total navigation time. From the experiments it was found that appropriate choice of the number of ants and the parameters can improve the efficiency of the algorithm. When the number of ants is small (ant no. 10), the ACA does not show clear signs of convergence, and an optimum solution is hard to obtain (as shown in Fig. 4). This is also the case when the ant number is larger (ant no. = 20) and parameters α and β are of low value (both ≤ 3). When α and β are larger (both ≥ 4), convergence is more evident, but a large number of iterations is required. When ant no. ≥ 50 and α, β both > 4, a better convergence is achieved; however, the solution fell into a local optimum on many occasions (see Fig. 5).

It was found that when the number of ants is relatively large and the parameters are such that α < β (α = 2, β = 3), better convergence was achieved through the ACA and a near-optimum solution was more readily obtained. Therefore the parameters for deriving the optimum shipping route are set as follows:

$$\alpha = 2,\ \beta = 3,\ \rho = 0.5,\ m = 200 \text{ and } N = 100$$

In addition, in order to validate the results the simulated results from east bound and west bound navigation were compared with those from navigation following the Great Circle Route. The performance of the simulation program under different weather conditions was observed. The simulated

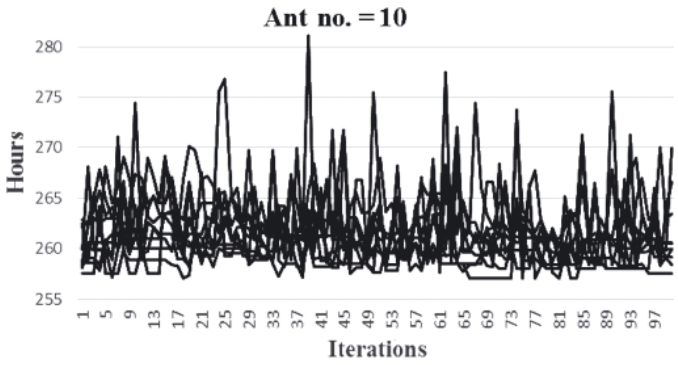


*Fig. 4. Poor convergence for a small number of ants. It is difficult to obtain a near-optimum solution.* ***Notation****: Ant no. stands for number of ants (Fig. 5)*

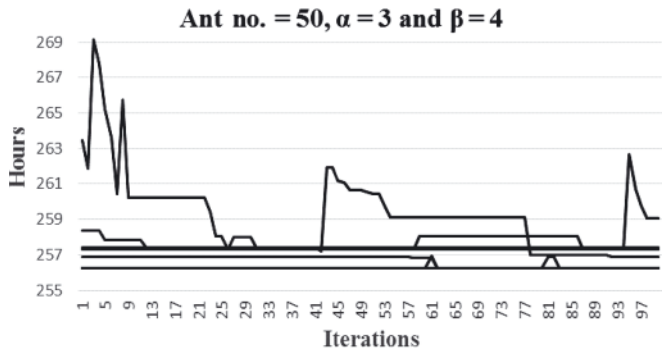


*Fig. 5. When α = 3 and β = 4, the solution achieved through ACA is often the local optimum.* ***Notation****: Ant no. stands for number of ants*

results are shown in Fig. 6 where the purple route is the Great Circle Route, the black route is the optimum route produced by the ACA, and the yellow routes are the alternative routes generated in the search process. During the east bound navigation, due to the influence of strong winds and stormy seas in the low pressure region, the ACA simulation suggests that the navigation route should be shifted south of the Great Circle Route (Fig. 7). If the ship followed the Great Circle Route for which the distance is 4518.6 nautical miles, and travelled with the calm water speed of 18 knots, the navigation time under the weather conditions was 261.8 h (Fig. 8) and the average speed was 17.26 knots. Although the distance generated by the ACA (equal to 4571.6 NM) is longer than that of the Great Circle Route, the navigation time was only 255.8 h and the average speed was 17.87 knots. Then 6 h and the corresponding amount of fuel can be saved compared with the Great Circle Route. For the west bound navigation, i.e. on the southern route, a ship encountered a head wind and head seas due to low pressure to the south of the Aleutian Islands. This casted an adverse effect on the navigation. The ACA algorithm therefore modified the route and caused it to deviate to the north off the Great Circle Route. The route entered the Bering Sea to the north of Aleutian Islands, and met favourable following seas and good weather, as shown in Fig. 9 and 10. In this case, the navigation time following the Great Circle Route was 267.2 h and the average speed was16.91 knots. The route produced by the ACA had a longer distance of 4571.72 NM, but the navigation time was only 264.7 h (refer to Fig. 11) and the average speed was 17.27 knots. The saving of 2.5 h and the corresponding amount of fuel was achieved. The simulation results shows that the weather routing by means of the ACA makes use of favourable meteorological conditions and avoids to some extent encountering head seas and heavy wind regions, reducing this way the risk of ship damage and cargo loss. As regards the execution time, although algorithm efficiency for the entire program has not been optimized, the average execution time was about 5 min, which is sufficient for decision-making in real-time navigation.

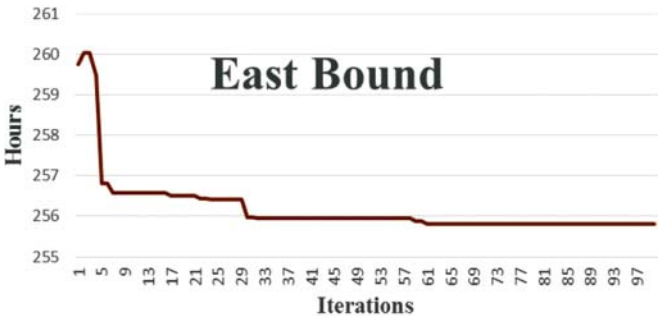


*Fig. 8. Iteration history of optimum navigation time for east bound navigation*

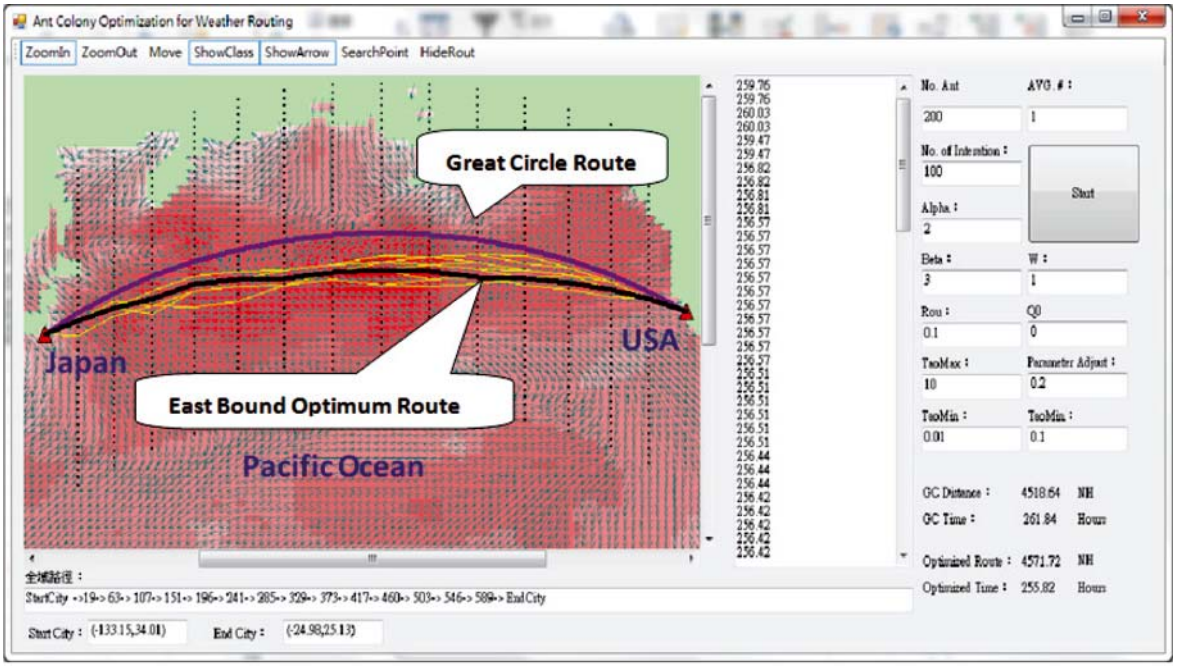


*Fig. 6. Route simulation results for east bound navigation*

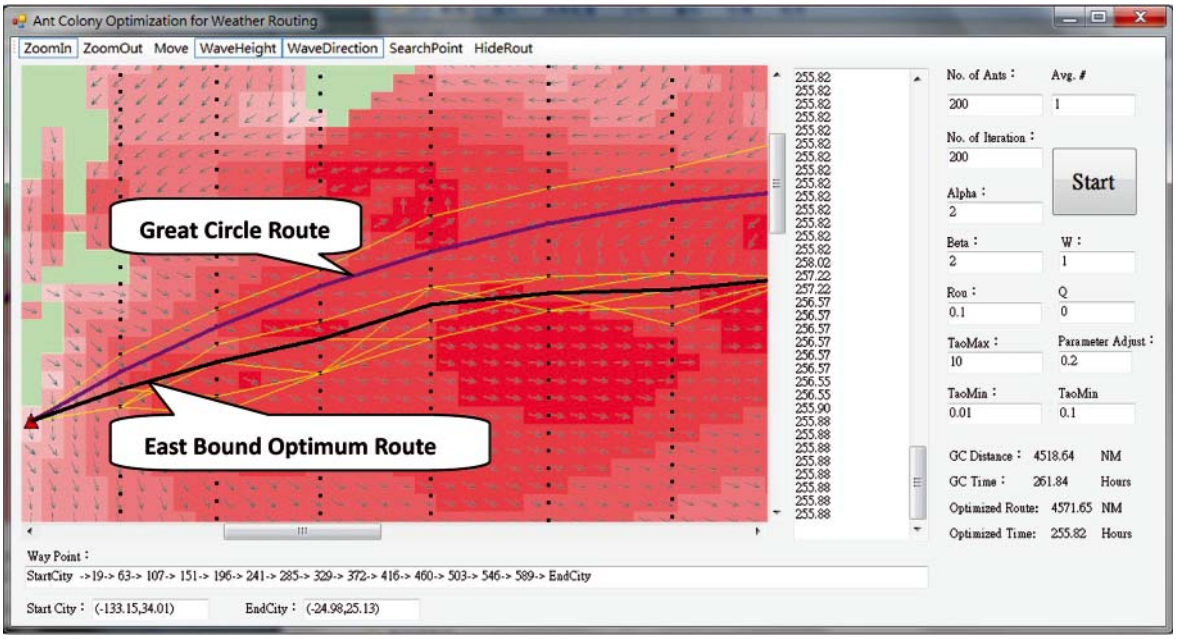


*Fig. 7. Weather conditions and simulated route for east bound navigation*

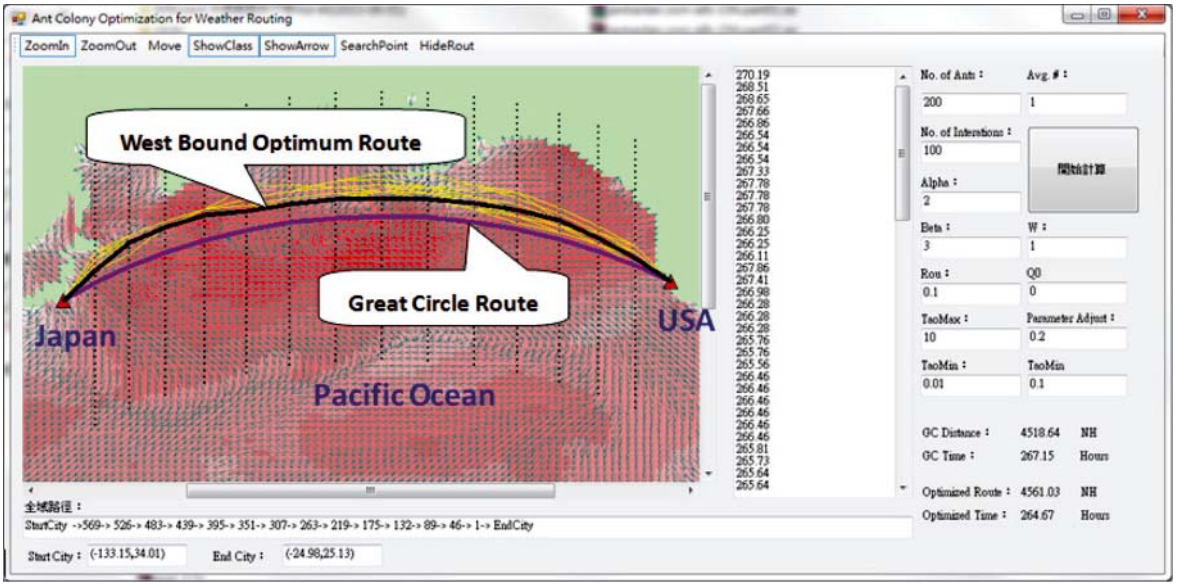


*Fig. 9. Route simulation results for west bound navigation*

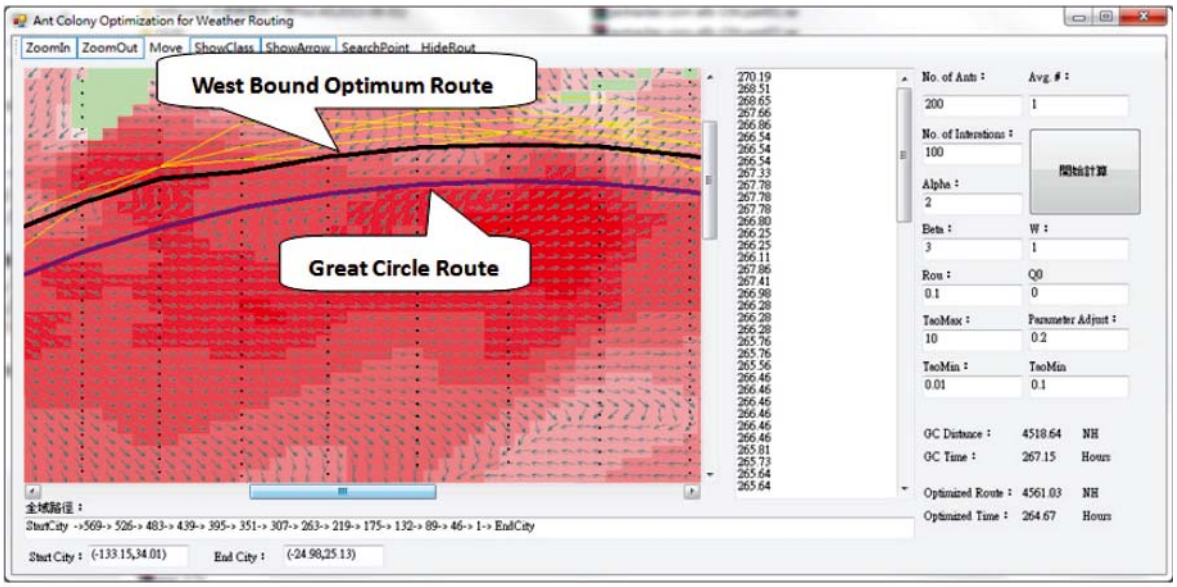


*Fig. 10. Weather conditions and the simulated route for west bound navigation*

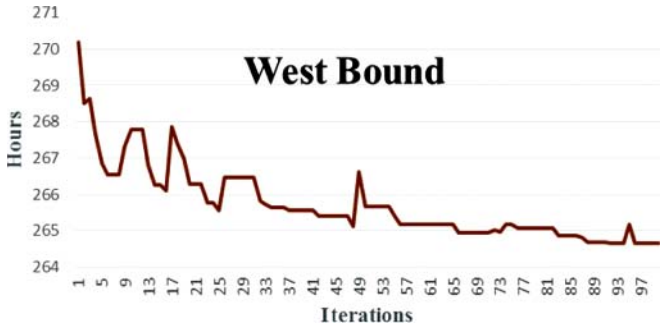


***Fig. 11.*** *Iteration history of optimum navigation time for west bound navigation*

## 6. CONCLUSIONS

With the substantial rise in international oil prices, and global warming on the rise, to reduce operational fuel consumption and decrease air pollution has become one of the key goals of green shipping. In order to reach the goal, ships in operation can be fitted with energy-conserving equipment. However, optimum ship routing is the most direct and economical method. Therefore, application of decision support tools to help the routing of transoceanic crossings, not only can enable route planning automation, achieve the aim of carbon oxide reduction and energy conservation but also provide a reference for decision making in route planning. In this study a proper grid system and the improved ACA was used to establish a route searching model that simulates a living organism's optimum behaviour. In addition, GA's crossover and mutation computations, a ship's critical speed function, and GIS's spatial analysis and computation capability were integrated to automate the generation of a transoceanic crossing route, in consequence increasing route planning speed and quality, and lowering the ship crew's burden. With the growing popularity of distributed computing environments, many applications of parallel processing and distributed processing have been widely implemented. Considering the efficiencies brought about by distributed processes, the using of the distributed parallel processing structure together with the feedback mechanism of the ACA collective intelligence can further enhance ACA resolution efficiency. And, the computational speed will be higher than that of other resolution methods. Therefore, in the future the size of the grid system can be reduced to conduct more refined simulations by means of the combination of more waypoints. Also, in this study the candidate routes that pass through obstacles was removed without integrating an obstacle avoidance mechanism (such as island avoidance navigation). A relevant coastal navigation routing technique, suggested by Tsou [23], could be added in the future so that the results might better satisfy requirements of real time navigation decision support and enhance the energy conservation effect.

### *Acknowledgements*

The authors would like to thank the National Science Council, Taiwan, R.O.C., for financial support under contract number: 100-2410-H-022-006.

**BIBLIOGRAPHY**

1. Bijlsma, S. J.,: *A Computational Method for the Solution of Optimal Control Problems in Ship Routing.* NAVIGATION, Journal of the Institute of Navigation, Vol. 48, pp. 145-154, 2001.
2. Bijlsma, S. J.: *On the Application of Optimal Control Theory and Dynamic Programming in Ship Routing.* NAVIGATION, Journal of the Institute of Navigation, Vol. 49, pp. 71-80, 2002.
3. Bijlsma, S. J.: *Minimal Time Route Computation for Ships with Pre-Specified Voyage Fuel Consumption*. The Journal of Navigation, Vol. 61, pp. 723-733, 2008.
4. Boditch, N.: *The American Practical Navigator – 2002 Bicentennial Edition*. National Imagery and Mapping Agency, U.S. Government, 2002.
5. Dorigo, M., Manizzzo, V. and Colomi, A.: *Ant system optimization by a colony of cooperating agents.* IEEE Transaction on System, Man and Cybernetics- Part B: Cybernetics, Vol. 26, No. 1, pp. 29-41, 1991.
6. Flecks, J.: *Study Green Shipping*. HVB Global Shipping, Hamburg, pp. 4-5, 2009.
7. Hagiwara, H.:*Weather Routing of Sail Assisted Motor Vessels*. Ph. D. Thesis, Delft University, Holland, 1989.
8. Hanssen, G. L. and James, R. W., "Optimum Ship Routing," *The Journal of Navigation,* Vol. 13, pp. 253-272, 1960.
9. Ito, M., Zhang, F. and Yoshida, N.: *Collision avoidance of ship with genetic algorithm.* Proceedings of 1999 IEEE International Conference on Control Applications, pp. 1791–1796, 1999.
10. Khalilov, S. I.: *Stochastic dynamic programming method for computing the most advantageous ship navigation routes*. *Meteoro. Hydrol.,* No. II, 1980.
11. Kosmas, O. T., Vlachos, D. S. and Simos, T. E.: *Obstacle Bypassing in Optimal Ship Routing Using Simulated Annealing*. Proceedings of International Electronic Conference on Computer Science, Vol. 1060, pp. 79-82, 2008.
12. Lee, H., Kong, G. & Kim, S.: *Optimum Ship Routing and It's Implementation on the Web*. Lecture Notes in Computer Science, Vol. 2402/2002, pp. 11-34, 2002.
13. Montes, A. A.: *Network Shortest Path Application for Optimum Track Ship Routing*, Master Thesis, U.S. Naval Postgraduate School, Monterey, California, 2005.
14. Motte, R. Burns, R. S. and Calvert, S.: *An Overview of Current Methods Used in Weather Routeing.* The Journal of Navigation, Vol. 41, No. 1, pp. 101-114, 1988.
15. Motte, R. and Calvert, S.: *Operational Considerations and Constraints in Ship-based Weather Routeing Procedures*. The Journal of Navigation, Vol. 41, No. 3, pp. 417-433, 1988.
16. Motte, R. and Calvert, S.,: *On The Selection of Discrete Grid Systems for On-Board Micro-based Weather Routeing.* The Journal of Navigation, Vol. 43, No. 1, pp. 104-117, 1990.
17. Motte, R., Fazal, R., Epshteyn, M. Calvert, S. and Wojdylak, H.: *Design and Operation of a Computerized, On-Board, Weather Routeing System.* The Journal of Navigation, Vol. 47, No. 1, pp. 54-69, 1994.
18. Smierzchalski, R., Michalewicz, Z.: *Modeling of ship trajectory in collision situations by an evolutionary algorithm.* IEEE Transactions On Evolutionary Computation, Vol. 4, pp. 227-241, 2000.
19. Szlapczynska, J., Smierzchalski, R.: *Adopted Isochrone Method Improving Ship Safety in Weather Routing with Evolutionary Approach*. International Journal of Reliability Quality and Safety Engineering, Vol. 14, No. 6, pp. 635-646, 2007.
20. Tang, X.-T., Fen, G.-S., Zhao, W.-F.: *Application of Dynamic Programming in Designing Ship's Optimum Route,* in Chinese. Journal of Guangzhou Maritime College, Vol. 17, No. 2, pp. 18-20, 2009.
21. Tian, W. and Zhan, A.,: *Research on Path Planning for UCAV based on Improved Ant Colony Algorithm,* in Chinese. Fire Control and Command Control, Vol. 33, No. 11, pp. 69-72, 2008.
22. Tsou, M.-C., Kao, S.-L., Su, C.-M.: *Decision Support for Genetic Algorithms for Ship Collision Avoidance Route Planning*. The Journal of Navigation, Vol. 63, pp. 167-182, 2010.
23. Tsou, M.-C.,: *Integration of a Geographic Information System and Evolutionary Computation for Automatic Routing in Coastal Navigation*. The Journal of Navigation, Vol. 63, pp. 323-341, 2010.
24. Wang, F., Jia, C.: *The Study on The Optimal Ship Routing*, in Chinese. Journal of Dalian Maritime University, Vol. 24, No. 2, pp. 61-64, 1998.

25. Wei, X., Yu, Z., Wang, Z.: *Design of Optimum Ship Route Based on Dynamic Programming*, in Chinese Navigation of China, Vol. 57, pp. 16-18, 2003.
26. Wei, S., Zhou, P.: *Development of a 3D Dynamic Programming Method for Weather Routing*. International Journal on Marine Navigation and Safety of Sea Transportation, Vol. 6, No. 1, pp. 79-83, 2012.
27. Zhou, P., Chen, H.-W.: *Improved Calculation Method of the Shortest Time Route*, in Chinese. Science Technology and Engineering, Vol. 18, No. 21, pp. 5876-5880, 2008.

## CONTACT WITH THE AUTHORS

Ming-Cheng Tsou*), Associate Prof.
Department of Shipping Technology,
National Kaohsiung Marine University,
Kaohsiung, Taiwan, R.O.C.

Hung-Chih Cheng, Prof.
Department of Marine Environment and Engineering,
National Sun Yat-sen University,
Kaohsiung, Taiwan, R.O.C.

*)Author for correspondence: Ming-Cheng Tsou
(e-mail: d86228006@yahoo.com.tw)

**POLISH MARITIME RESEARCH** 3(79) 2013 Vol 20; pp. 39-44
10.2478/pomr-2013-0033

# Application of Shape From Shading Technique for Side Scan Sonar Images

**Krzysztof Bikonis**, Ph. D.
**Marek Moszynski**, Assoc. Prof.
**Zbigniew Lubniewski**, Ph. D.
Gdansk University of Technology, Poland

ABSTRACT

*Digital signal processing technology has revolutionized a way of processing, visualisation and interpretation of data acquired by underwater systems. Through many years side scan sonars were one of the most widely used imaging systems in the underwater environment. Although they are relatively cheap and easy to deploy, more powerful sensors like multibeam echo sounders and sonars are widely used today and deliver 3D bathymetry of sea bottom terrain. Side scan sonar outputs data usually in a form of grey level 2D acoustic images but the analysis of such pictures performed by human eye allows creating semi-spatial impressions of seafloor relief and morphology. Hence the idea of post-processing the side scan sonar data in a manner similar to human eye to obtain 3D visualisation.*

*In recently developing computer vision systems the shape from shading approach is well recognized technique. Applying it to side scan sonar data is challenging idea used by several authors. In the paper, some further extensions are presented. They rely on processing the backscattering information of each footprint (pixel in sonar image) along with its surroundings. Additionally, a current altitude is estimated from the size of shadow areas. Both techniques allow constructing 3D representation of sea bottom relief or other investigated underwater objects.*

**Key words**: side scan sonar data processing; shape from shading

## INTRODUCTION

Acoustic sensors offer robust insight into underwater environments, as they are characterised by longer range and wider angle coverage compared to video cameras or other sensors. Also, they are capable of providing satisfactory results of mapping the environment in turbid waters. Side scan sonar (SSS) is one of the most widely used imaging systems in underwater environment. It is relatively cheap and easy to deploy, in comparison to more powerful sensors like multibeam sonars. However, it has some limitations, such as its inability to recover the seafloor depth or submerged object information directly [1].

Conventional side scan sonars are used until today. They emit fan-shaped pulses down toward the seafloor across a wide angle perpendicular to the path of the sensor through the water, which may be towed from a surface vessel or mounted on the ship's hull. The intensity of the acoustic reflections from the seafloor of a fan-shaped beam is recorded in a series of cross-track slices. When stitched together along the direction of motion, these slices form an image of the sea bottom within the swath of the beam.

During years of evolution side scan sonar were improved including higher frequency systems and the dual-frequency sonars, and the combined side-scan and sub-bottom profiling sonar. Generally, increasing frequency improves resolution of obtained images. The development of digital signal processing technology made possible real time processing of acquired data to form synthetic aperture. The principle of such synthetic aperture sonars (SAS) is to move a sonar along a line and illuminate the same spot on the seafloor with several pings. This produces a synthetic array equal to the distance traveled. By coherent reorganization of the data from all the pings, a synthetic aperture image is produced with improved along-track resolution. In contrast to conventional side scan sonar, SAS processing provides range-independent along-track resolution. At maximum range the resolution can be magnitudes better than that of side scan sonars.

Until the development of so-called 3D side scan sonars the side scan sonar imagery were presented in the form of classical 2D images. 3D side scan sonars uses interferometric acoustic technology and by application of digital signal processing techniques it operates over a field of view larger than 90° with no blind spots under the survey track.

However, many SSS 2D images exist, that could be transformed into 3D representation in an algorithmic way using the echo intensity information contained in grayscale images. In the imaging sonar systems, the characteristics of acoustic

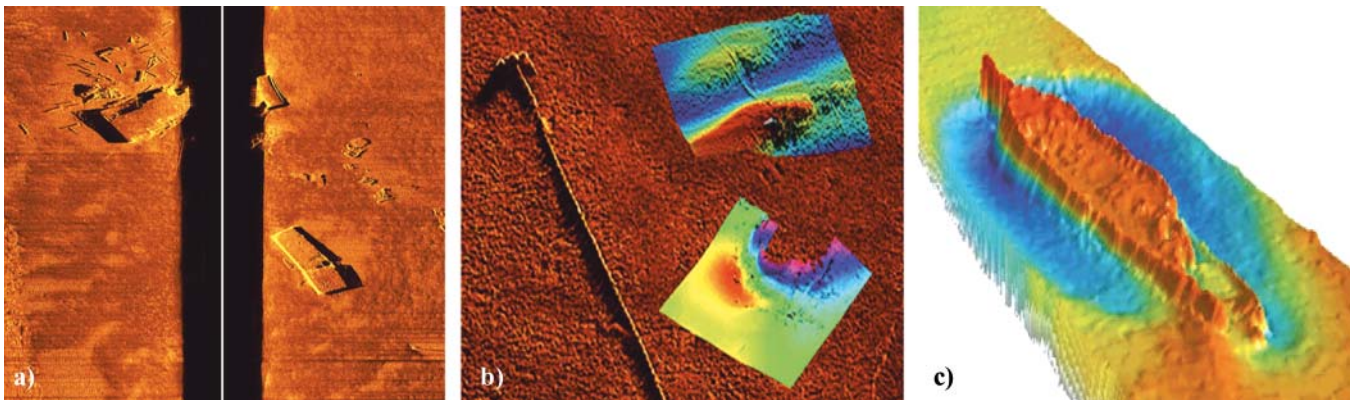


***Fig. 1.*** *Sample sea bottom images obtained by three generations of side scan acquisition systems* ***a)*** *conventional side scan sonar* ***b)*** *synthetic aperture sonar* ***c)*** *3D side scan sonar*

energy backscattering by a target localised on seafloor is utilised. Instead of arbitrarily using the formula like Lambert's law to describe the seabed backscattering dependence on an incident angle [2], the authors propose their own approach to derive this dependence locally from experimental data.

In this paper, two methods for 3D seafloor and submerged objects shape reconstruction from SSS images, based on shape from shading (SFS) approach, are presented. In the first method, for estimation of bottom local depth at a given pixel of sonar image, the information from both currently processed and previous ping is utilised. It allows the local seabed surface element orientation to have two degrees of freedom. Prior to the investigation of this approach on sidescan sonar field data, its verification on multibeam sonar backscatter data is presented, with use of the seabed 3D model (i.e. the set of (x, y, z) seabed surface points derived from multibeam soundings) as a reference.

The second method is used for 3D submerged object shape reconstruction and its imaging. The direct application of classical SFS technique seems not to be best suited to submerged object visualisation as it leads to obtaining very smooth shapes which differ significantly from actual forms of artificial objects. The proposed method, besides the utilisation of the local altitude gradient estimation by SFS algorithm with use of the backscattering coefficient angular dependence function derived experimentally, also estimates the elevation change on the basis of the dimension of acoustic shadow areas.

Several techniques of 3D geometry reconstruction for seabed surface or submerged objects using side-scan sonar images has been reported [3, 4, 5]. Mainly, they use the techniques based on the problem inverse to image formation, namely Shape from Shading (SFS), which is one of classical problems in computer vision (see [6] for a collection of significant papers on SFS). The goal is to derive a 3D scene description from one or more 2D images. Given a grey level image, the aim is to recover the light source and the surface shape at each pixel of the image.

Brief description of the SFS principles and basic methods along with literature references is given in [7].

## SHAPE FROM SHADING FOR SIDE SCAN SONAR IMAGERY

### *Seafloor relief reconstruction from sonar image*

In the construction of a seabed elevation map from side scan images, the SFS technique relays on calculating the local slope of bottom relief, given the image pixel intensity, the assumed dependence of bottom surface backscattering coefficient on incident angle (what corresponds to reflectance map in classical SFS), and the estimated local incident angle value. The presented algorithm for 3D seafloor relief reconstruction [8] has been developed assuming that the acoustic reflectivity model as well as the altitude H of the sonar transducer are given. The intensity (grey level) of a pixel in sonar image is treated as proportional to the acoustical intensity of backscattered echo. Also, the simple, straight line propagation path of acoustic wave in water column is assumed, and, the dimensions along vertical axis (z) of an object to be reconstructed are assumend to be small in comparison with the sonar transducer altitude.

The geometry used in derivation of the reconstruction algorithm is presented in Fig. 2. The beam of a side scan sonar covers an angular sector from $\varphi_{min}$ to $\varphi_{max}$.

The relation between the time instant $t_{ij}$ in an echo envelope and the across-track coordinate $x_j$ of a corresponding point $P_{ij}$ on seabed surface, may be expressed by:

$$x_j = \sqrt{\left(\frac{ct_{ij}}{2}\right)^2 - H^2} \tag{1}$$

where:
$t_{ij} \geq 2H/c$
$c$ – sound speed in water.

At the time instant $t_{ij}$, the seafloor surface $S_{ij}$ is insonified, the area of which may be for a flat bottom case expressed by the classical equation [2]:

$$S_{ij} = \theta_V R_{ij} \frac{c\tau}{2\sin\theta_{ij}} \tag{2}$$

where:
$\Theta_V$ – the along tract transducer beamwidth,
$R_{ij}$ – the range from the transducer to the point $P_{ij}$,
$\tau$ – the transmitted pulse length.

The 3D bottom relief was reconstructed by estimation of an altitude z(x, y) sequentially for consecutive discrete points (x, y) on a plane, using the scheme depicted in Fig. 2. For the (i, j) iteration (where i – number of processed line in the sonar image corresponding to one sonar ping, j – number of pixel belonging to this line), i.e. the point $P_{ij} = (x_j, y_i, z(x_j, y_i))$ altitude estimation, the local triangle facet was being taken into account, with vertices at two previously estimated points $P_{i-1\,j} = (x_j, y_{i-1}, z(x_j, y_{i-1}))$ and $P_{i\,j-1} = (x_{j-1}, y_i, z(x_{j-1}, y_i))$, and currently estimated point $P_{ij}$. Using the applied model, the value chosen for $z_{ij}$ allows for calculation of normal $\tilde{N}_{ij}$ to the surface facet, the angle $\Theta_{ij}$ and the local intensity $I_{ij}$ value, which then many be compared with that from the original sonar image.

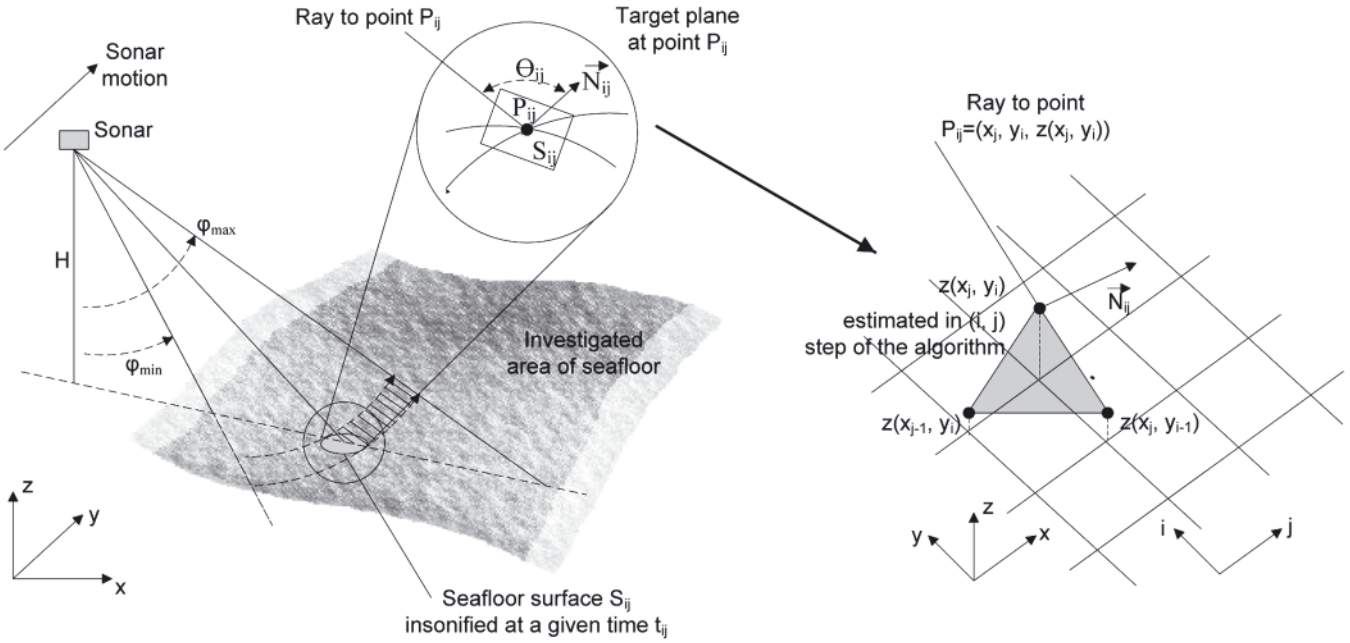


***Fig. 2.*** *The geometry used in derivation of the seafloor relief reconstruction algorithm and its grid approximation*

Optimal $z_{ij}$, i.e. that giving I equal to a measured value, may then be estimated [7].

The reliable reflectance model (namely, here: the seafloor acoustic backscattering coefficient dependence on an incident angle) is a crucial element of the SFS-like 3D object reconstruction procedure. Some authors suggest that the Lambert's Law provides a good fit to seabed backscattering dependence on an incident angle [2], but in general, the description of seafloor backscattering phenomenon is complicated. The backscatter from the seafloor is generally considered to be composed of a combination of surface and volume scattering, i.e. roughness interface scattering and scattering from inhomogeneities within the sediment volume. The detailed investigation of seafloor backscattering angular dependence, containing the theoretical modelling along with experimental verification, is described in [9]. It shows that although in several cases the application of Lambert Law might be allowed, in many others this law is not satisfied. This fact was also proved by further experiments. Taking it into account, the authors proposed their own approach here, which assumes the estimation of backscattering angular dependence coefficient locally for currently used experimental data. Assuming that we may choose the region within the processed sonar image, where the seabed surface is flat and composed of the material characterised by constant properties, we may state that the grey level of a given pixel in an analysed area should depend only on the experiment geometry (e.g. position of the source, the incident angle), the sonar calibration data, and the seafloor backscattering coefficient. If the investigated area covers some range of incident angle values, the backscattering coefficient angular dependence may be estimated for this range using pixel grey level values, as it is presented in the next section.

## *The use of shadow area dimension for object height estimation*

One extension has been made for the proposed 3D shape reconstruction algorithm from SSS data when used to artificial objects lying on seabed (like wrecks for instance). Such object usually have regular shapes and their sonar images often are full of shadow areas. The proposed algorithm extension assumes the utilisation of the information which may be derived from shadow areas. Namely, the height of an object element is being estimated from the size of a current shadow area. Shadow area include the pixels from SSS image witch values are below chosen threshold intensity value $I_{th}$. In a case of a shadow zone detection of a length j along x axis, the altitude values from $z_{i+1}$ to $z_{i+j}$ were set to unknown, and the $z_{i+j+1}$ value was calculated as:

$$z_{i+j+1} = z_i - \frac{\Delta x_{sh}}{\tan \varphi_i} \tag{3}$$

Fig. 3 presents in a schematic way the influence of the $I_{th}$ on the algorithm results for two cases of $I_{th}$ values. Figure 3a shows the sample dependence of the intensity value on x coordinate for a given fragment of one line in side scan sonar image, along with two $I_{th}$ values indicated. Figure 3b presents the reconstructed seabed altitude for these two cases. For $I_{th2}$ case, the larger shadow zone occurs and no reconstruction is obtained inside $[x_a, x_b]$ range.

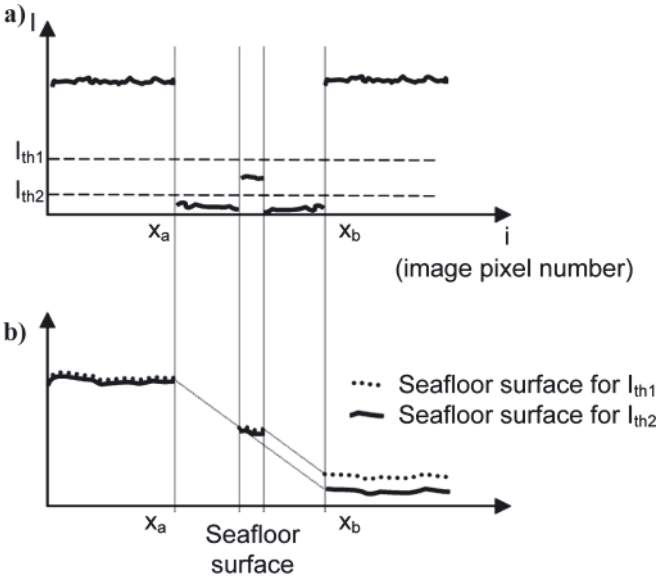


***Fig. 3.*** *The influence of the shadow threshold value $I_{th}$ on the altitude reconstruction algorithm results*

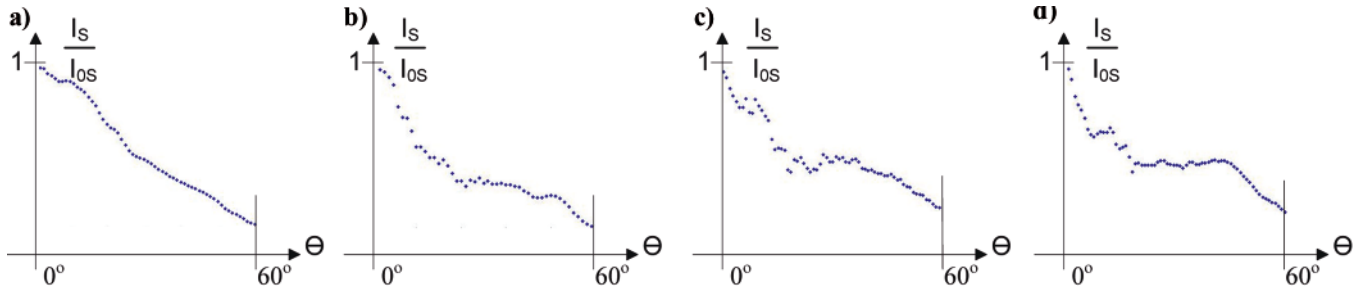


*Fig. 4. Seabed backscattering coefficient angular dependence averaged for 40 multibeam soundings for each of 4 sites*

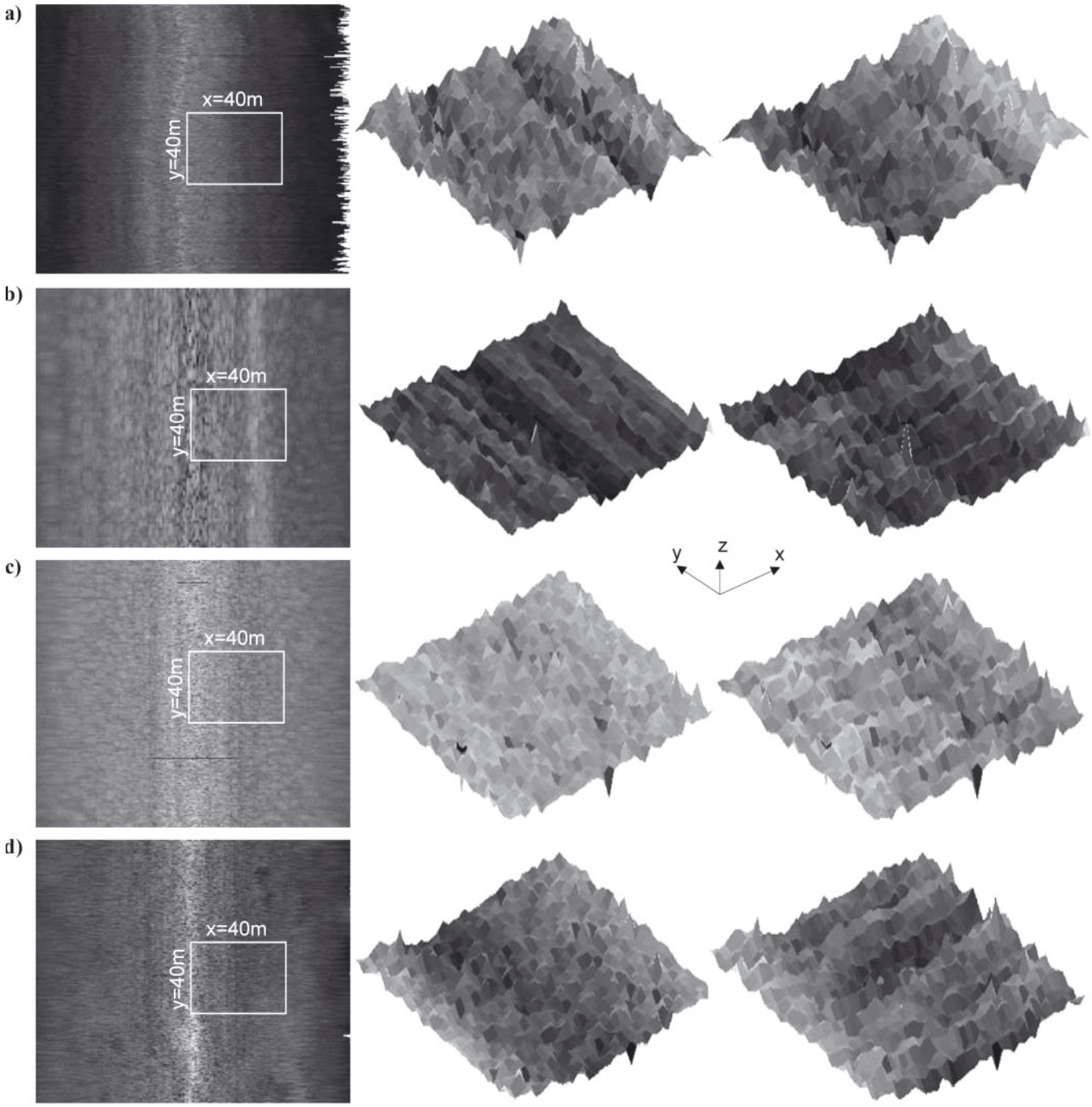


*Fig. 5. Verification results of 3D shape reconstruction method using multibeam sonar data for 4 sites in Gdansk Bay region. First column: sonar images constructed using backscattering strength of echoes corresponding to several multibeam soundings (horizontal lines in an image) and beams (vertical lines in an image). Central column: visualisations of seabed 3D models derived from multibeam soundings by the EM3002 sonar software in the form of sets of (x, y, z) seabed surface points – these seabed surfaces were used as a reference data. Right column: 3D seabed surface shapes reconstructed using the proposed SFS-like algorithm*

## EXPERIMENTS AND RESULTS

### *Experimental derivation of backscattering coefficient angular dependence*

As it has been introduced in the previous section, the seafloor backscattering coefficient angular dependence function, needed in the SFS-like 3D shape reconstruction procedure, has been derived experimentally by choosing flat surface area for this purpose.

The data used in this experiment were acquired by the Kongsberg EM 3002 multibeam sonar in Gdansk Bay region of the Baltic Sea for 4 separate sites characterised by different seafloor type. The sonar operating frequency was 300 kHz, the width of beams: 1.5° x 1.5°, the transmitted pulse length: 0.15 ms, the echo sampling rate: 14.3 kHz. The bottom depth was in a range approximately between 10 m and 100 m. 500 swaths from each of four seafloor types were processed. For each swath, 160 beams covered the angle sector from -65° to 65°.

Fig. 4 presents the seafloor backscattering coefficient angular dependence derived by the described approach and averaged for 40 multibeam soundings for each of 4 sites. The significant differences in the results between several cases are well visible. It proves the expectation that this dependence characterises the seabed locally and therefore it should be preferable to derive it experimentally in-situ.

### *Verification of the shape reconstruction procedure using multibeam sonar data*

The mutibeam data described in the precious subsection were also used in the verification procedure for the proposed algorithm of 3D shape reconstruction from acoustic data. The obtained results are presented in Fig. 5 for 4 different acquisition sites in Gdansk Bay. The seabed "sidescan sonar-like" images constructed from multibeam backscatter data (first column of pictures in Fig. 5) were processed by the proposed SFS-like algorithm to reconstruct the seafloor relief. The results are shown in the right column of pictures in Fig. 5 while the reference data, i.e. 3D seabed surfaces derived from multibeam data by EM3002 sonar software, are shown in the central column in this figure.

It is actually visible in Fig. 5 that although the proposed method introduces some "artifacts" in across-track direction (from bottom left to top-right on the pictures in Fig. 5), the differences between the reconstructed and the reference seabed surfaces are small enough to be primarily acceptable. For the quantitative estimation of the proposed method performance, the rms difference between the reconstructed and the reference surface has been calculated for each of 4 cases. The obtained rms values were between 3 cm for the first site (a) and 9 cm for the last site (d) what is a good result taking into account that the geometric dimensions of the experiment were of tens of meters.

### *Application of the 3D shape reconstruction procedure to side scan sonar data*

The developed procedure of 3D seafloor relief reconstruction was also tested on DF1000 dual frequency (100 and 500 kHz) side scan sonar data collected in the Gulf of Gdansk. For further processing the 500 kHz data were used as they represent the higher resolution entity. The specific areas were selected for calculation of seabed backscattering coefficient angular dependence. The results of 3D seabed surface reconstruction are presented in Fig. 6.

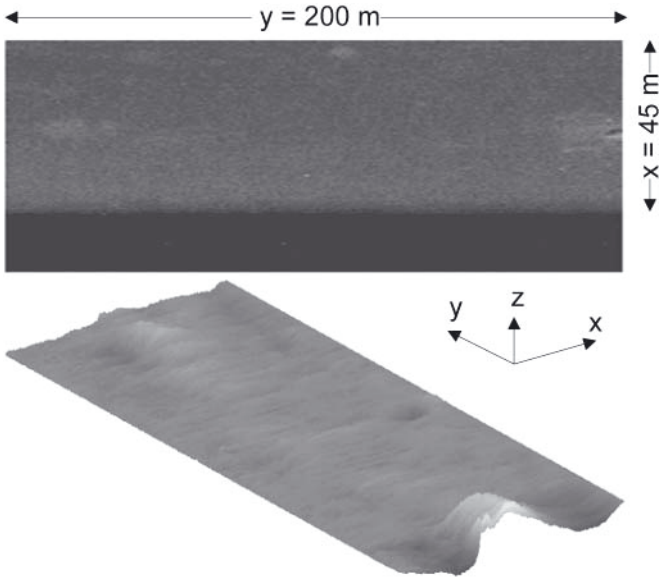


***Fig. 6.*** *The sample seabed image with selected areas used for seabed backscattering calculation [10]*

The developed procedure of object 3D shape reconstruction was tested on side scan sonar data downloadable from Marine Sonic Technology, Ltd. website. The sample car tire image acquired by side scan sonar is presented in Fig. 7 and its reconstruction is shown in Fig. 8.

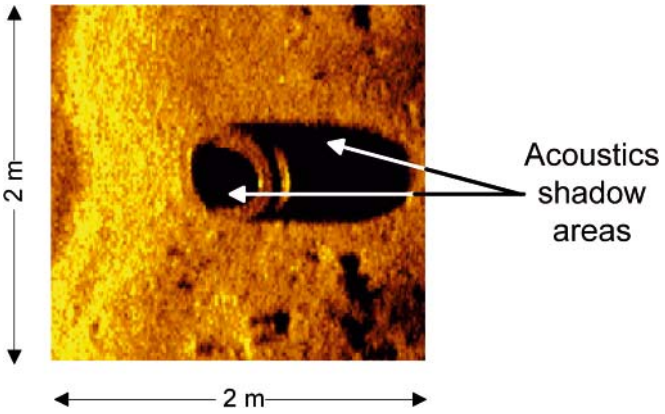


***Fig. 7.*** *Side scan sonar image of car tire from sonar operated at 2400 kHz [10]*

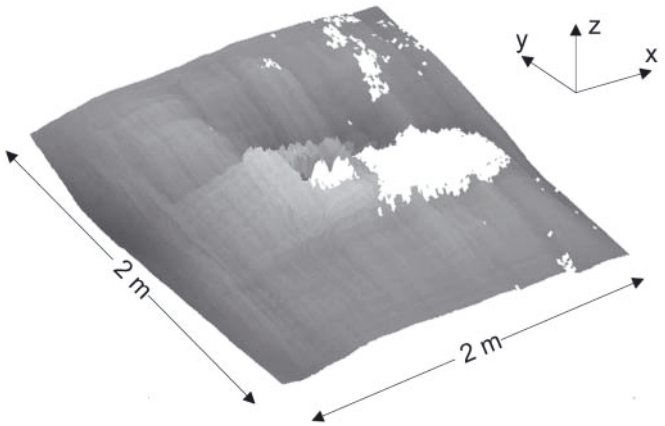


***Fig. 8.*** *The 3D car tire reconstruction*

The next test was performed on side scan sonar data containing the image of USS Utah as shown in Fig. 9. The image region within the rectangle was used to verify the performance of the algorithm.

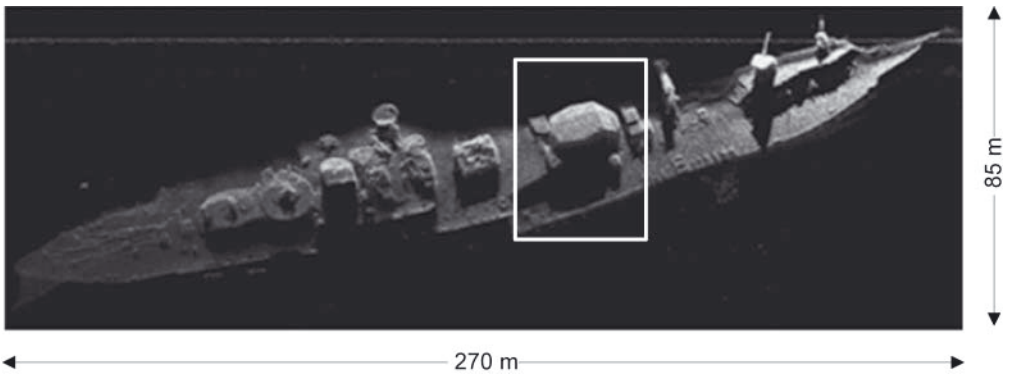


*Fig. 9. Image of the USS Utah, resting in Pearl Harbor near Ford Island, acquired by the U.S. Army 7th Engineer Detachment using Sea Scan Centurion system operated at 600 kHz [10]*

The comparison of the results obtained when applying two different shadow threshold values $I_{th1} = 0.05I_{max}$ and $I_{th2} = 0.1I_{max}$ is presented in Fig. 10. It may be seen that for lower $I_{th}$ value case (Fig. 10a), more details of the reconstructed shape may be visible than for higher $I_{th}$ value (Fig. 10b). But on the other hand, if the $I_{th}$ is too low, the artefacts may occur due to using the information from very dark, and possibly noised pixels, for the object local altitude slope estimation.

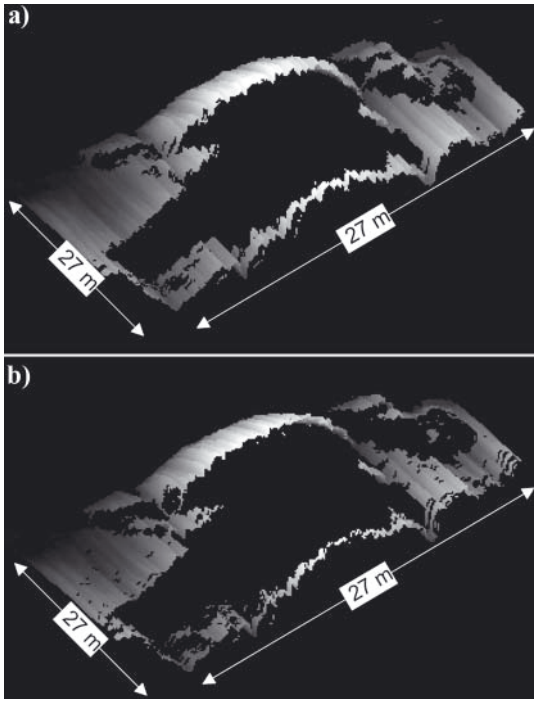


***Fig. 10.*** *3D wreck shape reconstruction results using two different values of shadow threshold*

## CONCLUSIONS

The methodology based on shape from shading approach for 3D reconstruction of seafloor and submerged objects from side scan sonar records was presented. It was verified using the data acquired by multibeam sonar system that contains both backscatter and bathymetry data and also tested on side scan sonar data. The principle advantage of the methods is their simplicity and the ability to produce the results within sequential, one-run processing. It was also shown that angular dependence of backscattering plays a significant role during image processing and should be estimated for a observed subareas.

At the current stage of the development the applicability of the presented solution might be questionable and further investigation are required. In particular, the authors expect that presented seafloor reconstruction algorithm performance can be improved by applying procedure similar to synthetic aperture sonar principle. The implementation of more advanced shape from shading algorithms could be required in more complex cases.

**BIBLIOGRAPHY**

1. Bikonis K., Moszynski M., Stepnowski A.: *Submerged object imaging using virtual reality modeling language*, Proceedings of International Congress on the Application of Recent Advances in Underwater Detection and Survey Techniques to Underwater Archeology, pp. 215-220, Bodrum, Turkey, 2004.
2. Urick J.: *Principles of underwater sound for engineers*, McGraw-Hill Book Company, New York, USA, 1975.
3. Bell J., Lane D., Dura E.: *Automatic 3D reconstruction of mine geometric using multiple side scan sonar images*, Paper presented at GOATS 2000 Conference, SACLANT-CEN, La Spezia, Italy, 2001.
4. Cushieri J. M., M. Hebert M.: *Three-dimensional map generation from side-scan sonar images*, Journal of Energy Resources Technology, 112, 96-102, 1990.
5. Coiras E., Petillot Y., Lane D.: *Automatic rectification of side scan sonar images*, Proceedings of the 1st International Conference on Underwater Acoustic Measurements: Technologies & Results (CD-ROM), Heraklion, Greece, 2005.
6. Zhang R., Tsai P. S., Cryer J. E., Shah M.: *Shape from shading: A survey*, IEEE Transactions on Pattern Analysis and Machine Intelligence, 21, 690-705, 1999.
7. Moszynski M., Bikonis K., Lubniewski Z.: *Reconstruction of 3Dshape from sidescan sonar images using Shape from Shading technique*, Hydroacoustics, 16, 181-188, 2013.
8. Bikonis K., Moszynski M., Lubniewski Z., Stepnowski A.: *Three-dimensional Imaging of Submerged Objects by Side-Scan Sonar Data Processing*, Proceedings of the 1st International Conference on Underwater Acoustic Measurements: Technologies & Results (CD-ROM), Heraklion, Greece, 2005.
9. Jackson D. R., Winebrenner D. P., Ishimaru A.: *Application of the composite roughness model to high-frequency bottom backscattering*, J. Acoust. Am, 79(5), 1410-1422, 1986.
10. Marine Sonic Technology, Ltd. website http://www.marinesonic.us, 2012.

**CONTACT WITH THE AUTHORS**

Krzysztof Bikonis, Ph. D.
Marek Moszynski, Assoc. Prof.
Zbigniew Lubniewski, Ph. D.
Faculty of Electronics,
Telecommunications and Informatics
Gdansk University of Technology
Narutowicza 11/12
80-233 Gdansk, POLAND
e-mail: binio@eti.pg.gda.pl

**POLISH MARITIME RESEARCH** 3(79) 2013 Vol 20; pp. 45-50
10.2478/pomr-2013-0034

# Gdansk Bay sea bed sounding and classification of its results

**Grażyna Grelowska**[1)], Prof.
**Eugeniusz Kozaczka**[1,2)], Prof.
**Sławomir Kozaczka**[1)], M.Sc.
**Wojciech Szymczak**[1)], M.Sc.
[1)] Polish Naval Academy, Poland
[2)] Gdansk University of Technology, Poland

ABSTRACT

*The main goal of this paper is to describe the results of sounding the Gdansk Bay sea bed by using a SES-2000 Standard parametric sub-bottom profiler. Quality of data obtained during trials depends inter alia on a proper location of transducer array to reduce influence of pitch, roll and heave motions as well as ship self noise (resulting from bubbles due to propeller and flow around hull, vibration generated by main engine and auxiliary devices). Furthermore, calibration of complementary units such as GPS, heading sensor, MRU-Z motion sensor and navigation devices make sea-bed investigating system capable of working with its whole capability. Results of so prepared surveys have been presented and discussed. They contain also an elaborated map of Gdansk Bay with preliminarily classified sea-bed materials and description of most interesting areas.*

**Key words**: sea bed sounding; parametric sub-bottom profiler; sea bed structure

## INTRODUCTION

Examination of the upper layer of sea bed can be performed with the use of invasive methods as well as non-invasive ones. The invasive methods apply only to the local structure of the sea bed, and are associated with geographical coordinates of the bore-hole point (point of evaluation). In addition, in such case a subtle structure of actual image of the bottom is destroyed. The non-invasive methods are mainly seismic ones which are rather suitable for determining the geological structure of the sea bed in relation to large depth [14, 16]. However, for the bottom layer they are relatively inaccurate. An alternative solution is to use acoustic methods which make accurate determining the sea-bed stratification, possible. These methods are non-invasive and relatively versatile. However there is a problem of penetration of bottom sediment by acoustic waves [1, 2, 9]. Attenuation of elastic waves by bottom sediments is about 1000 times larger than by the water [13]. For this reason the high-frequency waves are mostly reflected upon the water - bottom border surface.

With taking into account the relevant constraints a parametric source of acoustic waves can be applied in such case. The principle of operation of such source is that, as a result of the nonlinear interaction between two large-intensity acoustic beams in the area of common impact of the beams, a new wave is formed in the area of a volumetric character [12]. As the beams called primary, differ only slightly in frequency, we get a wave called the differential wave whose frequency is equal to the difference in frequency of the primary waves. Such wave maintain the features of primary waves and therefore is of a high directivity. Due to the area of its generation which is three-dimensional, it has no additionally adverse side lobe. The properties were used in the construction of the parametric sonar, *inter alia* in the SES 2000 Standard parametric echo-sounder [17]. Extensive research of sea bottom in Gdansk Bay waters was performed with the use of this echo sounders [3-8, 10, 11].

## RESEARCH VESSEL

The platform for sea trials was set on board s/y *Windspeel*, a small research vessel. The main device was the SES-2000 Standard sub-bottom echo sounder which consisted of the main unit situated below the deck and the transducer array mounted on aluminium arm starboard. The unit makes it possible to radiate low frequency sounding pulses set by the user within the range from 4 to 15 kHz and a definite changeable length. An interesting function during sounding was the option of obtaining sub-bottom data by applying two or three different pulses with user - defined frequencies. During the sea trials in question the frequencies of 4 kHz, 8 kHz and 12 kHz were set and combined to each other. As the best weather conditions are during calm sea which is not always achievable, hence a beam steering to compensate for vessel pitching and rolling was necessary.

The obtained data were stored on hard disc in the two formats: *.SES one which includes information about signal


***Fig. 1.*** *Research vessel with installed equipment*

envelope and *.RAW data containing full waveform. The whole unit was fed with 230V (AC) provided from DC-AC converter connected to the set of three 110 Ah gel batteries charged during trials from solar batteries and a generator driven by vessel's engine. During breaks in measurements the charging was provided by on-board 230 V Honda electric generating set. Additionally sea bed was sounded with the use of the multi-beam EM3002 echo sounder whose transmitted pulses were synchronized by means of an external trigger installed in the SES-2000 sounder that ensured undisturbed results. Complementary devices like the MRU-Z sensor of pitch, roll and heave motions precise GPS with heading sensor were installed and calibrated on the vessel. Signals from the sensors were distributed to the devicesby means of RS-232 splitters During the trials sound velocity profiles were stored in SD204 unit and put in to controlling programs of sub-bottom and multi-beam echo sounder. The investigated area and transects selection along which the sounding took place were determined on the basis of geological maps delivered by Państwowy Instytut Geologiczny (State Geological Institute) [15]. The appropriate data were delivered to the navigation software (Nobeltec) connected to autopilot, that ensured a satisfying accuracy of sounding along the set tracks. To help the skipper to control situation on sea two monitors were duplicated in cockpit to display navigation map and sounding results. The research vessel during measurement trials on Gdansk Bay is presented in Fig. 1.

The devices necessary to ensure proper work of the whole unit were placed on specially prepared working racks inside the vessel (Fig. 2). Before beginning the trails on sea the units were calibrated in harbour and checked during work with different parameters and configurations. Additionally, the electric system was tested and checked against possible emission of noise which could influence sounding equipment.

Special RS232 splitters were implemented into the system to avoid duplication of the units delivering information such as position and motion data.

## OBTAINING SEDIMENT SAMPLES

During all sea trials a diver prepared for such action was collecting samples of material taken from bottom's surface and other layers according to a type of sediment. The samples were

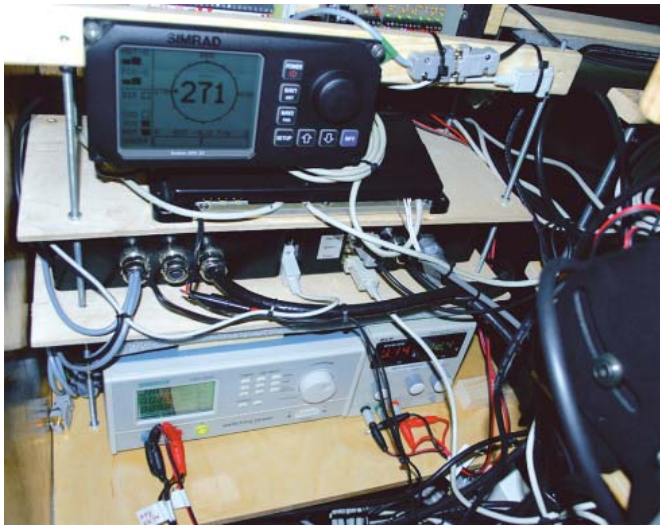


***Fig. 2.*** *Complementary devices*

stored in special containers, and then examined and classified. Additionally, it was necessary to collect enough amount of materials to be used during trials in 30 m long water tank of Gdansk University of Technology, where influence of different kind of materials on the parametric echo sounder records was measured and then used to prepare database for comparison of results from sea trials with data obtained during the "artificial sounding".

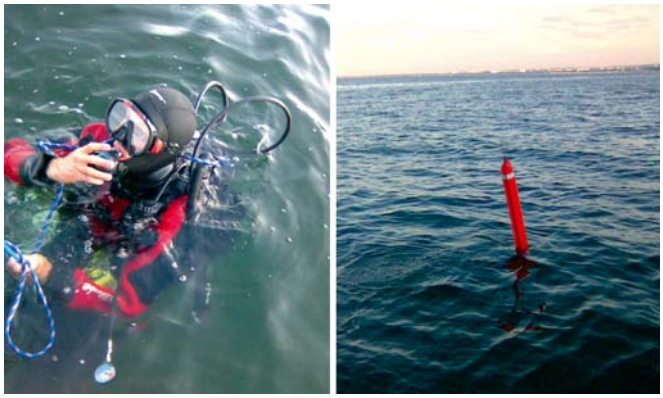

***Fig. 3.*** *Diver who prepares for taking bottom sediment samples*

***Fig. 4.*** *Mud dug out of sea bottom*

An example container filled with mud taken from sea bottom is presented below. Collecting such sediment was most difficult for the diver because of no visibility due to cloud of silt produced during digging the material.

Enlarged pictures of sediments are presented in Fig. 5 and 6. The example clearly shows difference in bottom layer structure. The example IV illustrates the sample of sand which results in high power echo compared with the sample of mud of a low penetration - example III.

Owing to the data which uncover clear parts of the cliff it was possible to elaborate pictures of the structure of such sediment layers by collecting the sediments and comparing them with the samples taken from sea bottom. Real image of such structure provides more information on its geological nature. In Fig. 7 is presented an example of enlarged pictures of materials taken from the pointed parts of the cliff material layers.

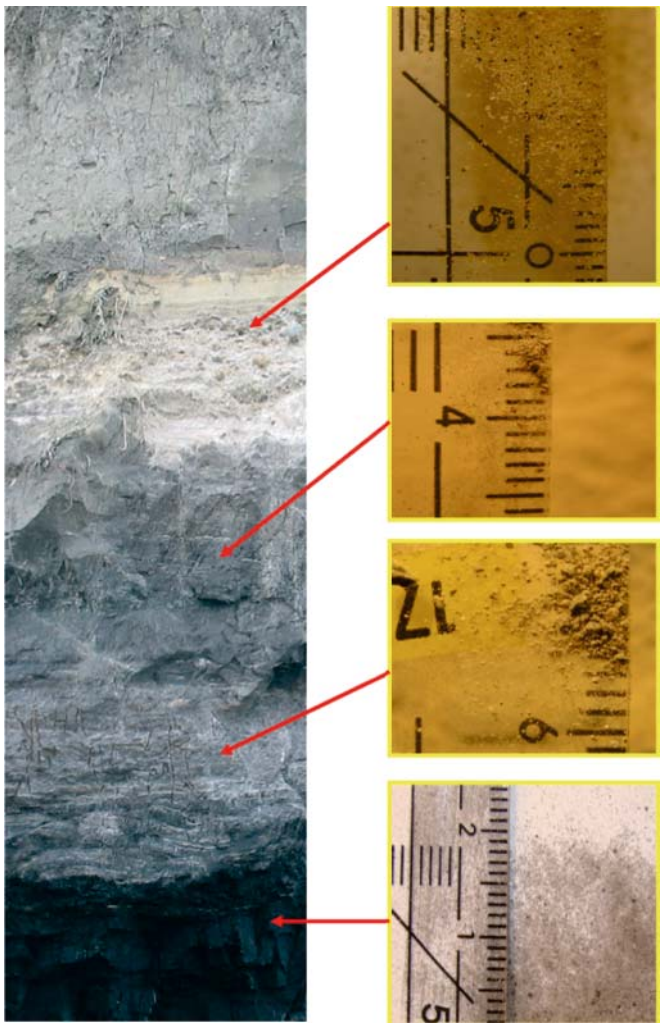

***Fig. 7.*** *Cliff material layered structure*

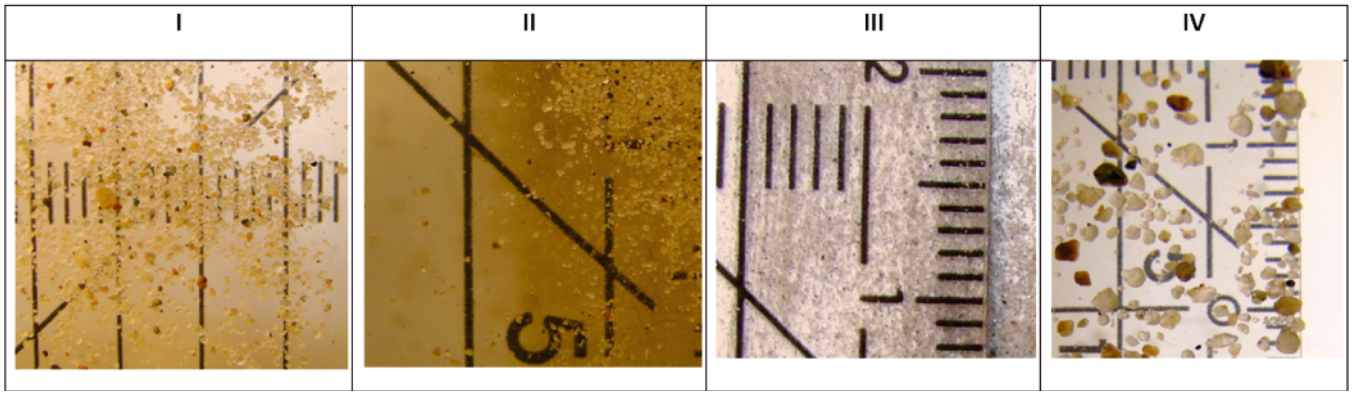


***Fig. 5.*** *Sediment samples in macro view, part 1*

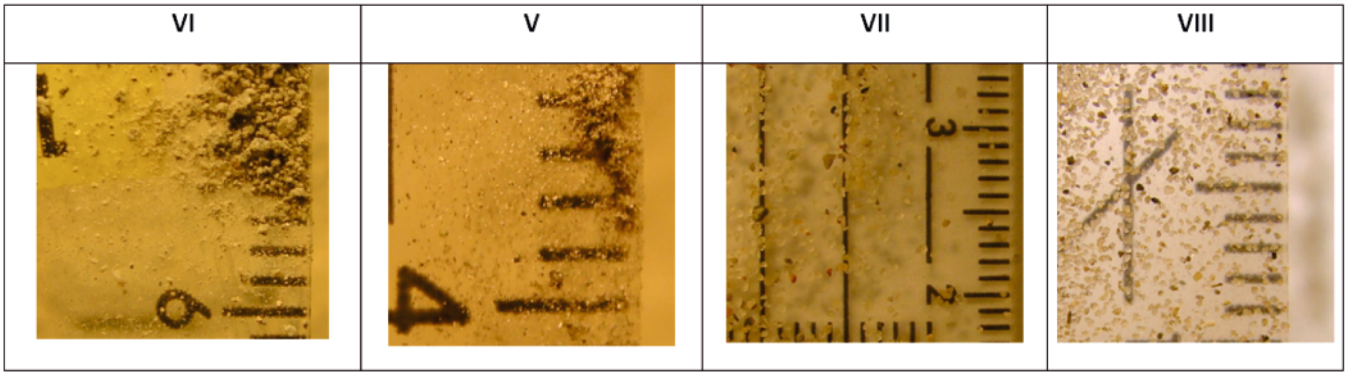


***Fig. 6.*** *Sediment samples in macro view, part 2*

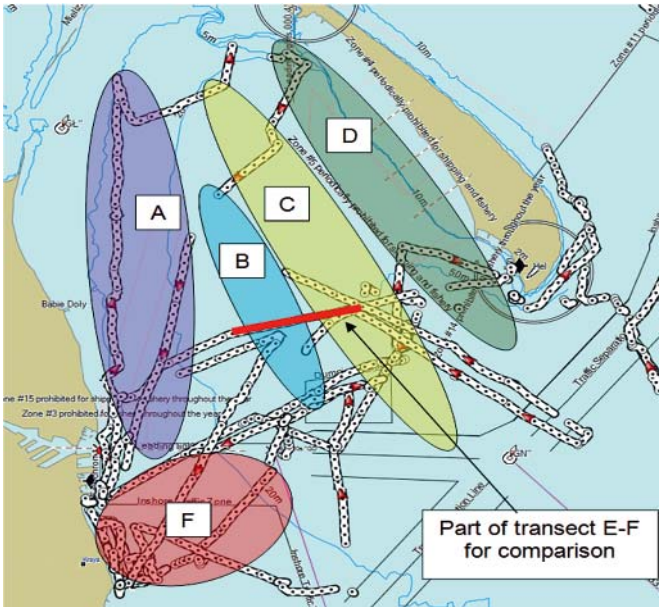


***Fig. 8.*** *Map of Gdansk Bay which shows classification of the bottom penetration areas.* ***A*** *- the area called "hilly sub-bottom";* ***B*** *- the area of medium sounding depth (up to 5 m penetration);* ***C*** *- the area of the deepest penetration (up to 30 m);* ***D*** *- the area of a highly reflective bottom (no penetration);* ***E*** *- the area of a mixed type of penetration (from 1 m up to 10 m);* ***Thick red line*** *- a part of the transect* ***E-F*** *- taken for comparison*

## EXAMPLES OF SEDIMENT CLASSIFICATION

After several trails in Gdansk Bay it was possible to elaborate a basic classification of sub-bottom penetration areas indicated on the map (Fig. 8) which shows five main types of the results.

Sample echograms corresponding to the marked areas are presented below: the first (Fig. 9) called "hilly sub-bottom", shows a typical bottom which reflects strong echo, and another bottom profile at first glance looking like "hills", where the top of it sometimes touches the bottom and even penetrates it e. g. in the point I. After examination, sediments of sand silt and clayey silts were found, what confirmed information taken from the geological map. From the point of view of the layered structure the area E is rather less interesting as it combines places with penetration up to 10 m with those of strong echo only and of no information of extra layers which corresponds to sediments like sand from which whole sounding pulse is reflected. The looking and analyzing of such long echograms gives possibility to determine permanence of sub-bottom layer.

The other results were also compared with the data delivered by Państwowy Instytut Geologiczny, representing a geological map of bottom structure (Fig. 11), prepared by using different methods including taking deep sediment samples. When analyzing echogram results shown in Fig. 12 one can notice that a part of sounding which dealt with sand characterized shallow penetration, and in the places where silt and clay

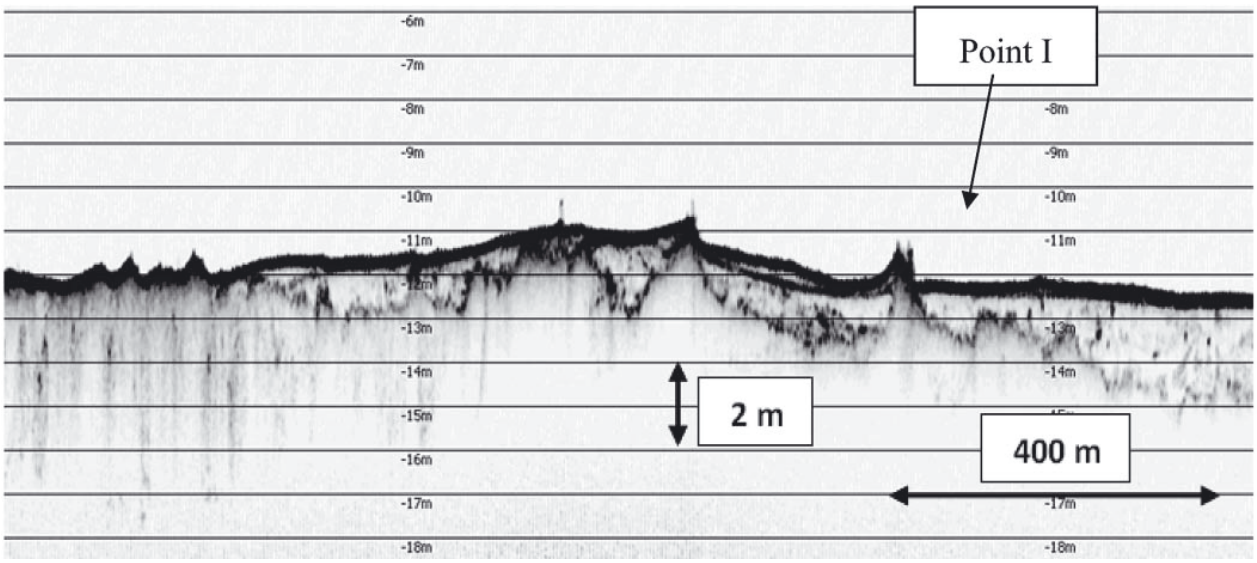


***Fig. 9.*** *Hilly sub-bottom profile – area A*

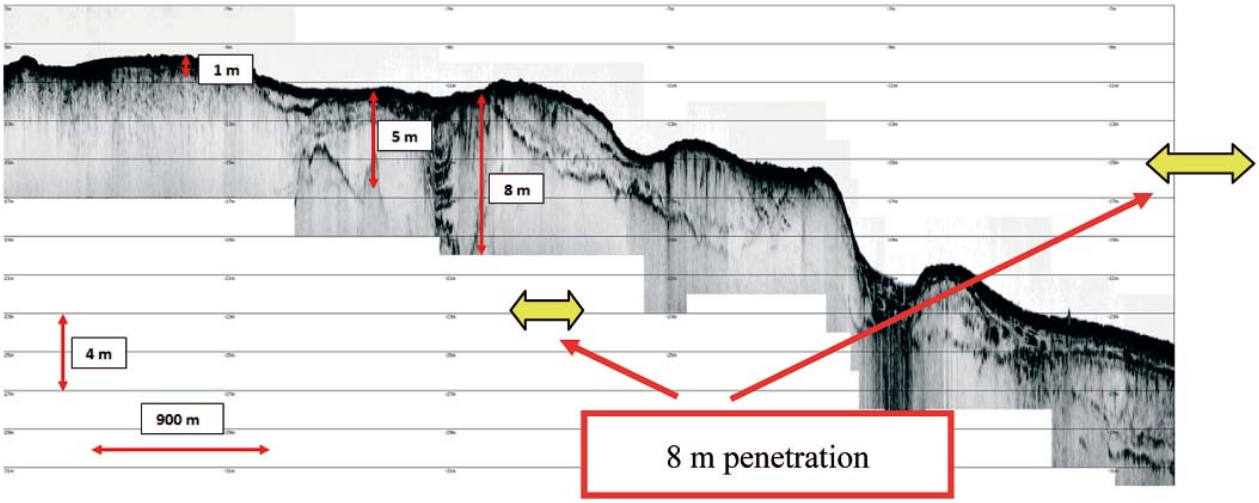


***Fig. 10.*** *The area of a mixed type of penetration depth (from 2 m up to 10 m) – area E*

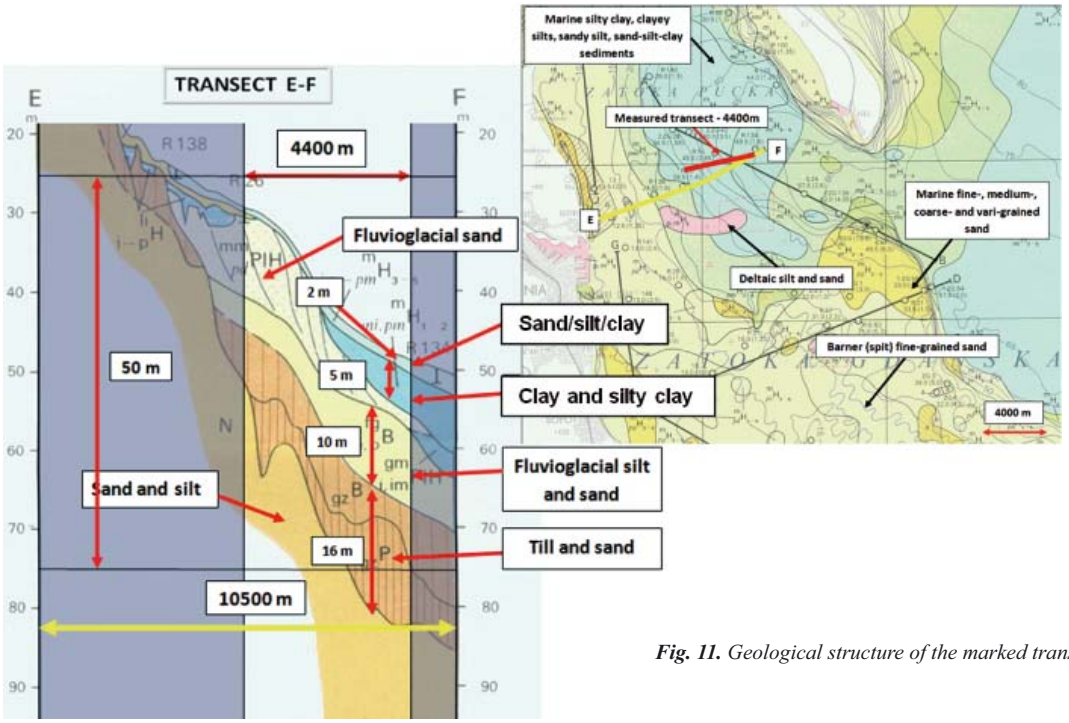


*Fig. 11. Geological structure of the marked transect*

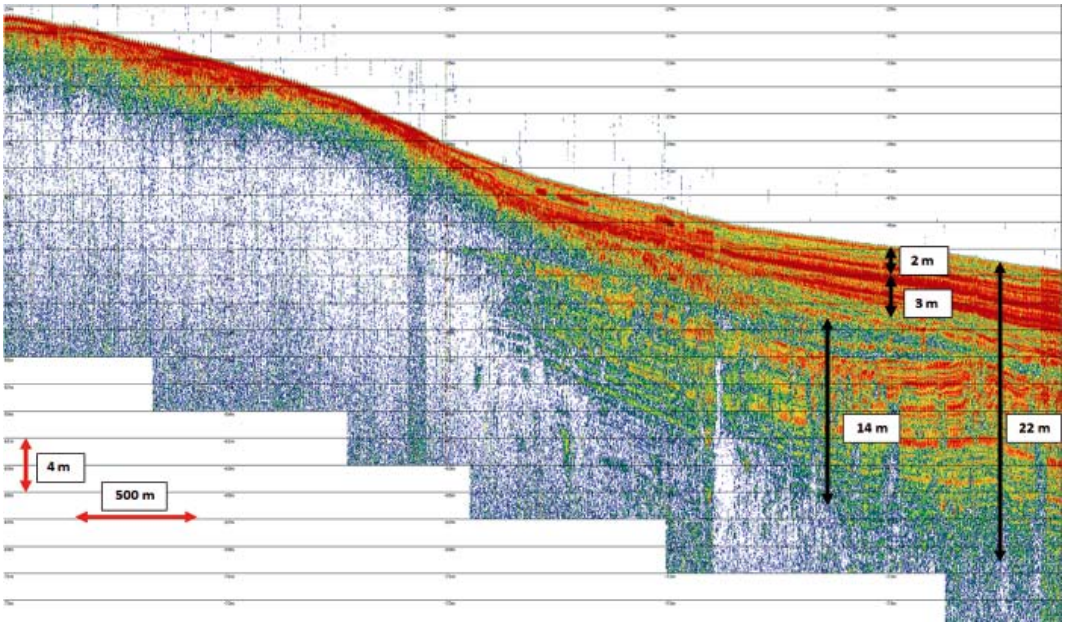


*Fig. 12. Echogram taken along the transect marked with red line in Fig. 11*

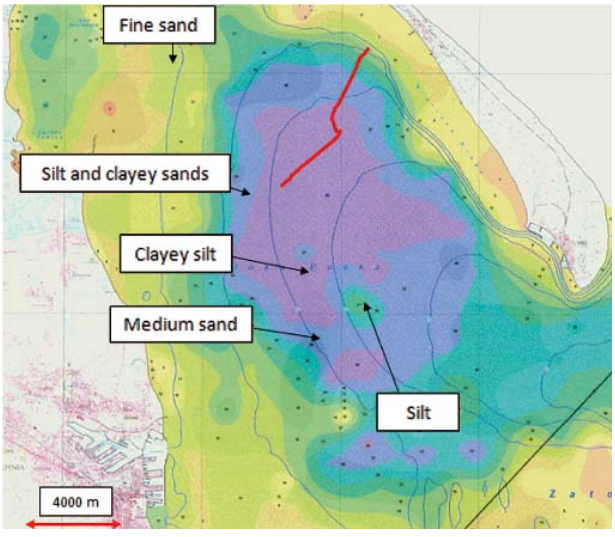


*Fig. 13. Geological map with the marked transect*

occurred deeper souding results were obtained. Comparison of the results was possible due to the use of devices to precisely contol of the research vessel motion and sail along selected transects. During the measurements the parametric echosounder was tested with different sounding pulse frequencies to acquire information about echosounder parameters during sounding the deep bottom penetration areas.

The last results come from the mixed areas B, C and D. They were taken along the transect marked with red line depicted on the geological map.

When analyzing of the results (Fig. 14) is started from the left side, the data obtained in the area B representing strong echo reflected from hard bottom are there visualized. When passing to B sector a deeper penetration can be noticed - not as deep as in the middle of this area but with the same characteristic structure. The end of the echoogram shows rapid change of penetration depth compared with bathymetric data and change of colour of the surface from orange to red which is related to a higher level of the bottom echo strength.

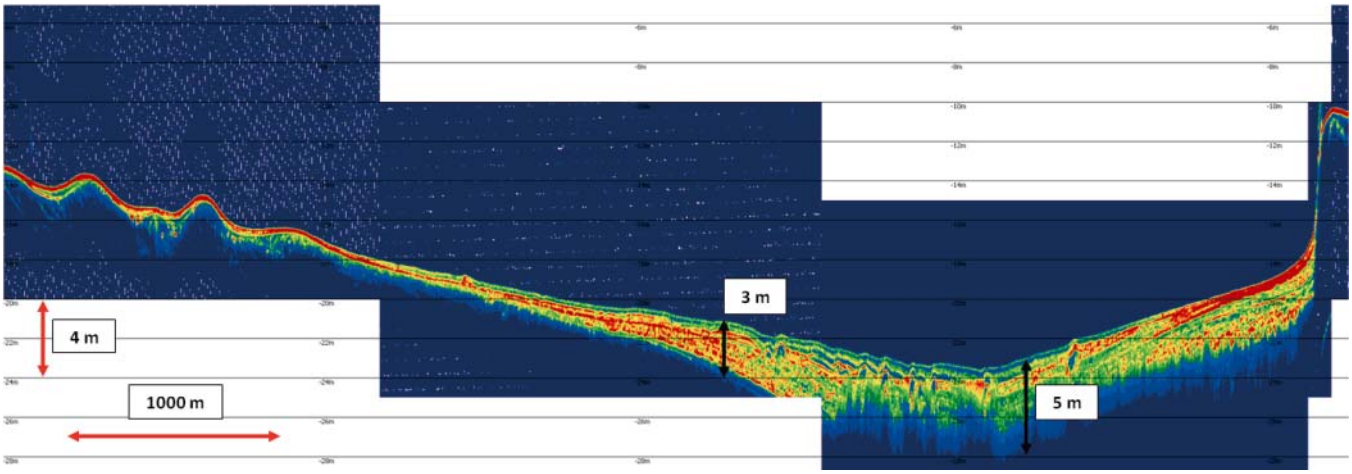


***Fig. 14.*** *Echogram taken along the transect marked on the geological map (Fig. 13)*

## SUMMARY

In the paper is presented an experimental acoustic method for determination of sea bed material as well as structure of the upper layer of the sea bottom.

After performance of trials and data processing, their results were analyzed and compared with those obtained during the trials in the water tankthat was satisfactorily implemented into the first step of classification of sediment layers.

Additionally experiments in preparing long echograms (over a few kilometers) clearly showing changes in sediment structure, have ended with good results that was confirmed by the promising spectrograms presented in this paper.

The systematic approach to the problem, consisted in starting with measurements of some acoustic parameters of sediments in laboratory conditions and then passing to the in situ investigations, resulted in determination of different properties of sea bottom in some areas of Gdansk Bay.

### *Acknowledgments*

The investigations was partially supported by the Ministry of Science and Higher Education in the frame of the fund for statutory activities of the Faculty of Navigation and Naval Weapons of the Polish Naval Academy.

### BIBLIOGRAPHY

1. P. Blondel, A. Caiti: *Buried Waste in the Seabed Acoustic Imaging and Bio-Toxicity.* University of Bath, UK, 2007
2. J. Galloway, W. Collins: *Dual frequency acoustic classification of seafloor habitat using the QTC view*. Oceans '98, Nice, France 1998.
3. G. Grelowska, E. Kozaczka, *Sounding of layered marine bottom - modeling investigations*, Acta Physica Polonica A, Vol. 118, No. 1, 66÷70, 2010
4. G. Grelowska, E. Kozaczka: *Selected results of the parametric soundings of the Gdansk Bay*. Hydroacoustics V. 11, 105÷112, 2008
5. G. Grelowska, E. Kozaczka, W. Szymczak: *Methods of data extraction from sub-bottom profiler's signal. Hydroacoustics*, 13, 109÷118, 2010
6. G. Grelowska: *The prevailing patterns of the sound speed distribution in the environment of the southern Baltic*. Archives of Acoustics, 25, 359÷368, 2000
7. G. Grelowska, S. Kozaczka. W. Szymczak: *Some methods of the sea bottom recognition.* Hydroacoustics, Vol. 12, 69÷76, 2009
8. G. Grelowska, E. Kozaczka, S. Kozaczka, W. Szymczak: *Detection of Objects Buried in the Sea Bottom with the Use of Parametric Echosounder*. Archives on Acoustics, Vol. 38, No 1, 99÷104, 2013
9. L. Hamilton, P. Mulhearn, R. Poeckert: *Comparison of RoxAnn and QTC-view acoustic bottom classification system performance for the Cairns area, Great Barier Reef, Australia.* Continental Shelf Research 19, 1577÷1597, 1999
10. E. Kozaczka, G. Grelowska, S. Kozaczka: *Images of the seabed of the Gulf of Gdansk obtained by means of the parametric sonar.* Acta Physica Polonica A, Vol. 118, No 1, 91÷94, 2010
11. E. Kozaczka, G. Grelowska, S. Kozaczka, W. Szymczak: *Processing data on sea bottom structure obtained by means of the parametric sounding.* Polish Maritime Research, 19, 4 (76), 3÷10, 2012
12. K. Naugolnykh, L. Ostrovsky: *Nonlinear Wave Processes in Acoustics.* Cambridge University, Cambridge, 1998
13. Sternlicht D. D., Moustier Ch. P: *Time-dependent seafloor acoustic backscatter (10-100) kHz*. J. Acoust. Soc. Am., 114, 2709÷2723, 2003
14. Turgut A.: *Method and apparatus of classifying marine sediment*. Technical Report U. S., 1998
15. Uscinowicz S., Zachowicz J.: *Geological map of the bottom of the Baltic Sea*. 8 sheets and pamphlet, scale 1:200, 000, Polish Geological Institute, Warsaw, 1994
16. Walter D., Lambert D., Young D., Stephens K.: *Mapping sediment acoustic impedance using remote sensing acoustic techniques in a shallow-water carbonate environment.* Geo-Marine Letters, 17, 260÷267, 1997
17. Wunderlich J., Müller S.: *High-resolution sub-bottom profiling using parametric acoustics*. International Ocean Systems, **7** (4), 6÷11, 2003.

### CONTACT WITH THE AUTHORS

Grażyna Grelowska[1)], Prof., ggrel@wp.pl
Eugeniusz Kozaczka[1, 2)], Prof., kozaczka@pg.gda.pl
Sławomir Kozaczka[1)], M.Sc., milites@vp.pl
Wojciech Szymczak[1)], M.Sc., ws2@o2.pl

1) Polish Naval Academy
Śmidowicza 69
81-103 Gdynia POLAND

2) Gdansk University of Technology,
11/12 G. Narutowicza
80-233 Gdańsk, POLAND


The Ship Handling Research and Training Centre at Ilawa is owned by the Foundation for Safety of Navigation and Environment Protection, which is a joint venture between the Gdynia Maritime University, the Gdansk University of Technology and the City of Ilawa.

**Two main fields of activity of the Foundation are:**

- Training on ship handling. Since 1980 more than 2500 ship masters and pilots from 35 countries were trained at Iława Centre. The Foundation for Safety of Navigation and Environment Protection, being non-profit organisation is reinvesting all spare funds in new facilities and each year to the existing facilities new models and new training areas were added. Existing training models each year are also modernised, that's why at present the Centre represents a modern facility perfectly capable to perform training on ship handling of shipmasters, pilots and tug masters.

- Research on ship's manoeuvrability. Many experimental and theoretical research programmes covering different problems of manoeuvrability (including human effect, harbour and waterway design) are successfully realised at the Centre.

The Foundation possesses ISO 9001 quality certificate.

**Why training on ship handling?**

The safe handling of ships depends on many factors - on ship's manoeuvring characteristics, human factor (operator experience and skill, his behaviour in stressed situation, etc.), actual environmental conditions, and degree of water area restriction.

Results of analysis of CRG (collisions, rammings and groundings) casualties show that in one third of all the human error is involved, and the same amount of CRG casualties is attributed to the poor controllability of ships. Training on ship handling is largely recommended by IMO as one of the most effective method for improving the safety at sea. The goal of the above training is to gain theoretical and practical knowledge on ship handling in a wide number of different situations met in practice at sea.

For further information please contact:
**The Foundation for Safety of Navigation and Environment Protection**

Head office:
36, Chrzanowskiego Street
80-278 GDAŃSK, POLAND
tel./fax: +48 (0) 58 341 59 19

Ship Handling Centre:
14-200 IŁAWA-KAMIONKA, POLAND
tel./fax: +48 (0) 89 648 74 90
e-mail: office@ilawashiphandling.com.pl
e-mail: office@portilawa.com

## GDANSK UNIVERSITY OF TECHNOLOGY

is the oldest and largest scientific and technological academic institution in the Pomeranian region. The history of Gdansk University of Technology is marked by two basic dates, namely: October 6, 1904 and May 24, 1945.

The first date is connected with the beginning of the technical education at academic level in Gdansk. The second date is connected with establishing of Gdansk University of Technology, Polish state academic university. Gdansk University of Technology employ 2,500 staff, 1,200 whom are academics. The number of students approximates 20,000, most of them studying full-time. Their career choices vary from Architecture to Business and Management, from Mathematics and Computer Science to Biotechnology and Environmental Engineering, from Applied Chemistry to Geodesics and Transport, from Ocean Engineering to Mechanical Engineering and Ship Technology, from Civil Engineering to Telecommunication, Electrical and Control Engineering. Their life goals, however, are much the same - to meet the challenge of the changing world. The educational opportunities offered by our faculties are much wider than those of other Polish Technical universities, and the scientific research areas include all of 21st Century technology. We are one of the best schools in Poland and one of the best known schools in Europe – one that educates specialists excelling in the programming technology and computer methods used in solving complicated scientific, engineering, organizational and economic problems.

## THE FACULTY OF OCEAN ENGINEERING AND SHIP TECHNOLOGY

The Faculty of Ocean Engineering and Ship Technology (FOEST) as the only faculty in Poland since the beginning of 1945 has continuously been educating engineers and doctors in the field of Naval Architecture and Marine Technology.

The educational and training activities of FOEST are supported by cooperation with Polish and foreign universities, membership in different international organizations and associations, as well as participation in scientific conferences and symposia. Hosting young scientists and students from different countries is also a usual practice in FOEST.

The activities of Faculty departments are related to: mechanics and strength of structures, hydromechanics, manufacturing, materials and system quality, power plants, equipment and systems of automatic control, mostly in shipbuilding, marine engineering and energetic systems.

FOEST is a member of such organizations like WEGEMT; The Association of Polish Maritime Industries and the co-operation between Nordic Maritime Universities and Det Norske Veritas. The intensive teaching is complemented and supported by extensive research activities, the core of which is performed in close collaboration between FOEST staff and industry. We take great care to ensure that the applied research meet both the long term and short term needs of Polish maritime industry. FOEST collaborates with almost all Polish shipyards. Close links are maintained with other research organizations and research institutions supporting the Polish maritime industry, such as Ship Design and Research Centre and Polish Register of Shipping, where several members of the Faculty are also members of the Technical Board.

The Faculty of Ocean Engineering and Ship Technology is a unique academic structure, which possesses numerous highly qualified and experienced staff in all above mentioned specific research areas. Moreover, the staff is used to effective co-operation and exchange of ideas between specialists of different detailed areas. This enables a more integrated and comprehensive treatment of research and practical problems encountered in such a complicated field of activity as naval architecture, shipbuilding and marine engineering.

The staff of the Faculty has strong international links worldwide, being members or cooperating with international organizations like International Maritime Organization IMO, International Towing Tank Conference ITTC, International Ship and Offshore Structures Congress ISSC, International Conference on Practical Design of Ship and other floating Structures PRADS just to name a few.

GDANSK UNIVERSITY OF TECHNOLOGY
Faculty of Ocean Engineering and Ship Technology
11/12 Narutowicza Street, 80-233 Gdansk, Poland
Tel (+48) 58 347 1548 ; Fax (+48) 58 341 4712
e-mail: sekoce@pg.gda.pl